

MICROCOPY RESOLUTION TEST CHART
NATIONAL BUREAU OF STANDARDS-1963-A

2

AD-A161 444

REPORT DOCUMENTATION PAGE		READ INSTRUCTIONS BEFORE COMPLETING FORM
1. REPORT NUMBER ARO 18054.16-EL	2. GOVT ACCESSION NO. AD-A161444 N/A	3. RECIPIENT'S CATALOG NUMBER N/A
4. TITLE (and Subtitle) MILLIMETER-WAVE INTEGRATED CIRCUITS		5. TYPE OF REPORT & PERIOD COVERED Final Report 15 March 1982 to 20 Mar 1985
7. AUTHOR(s) Raj Mittra		6. PERFORMING ORG. REPORT NUMBER EC-85-8; UILU-ENG-85-2568
9. PERFORMING ORGANIZATION NAME AND ADDRESS Department of Electrical and Computer Engineering University of Illinois 1406 W. Green Street, Urbana, IL 61801		8. CONTRACT OR GRANT NUMBER(s) DAAG29-82-K-0084
11. CONTROLLING OFFICE NAME AND ADDRESS U. S. Army Research Office Post Office Box 12211 Research Triangle Park, NC 27709		10. PROGRAM ELEMENT, PROJECT, TASK AREA & WORK UNIT NUMBERS N/A
14. MONITORING AGENCY NAME & ADDRESS (if different from Controlling Office)		12. REPORT DATE October 1985
		13. NUMBER OF PAGES 106
		15. SECURITY CLASS. (of this report) Unclassified
		15a. DECLASSIFICATION/DOWNGRADING SCHEDULE
16. DISTRIBUTION STATEMENT (of this Report) Approved for public release; distribution unlimited.		
17. DISTRIBUTION STATEMENT (of the abstract entered in Block 20, if different from Report) NA		
18. SUPPLEMENTARY NOTES The view, opinions, and/or findings contained in this report are those of the author(s) and should not be construed as an official Department of the Army position, policy, or decision, unless so designated by other documentation.		
19. KEY WORDS (Continue on reverse side if necessary and identify by block number) microwave transmission lines modal characteristics discontinuities in transmission lines microstrip thin lines		
20. ABSTRACT (Continue on reverse side if necessary and identify by block number) In this report, a number of topics are considered that concern printed circuits and printed circuit discontinuities. First, propagating and evanescent modes of a shielded microstrip are calculated using the spectral Galerkin technique. The characteristic impedance and field configurations of these modes are also calculated. These modes are then used in a mode matching technique, in order to calculate the scattering from abrupt discontinuities in the microstrip. Results are given for various configurations of single and cascaded discontinuities. Next, the singular integral equation technique is used as an alternative		

DTIC
 ELECTE
 NOV 22 1985
 S E

DTIC FILE COPY

to the spectral Galerkin technique, to calculate modes in a shielded microstrip. These results are compared to those generated by the spectral Galerkin technique. Finally, the coupling between multiple transmission lines is considered, by using the coupled-mode theory. Results for the propagation constants of the various modes of propagation, as well as for the transfer of current from one line to the next, are presented.

UNCLASSIFIED

ARU 18054.16-EL

UILU-ENG-85-2568

ELECTROMAGNETIC COMMUNICATION LABORATORY REPORT NO. 85-8

MILLIMETER-WAVE INTEGRATED CIRCUITS

Final Report

U. S. Army Research Office
DAAG29-82-K-0084

Raj Mittra

University of Illinois
at Urbana-Champaign

Accession For	
NTIS GRA&I	<input checked="" type="checkbox"/>
DTIC TAB	<input type="checkbox"/>
Unannounced	<input type="checkbox"/>
Justification	<input type="checkbox"/>
By _____	
Distribution/	
Availability Codes	
Dist	Avail and/or Special
A-1	



October 1985

Approved for Public Release
Distribution Unlimited

85 11 18 256

TABLE OF CONTENTS

Chapter	Page
1. INTRODUCTION.....	1
2. UNIFORM MICROSTRIP ANALYSIS	3
2.1 Introduction.....	3
2.2 The Spectral Domain Immitance Approach	3
2.3 The Spectral Galerkin Technique	11
2.4 Basis Functions.....	13
2.5 Characteristic Impedance	16
2.6 Fin Line Calculations	20
2.7 Field Configurations.....	24
2.8 Results for Uniform Microstrip and Fin Line	24
2.9 Conclusion	36
3. DISCONTINUITY CALCULATIONS	37
3.1 Introduction.....	37
3.2 Mode Matching.....	38
3.3 Orthogonality of Inner Products.....	43
3.4 Condition Number of the Matrix.....	44
3.5 Matrix Theory for Cascaded Discontinuities.....	44
3.6 Results for the Single Discontinuity	49
3.7 Results for Other Discontinuities.....	53
3.8 Conclusion	57
4. THE SINGULAR INTEGRAL EQUATION TECHNIQUE	62
4.1 Introduction.....	62
4.2 Overview of the Method	62
4.3 Calculations of P_{mq} , K_n , and D_{nm}	70
4.4 Results	74
4.5 Conclusion	75
5. COUPLED-MODE ANALYSIS OF MULTICONDUCTOR MICROSTRIP LINES	76
5.1 Introduction.....	76
5.2 Calculation of Modes	78
5.3 Coupled-mode Theory.....	80
5.4 Results	81
5.5 Conclusion	83
6. SUMMARIES OF OTHER ACTIVITIES AND IMPORTANT RESULTS	88
LIST OF PUBLICATIONS AND TECHNICAL REPORTS.....	90
SCIENTIFIC PERSONNEL AND DEGREES AWARDED.....	93
REFERENCES.....	94

LIST OF FIGURES

	Page
Figure 2.1. Shielded microstrip.	4
Figure 2.2. Coordinate transformation in the spectral domain.	7
Figure 2.3. Equivalent transmission lines for the TE and TM components of microstrip fields in the transform domain.	10
Figure 2.4. Basis functions for $J_z(x)$	14
Figure 2.5. Basis functions for $J_x(x)$	15
Figure 2.6. Dimensions for a fin line.	21
Figure 2.7. Equivalent transmission lines for the TE and TM components of fin-line fields in the transform domain.	22
Figure 2.8. The dispersion characteristics of the dominant and first two even higher-order modes of a microstrip. Two basis functions and 100 spectral terms were used.	26
Figure 2.9. The characteristic impedance of a microstrip, calculated with two definitions. One basis function and 50 spectral terms were used.	27
Figure 2.10. Dispersion curve of a fin line. One basis function and 50 spectral terms were used. A comparison is made to the results of Helard et al. [17].	28
Figure 2.11. Plots of $E_x(x,y)$ and $E_y(x,y)$ for the dominant mode of a microstrip. For this plot, $h = 0.4445$ mm, $b = 0.381$ mm, $t = 0.127$ mm, $s = 0.0635$ mm, $\epsilon_r = 9.6$ mm, $\text{freq} = 20$ GHz, and $\beta = 1037.01$ rad/m.	29
Figure 2.12. H_x and H_y of the dominant mode for the same configuration as that in Figure 2.11.	30
Figure 2.13. E_z and H_z of the dominant mode for the same configuration as that in Figure 2.11.	31
Figure 2.14. E_x and E_y of the second mode for the same configuration as that in Figure 2.9. For this mode, $\beta = -j4068.72$ rad/m.	32
Figure 2.15. E_x and E_y of the third mode for the same configuration as that in Figure 2.9. For this mode, $\beta = -j10478.5$ rad/m.	33
Figure 2.16. E_x and E_y of the fourth mode for the same configuration as that in Figure 2.9. For this mode, $\beta = -j14694.4$ rad/m.	34

Figure 2.17. E_x and E_y of the fifth mode for the same configuration as that in Figure 2.9. For this mode, $\beta = -j14897.1$ rad/m.	35
Figure 3.1. Various microstrip discontinuities in the center conductor.	39
Figure 3.2. Dimensions for a single-step discontinuity in strip width and the corresponding equivalent circuit.	42
Figure 3.3. Symmetrical discontinuities, and the method of taking advantage of the symmetry by symmetrical and antisymmetrical excitation of the discontinuity.	46
Figure 3.4. Input and output parameters of an arbitrary circuit, and a cascade of such circuits.	47
Figure 3.5. Dimensions for a symmetrical double step discontinuity in strip width.	54
Figure 3.6. Dimensions for a model of a microstrip taper, modeled as a cascade of discrete discontinuities.	58
Figure 3.7. Dimensions for a step discontinuity in dielectric constant, strip width, and substrate thickness.	60
Figure 4.1. Dimensions of a shielded microstrip for this chapter.	63
Figure 5.1. Configuration of microstrip with five lines. For these calculations, $t = 2s = 1$ mm, $2s_1 = 0.2$ mm, and $\epsilon_r = 10$	77
Figure 5.2. Dispersion curves for the first five modes of propagation of a microstrip with five lines. The dimensions are the same as those in Figure 5.1.	82
Figure 5.3. $J_7(x)$ for the first even mode.	84
Figure 5.4. $J_7(x)$ for the second even mode.	84
Figure 5.5. $J_7(x)$ for the third even mode.	85
Figure 5.6. $J_2(x)$ for the first odd mode.	85
Figure 5.7. $J_2(x)$ for the second odd mode.	86
Figure 5.8. Variation of I' with z at 1 GHz for each of the five strips.	87
Figure 5.9. Variation of I' with z at 10 GHz for each of the five strips.	87

CHAPTER 1

INTRODUCTION

The primary objective of this effort has been the investigation of dominant and higher-order mode characteristics of microstrip lines and fin lines that find application in millimeter-wave integrated circuits. The investigation of higher-order modes is important for the analysis of discontinuity problems in planar transmission lines; these problems have been the focus of attention in this project during the entire grant period. The study of the discontinuity problems is of interest from the point of view of designing practical components, e.g., filters, impedance matching networks, and transitions between rectangular waveguides and planar transmission lines. The higher-order modes have been analyzed using the spectral domain technique introduced by Itoh and Mittra [1, 2]. The propagation constant, characteristic impedance and field configuration are obtained for the dominant and higher-order modes in planar lines. The model characteristics are then employed to analyze some typical discontinuities in planar lines using the mode-matching procedure [3, 4], which has been extensively employed in the past for the solution of similar problems in other types of waveguides. However, the situation with regard to the application of the mode-matching procedure is found to be quite different for the case of planar waveguides when compared to that of rectangular guides because accurate generation of higher-order mode fields becomes a formidable problem in planar guides, whereas this task is quite straightforward for rectangular guides. Thus, it becomes important to investigate effectiveness of the mode-matching procedure when only a relatively small number of modes are available and the higher-order modes are known only approximately.

In an attempt to enhance the accuracy of the higher-order mode computation, the singular integral equation technique is used. This technique was originally employed by Mittra and Itoh [5] for the analysis of planar transmission lines. This technique is further developed in this work and the results obtained via the application of the singular integral

equation technique are compared with those derived from the spectral domain approach. Another interesting problem in planar transmission lines, viz., the coupled multiconductor lines is analyzed in this work using the spectral domain approach.

To the best of our knowledge a full-wave coupled line analysis of n planar transmission lines has not appeared elsewhere in the literature.

CHAPTER 2

UNIFORM MICROSTRIP ANALYSIS

2.1 Introduction

The analysis of various printed circuits has been of interest for a number of years. We find it of interest here, because the first step of the mode matching procedure is to generate the dominant and higher-order modes in a uniform microstrip. A cross section of a shielded microstrip is shown in Figure 2.1. This and related structures have been analyzed by a number of workers using a variety of techniques. These techniques include various quasi-static methods [6-9], nonuniform discretization of integral equations [10], a modified Weiner-Hopf technique [11], a singular integral equation technique [5], and the spectral Galerkin technique [1,2,12-17]. The method that is simplest to implement while giving excellent results is the spectral Galerkin technique. This is the method considered in this chapter.

In order to allow mode matching work to a high degree of accuracy, it is necessary to calculate as many evanescent modes as possible. The feasibility of generating a large number of higher-order modes imposes the largest constraint upon the accuracy of the mode matching solutions. To date, there is little information available on evanescent modes in a shielded microstrip, although the propagating modes have been well studied.

In this chapter, we present data on the dominant and first few evanescent modes of a microstrip, showing dispersion curves, characteristic impedance calculations, and field distributions. Let us proceed now with the analysis of a uniform microstrip.

2.2 The Spectral Domain Immitance Approach

In order to find information about waveguide modes, the quantity of most immediate interest is the propagation constant, β . To find β , a matrix equation must be found of the form

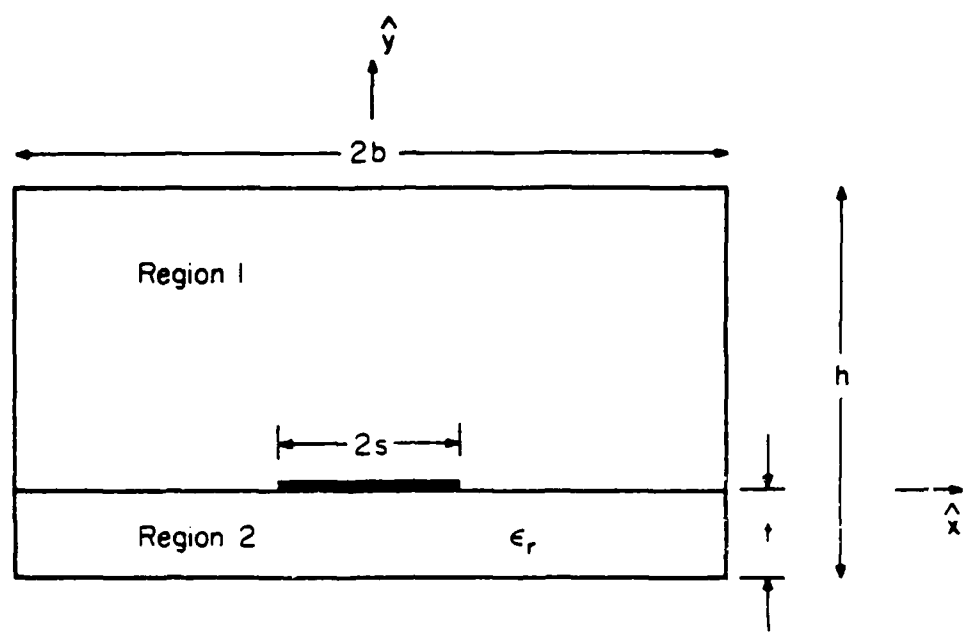


Figure 2.1. Shielded microstrip.

$$\begin{pmatrix} \tilde{Z}_{zz}(\beta) & \tilde{Z}_{zx}(\beta) \\ \tilde{Z}_{xz}(\beta) & \tilde{Z}_{xx}(\beta) \end{pmatrix} \begin{pmatrix} \tilde{J}_z \\ \tilde{J}_x \end{pmatrix} = \begin{pmatrix} \tilde{E}_z(\beta) \\ \tilde{E}_x(\beta) \end{pmatrix} \quad (2.1)$$

where \tilde{J} and \tilde{E} are the Fourier transforms of the current and electric field in the plane $z=0$, and the \tilde{Z} 's form the components of a dyadic Green's function. In order to find this Green's function, we use the spectral domain immittance approach. This approach is a method of generating the dyadic Green's function in a straightforward manner, that will be useful for many different kinds of printed circuits, including microstrip, fin line, and coplanar waveguides. The work in this section follows Itoh [13].

We begin by setting up a scalar Helmholtz equation in each of the regions 1 and 2, as shown in Figure 1. Assuming an $e^{j(\omega t - \beta z)}$ dependence, we obtain

$$(\nabla^2 + \epsilon_i k_0^2) \begin{pmatrix} \phi_i(x, y) \\ \psi_i(x, y) \end{pmatrix} = 0 \quad (2.2a)$$

where

$$\epsilon_i = \begin{cases} \epsilon_0 & \text{Region 1} \\ \epsilon_0 \epsilon_r & \text{Region 2} \end{cases} \quad (2.2b)$$

As the equations now stand, the TE_y and TM_y fields are coupled. In order to decouple these equations we must work in the Fourier transform domain. Thus, for example,

$$\tilde{\phi}(n, y) = \int_{-\infty}^{\infty} \phi(x, y) e^{j\alpha_n x} dx \quad (2.3a)$$

$$\phi(x, y) = \frac{1}{2b} \sum_{-\infty}^{\infty} \tilde{\phi}(n, y) e^{-j\alpha_n x} \quad (2.3b)$$

$$\alpha_n = \frac{(n - 1/2) \pi}{b} \quad (2.3c)$$

The above choice of α_n is suitable for modes that are even in J_z , such as the dominant mode. This choice enforces the boundary conditions at $x = \pm b$. For modes that are odd in

J_z we choose $\alpha_n = n\pi/b$. In the transform domain, the Helmholtz equations become

$$\left(-\alpha_n^2 + \frac{\partial^2}{\partial y^2} - \beta^2 + \epsilon_i k_o^2\right) \begin{pmatrix} \bar{\phi}_i(n) \\ \bar{\psi}_i(n) \end{pmatrix} = 0 \quad (2.4)$$

or

$$\left(\frac{\partial^2}{\partial y^2} - \gamma_i^2\right) \begin{pmatrix} \bar{\phi}_i(n) \\ \bar{\psi}_i(n) \end{pmatrix} = 0 \quad (2.5)$$

where

$$\gamma_i^2 = \alpha_n^2 + \beta^2 - \epsilon_i k_o^2 \quad (2.6)$$

Thus, in the transform domain we can reduce the problem to two transmission line equations.

Let us now introduce the transformations

$$\begin{pmatrix} z \\ x \end{pmatrix} = \begin{pmatrix} N_z & N_x \\ N_x & -N_z \end{pmatrix} \begin{pmatrix} v \\ u \end{pmatrix} \quad (2.7)$$

where

$$N_z = \frac{\beta}{\sqrt{\alpha_n^2 + \beta^2}} = \sin \theta \quad (2.8a)$$

$$N_x = \frac{\alpha_n}{\sqrt{\alpha_n^2 + \beta^2}} = \cos \theta \quad (2.8b)$$

This transformation is shown in Figure 2.2. With this transformation, we see that all scalar potentials and fields are of the form

$$\bar{\phi}(n, y) e^{-j\beta z} = \int_{-\infty}^{\infty} \phi(x, y) e^{-j(\alpha_n x + \beta z)} \quad (2.9)$$

The transformed equations are dependent only upon v ; hence $\frac{\partial}{\partial u} = 0$. This decouples

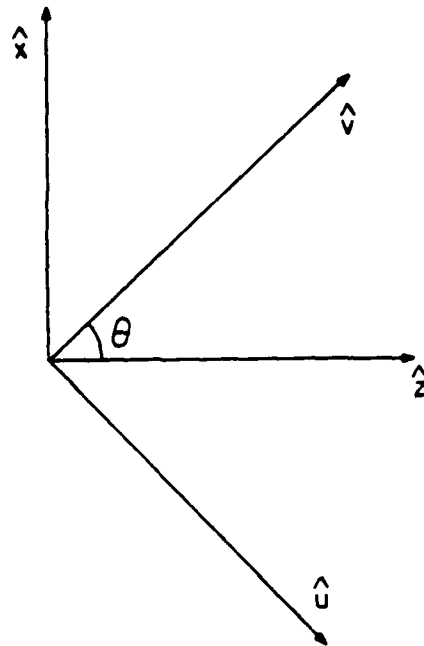


Figure 2.2. Coordinate transformation in the spectral domain.

Equation 2.5 into TE_y components (\tilde{H}_y , \tilde{E}_u , and \tilde{H}_v) and TM_y components (\tilde{E}_y , \tilde{E}_v , and \tilde{H}_u). We now show how this separation takes place, and that the TE_y components are due to \tilde{J}_u , and the TM_y components are due to \tilde{J}_v .

Let us derive the expressions for the field components. To begin, we express the vector potentials as

$$\tilde{F}_i = \hat{y} \phi_i(x, y) \quad (2.10a)$$

$$\tilde{A}_i = \hat{y} \psi_i(x, y) \quad (2.10b)$$

Adapting some results from Harrington [18] on the separation of TE and TM fields, and using the fact that $\frac{\partial}{\partial y} = \gamma_i$ and $\frac{\partial}{\partial u} = 0$, we obtain the TE components

$$\tilde{E}_v = \tilde{E}_y = 0 \quad (2.11a)$$

$$\tilde{E}_u = -\frac{\partial \tilde{\psi}_i}{\partial v} \quad (2.11b)$$

$$\tilde{H}_v = \frac{\gamma_i}{j\omega\mu_0} \frac{\partial \tilde{\psi}_i}{\partial v} \quad (2.11c)$$

$$\tilde{H}_y = \frac{1}{j\omega\mu_0} (\gamma_i^2 + k_i^2) \tilde{\psi}_i \quad (2.11d)$$

$$\tilde{H}_u = 0 \quad (2.11e)$$

and the TM components

$$\tilde{E}_v = \frac{\gamma_i}{j\omega\epsilon_1} \frac{\partial \tilde{\phi}_i}{\partial v} \quad (2.12a)$$

$$\tilde{E}_y = \frac{1}{j\omega\epsilon_1} (\gamma_i^2 + k_i^2) \tilde{\phi}_i \quad (2.12b)$$

$$\tilde{E}_u = 0 \quad (2.12c)$$

$$\tilde{H}_v = \tilde{H}_y = 0 \quad (2.12d)$$

$$\tilde{H}_u = \frac{\partial \tilde{\phi}_t}{\partial v} \quad (2.12e)$$

From these equations, we can set up equivalent transmission lines for the TE and TM cases.

The characteristic impedance of each line is

$$Z_{TE_i} = -\frac{\tilde{E}_u}{\tilde{H}_v} = \frac{j\omega\mu_0}{\gamma_i} \quad (2.13a)$$

$$Z_{TM_i} = \frac{\tilde{E}_v}{\tilde{H}_u} = \frac{\gamma_i}{j\omega\epsilon_i} \quad (2.13b)$$

The propagation constant for each line is γ_i , and the sources for the lines are \tilde{J}_v for the TE line and \tilde{J}_u for the TM line. These equivalent lines are shown in Figure 2.3. From the input impedance of the shorted line sections, we obtain the input impedance at $z = 0$ as

$$\tilde{Z}^e = \frac{1}{\frac{1}{Z_{TM_1} \tanh \gamma_1(h-t)} + \frac{1}{Z_{TM_2} \tanh \gamma_2 t}} \quad (2.14a)$$

$$\tilde{Z}^h = \frac{1}{\frac{1}{Z_{TE_1} \tanh \gamma_1(h-t)} + \frac{1}{Z_{TE_2} \tanh \gamma_2 t}} \quad (2.14b)$$

Given this input impedance, we may now write

$$\tilde{E}_v(n, y=0) = \tilde{Z}^e \tilde{J}_u(n, y=0) \quad (2.15a)$$

$$\tilde{E}_u(n, y=0) = \tilde{Z}^h \tilde{J}_v(n, y=0) \quad (2.15b)$$

Furthermore, we can transform these equations back into x and z coordinates using Equations 2.7 and 2.8 to obtain

$$\begin{bmatrix} \tilde{Z}_{zz}(\alpha_n, \beta) & \tilde{Z}_{zx}(\alpha_n, \beta) \\ \tilde{Z}_{xz}(\alpha_n, \beta) & \tilde{Z}_{xx}(\alpha_n, \beta) \end{bmatrix} \begin{bmatrix} \tilde{J}_z(\alpha_n) \\ \tilde{J}_x(\alpha_n) \end{bmatrix} = \begin{bmatrix} \tilde{E}_z(\alpha_n, \beta) \\ \tilde{E}_x(\alpha_n, \beta) \end{bmatrix} \quad (2.16)$$

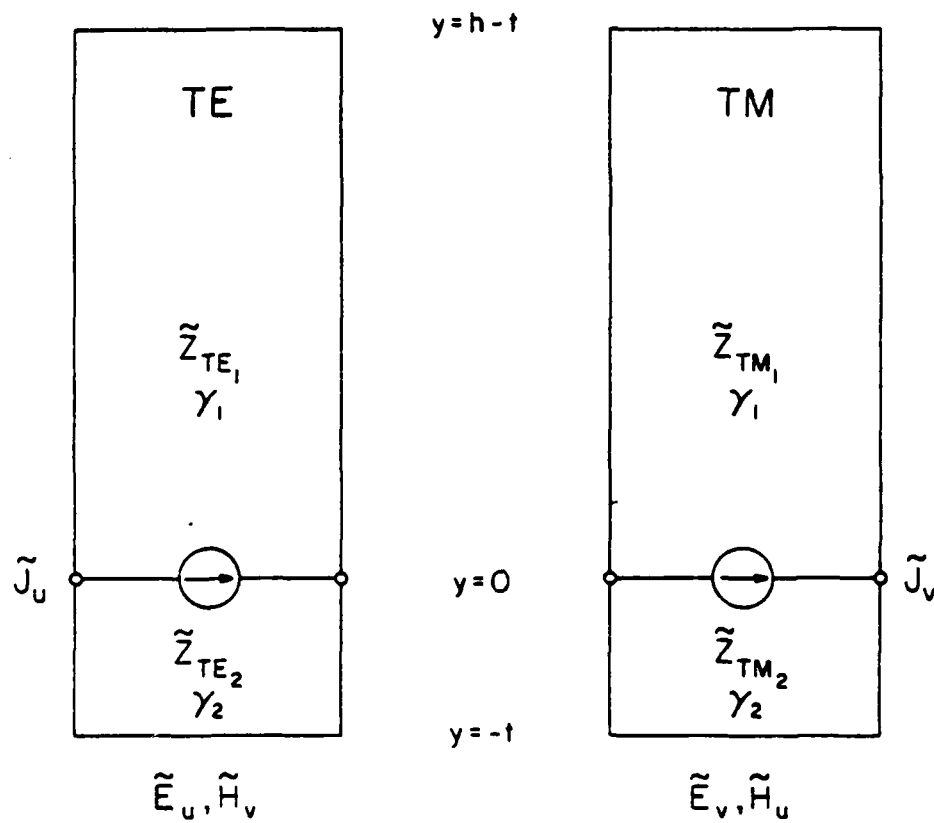


Figure 2.3. Equivalent transmission lines for the TE and TM components of microstrip fields in the transform domain.

where

$$\tilde{Z}_{zz} = N_z^2 \tilde{Z}^e + N_x^2 \tilde{Z}^h \quad (2.17a)$$

$$\tilde{Z}_{zx} = \tilde{Z}_{xz} = N_x N_z (- \tilde{Z}^e + \tilde{Z}^h) \quad (2.17b)$$

$$\tilde{Z}_{xx} = N_x^2 \tilde{Z}^e + N_z^2 \tilde{Z}^h \quad (2.17c)$$

This is the equation that must be solved to find β . Once β is found, all other quantities of interest, such as field configurations and characteristic impedance, may be found.

It is helpful at this point to briefly discuss the applicability of the spectral domain immittance approach to structures related to the microstrip. Since the equations are separable in the transform domain, we see that if we have multiple layers of dielectric, this will be equivalent to having extra sections in the transmission line model. Furthermore, multiple strips can be represented as extra current sources, and slots can be represented by voltage sources. Therefore, we can use this method of generating the dyadic Green's function for a large class of planar waveguide structures. These include fin line, coplanar waveguide, and slot line. The generality in this procedure for generating the Green function maintains the generality of the mode matching procedure.

2.3 The Spectral Galerkin Technique

Now that we have found Equation 2.16, we must solve it for β with the spectral Galerkin technique. The work in this section follows Schmidt and Itoh [15].

We proceed by expanding the currents on the strip as a sum of basis functions

$$J_z(x) = \sum_{i=1}^N c_i \xi_i(x) \quad (2.18a)$$

$$J_x(x) = \sum_{i=1}^N d_i \eta_i(x) \quad (2.18b)$$

These basis functions are now Fourier transformed according to Equation 2.3 and

substituted into Equation 2.16. By taking the inner product of the resulting equation with $\xi_i(x)$ and $\eta_i(x)$, we can eliminate the E-fields in this equation. This is true because $\xi_i(x)$ and $\eta_i(x)$ are non-zero only where E_z and E_x are constrained to be zero, since they are tangential to the strip. Since this is true in the space domain, Parseval's theorem [18] guarantees that it will also be true in the spectral domain. Hence, we obtain the equations

$$\sum_{i=1}^M K_{pi}^{zz} c_i + \sum_{j=1}^N K_{pj}^{zx} d_j = 0 \quad p=1, \dots, M \quad (2.19a)$$

$$\sum_{i=1}^M K_{qi}^{xz} c_i + \sum_{j=1}^N K_{qj}^{xx} d_j = 0 \quad q=1, \dots, N \quad (2.19b)$$

where

$$K_{pi}^{zz} = \sum_{n=-\infty}^{\infty} \bar{\xi}_p(n) \bar{Z}_{zz}(n, \beta) \bar{\xi}_i(n) \quad (2.20a)$$

$$K_{pj}^{zx} = \sum_{n=-\infty}^{\infty} \bar{\xi}_p(n) \bar{Z}_{zx}(n, \beta) \bar{\eta}_j(n) \quad (2.20b)$$

$$K_{qi}^{xz} = \sum_{n=-\infty}^{\infty} \bar{\eta}_q(n) \bar{Z}_{xz}(n, \beta) \bar{\xi}_i(n) \quad (2.20c)$$

$$K_{qj}^{xx} = \sum_{n=-\infty}^{\infty} \bar{\eta}_q(n) \bar{Z}_{xx}(n, \beta) \bar{\eta}_j(n) \quad (2.20d)$$

A solution to this equation exists if and only if the determinant of the coefficient matrix is equal to zero. Thus,

$$0 = f(\beta) = \begin{vmatrix} K^{zz} & K^{zx} \\ K^{xz} & K^{xx} \end{vmatrix} \quad (2.21)$$

where, for example, K^{zz} is the matrix of coefficients given in Equation 2.20a. We may now find the zeros of $f(\beta)$ with a zero-finding algorithm such as Newton's method, thus completing the solution for β .

2.4 Basis Functions

One of the most important aspects of the spectral Galerkin procedure involves the choice of basis functions. A good set of basis functions can greatly increase the efficiency of the solution, as well as its accuracy.

The basis functions should satisfy three conditions. First, they must be analytically Fourier transformable, since they are used in the transform domain in Equation 2.16. Second, they should have a shape that is similar to that for the current we expect to find on the strip. Having this property will reduce the size of the matrix equation. Finally, they should have the properties that $J_z(x)$ has a $1/\sqrt{x}$ singularity at the strip edges and that $J_x(x)$ is zero at the strip edges. This is the result expected for the current parallel and perpendicular to a knife edge. By not satisfying this last condition, more basis functions will be required to represent the currents, resulting again in an increased matrix size.

One appropriate choice of basis functions for modes that are even in $J_z(x)$ is suggested in [15] as

$$\xi_i(x) = \frac{\cos \{ (i-1) \pi (x/s + 1) \}}{\sqrt{1 - (x/s)^2}} \quad (2.22a)$$

$$\eta_i(x) = \frac{\sin [i \pi (x/s + 1)]}{\sqrt{1 - (x/s)^2}} \quad (2.22b)$$

These functions satisfy all the above criteria. In particular, note that $\xi_i(x)$ has a $1/x$ singularity at $x = \pm s$ and that $\eta_i(x = \pm s) = 0$, which can be shown by l'Hopital's rule. The first few functions are shown in Figures 2.4 and 2.5. The Fourier transforms of these functions are

$$\tilde{\xi}_i(n) = \frac{(-1)^{i-1} s \pi}{2} [J_0(\alpha_n s + (i-1)\pi) + J_0(\alpha_n s - (i-1)\pi)] \quad (2.23a)$$

$$\tilde{\eta}_i(n) = \frac{(-1)^i s \pi}{2j} [J_0(\alpha_n s + i\pi) - J_0(\alpha_n s - i\pi)] \quad (2.23b)$$

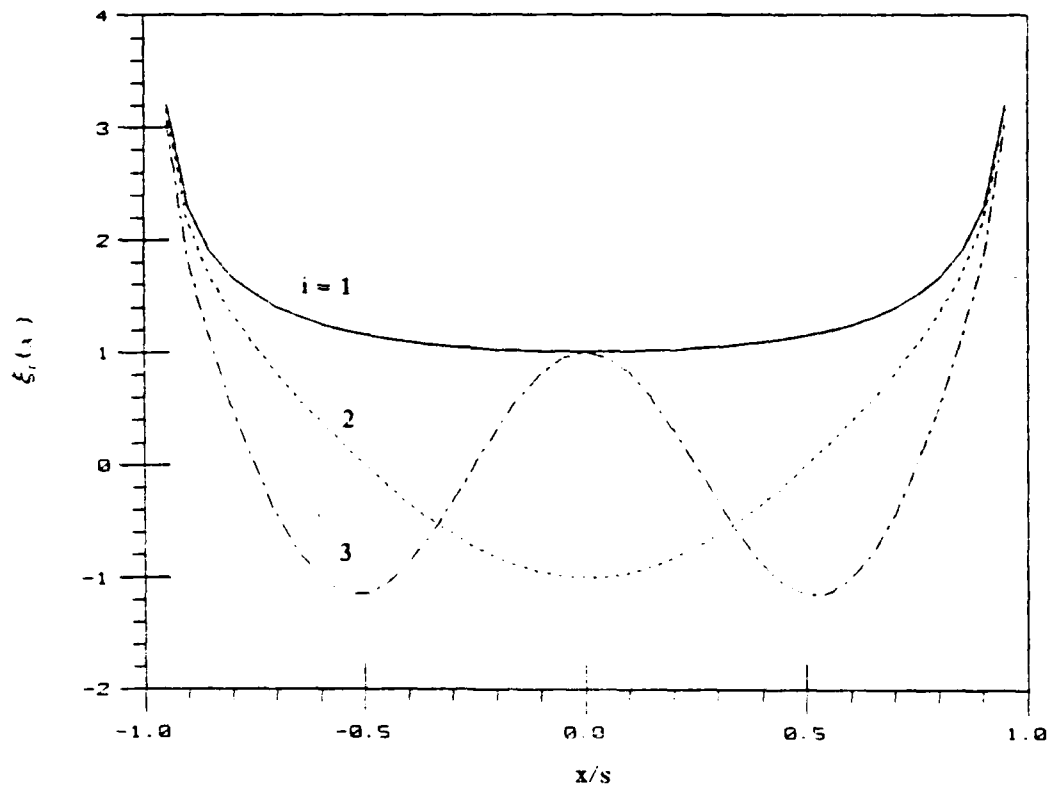


Figure 2.4. Basis functions for $J_2(x)$

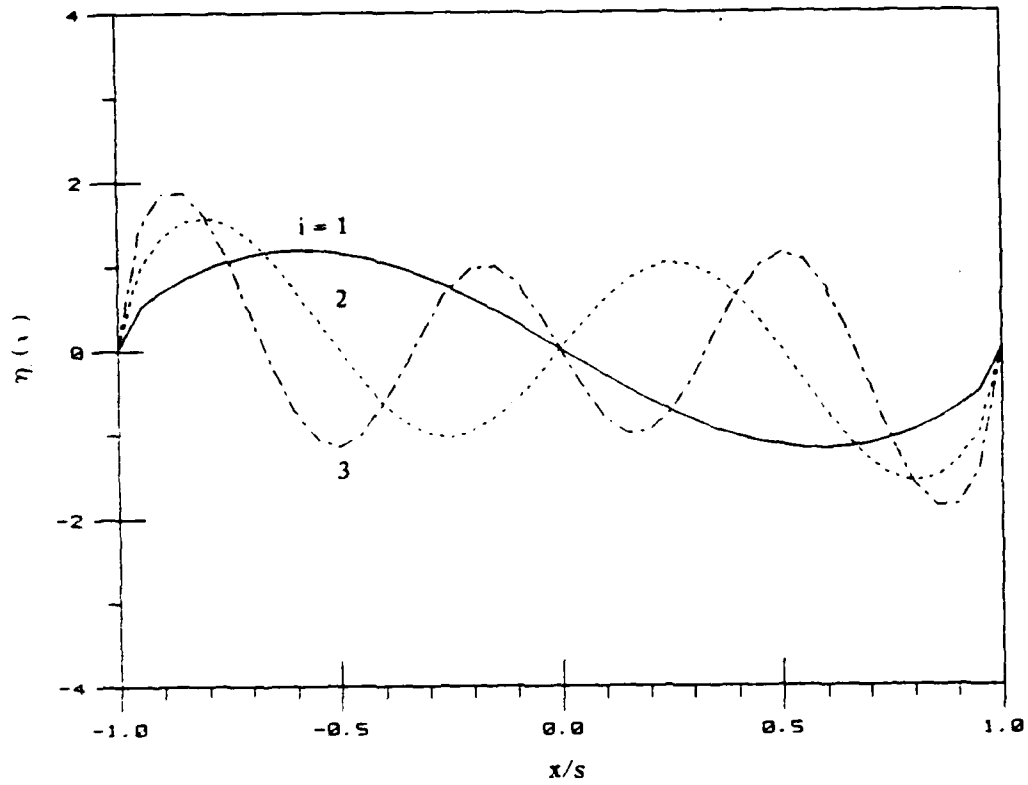


Figure 2.5. Basis functions for $J_1(x)$

where $j = \sqrt{-1}$ and $J_0(x)$ is the zeroth order Bessel function. A formula that is useful in deriving the above transforms comes from the Bateman Manuscripts [19]. Hence,

$$\int_{-\infty}^{\infty} \frac{T_n(x) e^{-jxy}}{\sqrt{1-x^2}} dx = (-1)^n i^n \pi J_n(y) \quad (2.24)$$

where $T_n(x)$ is the n th order Chebychev polynomial in the interval $|x| < 1$ and zero elsewhere, and $T_0(x) = 1$.

2.5 Characteristic Impedance

The characteristic impedance of a microstrip is a useful parameter to calculate for several reasons. It serves not only as a useful design tool, but also as a check on the accuracy of the dominant mode propagation constant. In addition, the inner product we use in the mode matching procedure uses an inner product that is very similar to characteristic impedance. Hence, it will be useful to compare our calculated values of characteristic impedance to previous calculations [11,12].

At this point, mention should be made of the ambiguity inherent in this characteristic impedance calculation. The characteristic impedance of a transmission line is usually thought to be a characteristic of TEM transmission lines. The dominant mode of the microstrip is only quasi-TEM, however, so there are several definitions of characteristic impedance in this case that make sense and yield similar, but unequal results. A number of authors have discussed the relative merits of the various definitions [20-23]. These definitions include

$$Z_0 = \frac{2P}{II'} \quad (2.25)$$

$$Z_0 = \frac{V}{I} \quad (2.26)$$

and

$$Z_0 = \frac{VV^*}{2P} \quad (2.27)$$

where

$$P = \frac{1}{2} \operatorname{Re} \int_{-a}^{a} \int_{-b}^b \vec{E} \times \vec{H}^* \cdot \hat{z} \, dx \, dy \quad (2.28)$$

$$I = \int_{-a}^a J_z(x) \, dx \quad (2.29)$$

$$V = - \int_{-a}^a E_y(x=0,y) \, dy \quad (2.30)$$

These are the so-called power-current, voltage-current, and power-voltage definitions. It turns out that the definition most widely accepted is the power-current definition, and that is what we calculate here. For comparison, we also calculate the characteristic impedance with the voltage-current definition. Thus, we need to calculate P , I , and V .

First, let us calculate I and V . Proceeding from Equations 2.29 and 2.30, it is straightforward to show that

$$I = \sum_{i=1}^N c_i \tilde{\xi}_i(n=0) \quad (2.31)$$

$$V = \frac{-1}{2b} \sum_{n=-\infty}^{\infty} \int_{-a}^a \tilde{E}_y(n,y) \, dy \quad (2.32)$$

Next, we proceed to the power calculation. Beginning with Equation 2.28, and subsequently using Parseval's theorem [24], we obtain

$$P = \frac{1}{4b} \sum_{n=-\infty}^{\infty} f(n) \quad (2.33)$$

where

$$f(n) = \int_{-a}^a (\tilde{E}_x \tilde{H}_y^* - \tilde{E}_y \tilde{H}_x^*) \, dy \quad (2.34)$$

The task now becomes one of finding expressions for the field components in the transform domain. In order to find these, we first need to solve the transmission line problem shown previously in Figure 2.3. The solution is straightforward, and can be adapted from a number of standard textbooks, for example, Mayes [25]. This results in the following set of equations

$$\tilde{H}_w(n, y) = A_i^{TE}(n) X_i^C(y) \quad (2.35a)$$

$$\tilde{E}_w(n, y) = -A_i^{TE}(n) X_i^S(y) \quad (2.35b)$$

$$\tilde{H}_w(n, y) = A_i^{TM}(n) X_i^S(y) \quad (2.35c)$$

$$\tilde{E}_w(n, y) = A_i^{TM}(n) X_i^C(y) \quad (2.35d)$$

where

$$X_i^C = \begin{cases} \frac{\cosh \gamma_1(y - (h - t))}{\sinh \gamma_1(h - t)} & i = 1 \\ \frac{\cosh \gamma_2(y + t)}{\sinh \gamma_2 t} & i = 2 \end{cases} \quad (2.36a)$$

$$X_i^S = \begin{cases} \frac{\sinh \gamma_1(y - (h - t))}{\sinh \gamma_1(h - t)} & i = 1 \\ \frac{\sinh \gamma_2(y + t)}{\sinh \gamma_2 t} & i = 2 \end{cases} \quad (2.36b)$$

and

$$\frac{A_2^{TE}}{A_1^{TE}} = \frac{-Z_1^{TE} \sinh \gamma_1(h - t)}{Z_2^{TE} \sinh \gamma_2 t} \quad (2.37a)$$

$$\frac{A_2^{TM}}{A_1^{TM}} = \frac{-Z_1^{TM} \sinh \gamma_1(h - t)}{Z_2^{TM} \sinh \gamma_2 t} \quad (2.37b)$$

$$A_1^{TE} = \frac{-\tilde{J}_u(n)}{\coth \gamma_1(h-t) - \left| \frac{A_2^{TE}}{A_1^{TE}} \right| \coth \gamma_2 t} \quad (2.37c)$$

$$A_1^{TM} = \frac{\tilde{J}_v(n)}{\coth \gamma_1(h-t) - \left| \frac{A_2^{TM}}{A_1^{TM}} \right| \coth \gamma_2 t} \quad (2.37d)$$

The signs of the current terms in the above equations are determined by the boundary condition [26]

$$\hat{y} \times (\bar{H}_1 - \bar{H}_2) = \bar{J}, \quad (2.38)$$

where \bar{H}_1 and \bar{H}_2 are the H-fields just above and below the strip. In the spectral domain this condition is

$$\tilde{H}_{1u} - \tilde{H}_{2u} = \tilde{J}_v, \quad (2.39a)$$

$$\tilde{H}_{1v} - \tilde{H}_{2v} = -\tilde{J}_u \quad (2.39b)$$

This completes the derivation of the fields in the decoupled u,v coordinates.

In order to express the fields in x,y,z coordinates, we need to invoke the coordinate transformation given previously in Equation 2.7 and then combine the TE and TM parts of the fields. This results in the following set of equations:

$$\tilde{E}_{xi}(n,y) = \left[N_z A_i^{TE} Z_i^{TE} + N_x A_i^{TM} Z_i^{TM} \right] X_i^S \quad (2.40a)$$

$$\tilde{E}_{yi}(n,y) = \frac{\sqrt{\alpha_n^2 + \beta^2}}{\omega \epsilon_1} A_i^{TM} X_i^C \quad (2.40b)$$

$$\tilde{E}_{zi}(n,y) = \left[-N_x A_i^{TE} Z_i^{TE} + N_z A_i^{TM} Z_i^{TM} \right] X_i^S \quad (2.40c)$$

$$\tilde{H}_{xi}(n,y) = \left[N_x A_i^{TE} - N_z A_i^{TM} \right] X_i^C \quad (2.40d)$$

$$\tilde{H}_{yi}(n, y) = \frac{\sqrt{\alpha_n^2 + \beta^2}}{\omega\mu_0} A_i^{TE} Z_i^{TE} X_i^S \quad (2.40e)$$

$$\tilde{H}_{zi}(n, y) = \left(N_z A_i^{TE} + N_x A_i^{TM} \right) X_i^C \quad (2.40f)$$

The y dependence is contained in X_i^C and X_i^S . These fields can now be substituted into Equation 2.7 to calculate $f(n)$. In order to carry out the integration of $f(n)$, we need only integrate over the products of hyperbolic cosines and sines, which can be carried out analytically. This concludes the power calculations and, hence, the characteristic impedance calculation.

2.6 Fin Line Calculations

Although it is very easy to verify the dominant mode microstrip calculations, very little data exist for the evanescent modes. We would, however, like to have a comparison for our calculated evanescent modes. It turns out that fin line evanescent modes have been calculated. In order to verify our evanescent modes, therefore, the best we can do is to alter our program to calculate fin line evanescent modes, and compare these to those in the literature [17]. A diagram of fin line is shown in Figure 2.6.

In order to adapt the spectral domain immittance approach to the fin line, we need to use a different matrix equation. This is of the form

$$\begin{bmatrix} \tilde{Y}_{xx} & \tilde{Y}_{xz} \\ \tilde{Y}_{zx} & \tilde{Y}_{zz} \end{bmatrix} \begin{bmatrix} \tilde{E}_x \\ \tilde{E}_z \end{bmatrix} = \begin{bmatrix} \tilde{J}_x \\ \tilde{J}_z \end{bmatrix} \quad (2.41)$$

where \tilde{E}_x and \tilde{E}_z in the fin line are analogous to \tilde{J}_z and \tilde{J}_x in the microstrip, respectively. In order to find the admittances, we must set up transmission lines analogous to those in Figure 2.3. These are shown in Figure 2.7. From these transmission lines we obtain the dyadic admittance matrix

$$\tilde{Y}_{xx} = N_x^2 \tilde{Y}^e + N_z^2 \tilde{Y}^h \quad (2.42a)$$

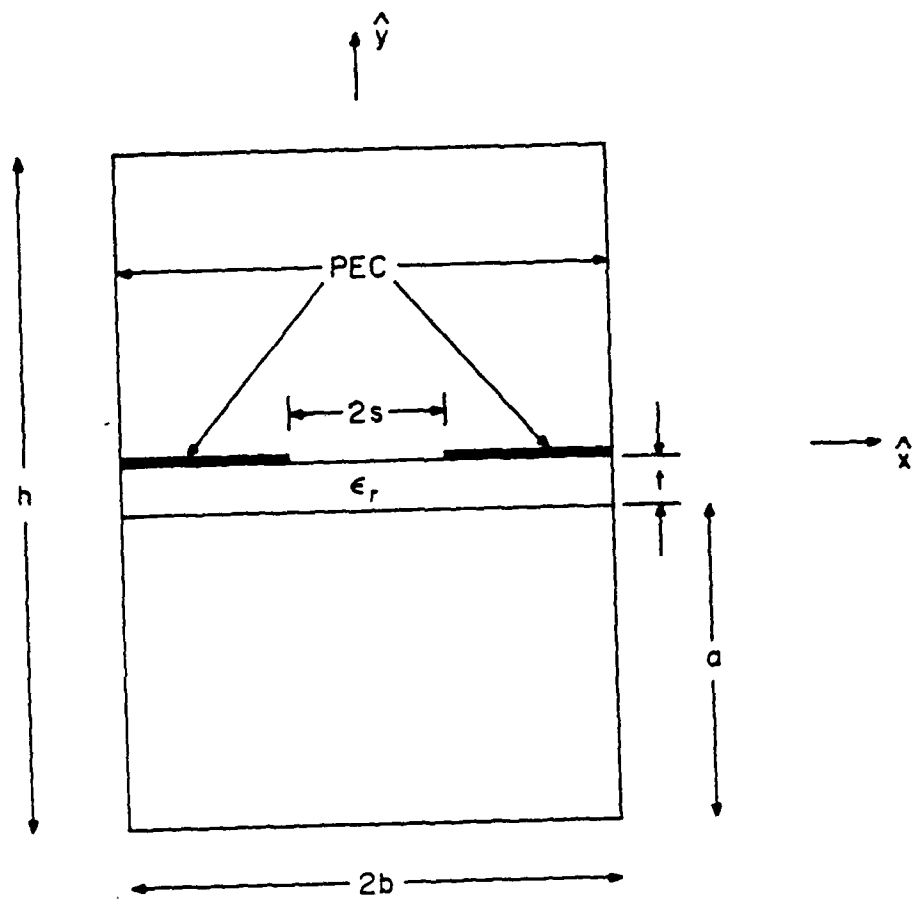


Figure 2.6. Dimensions for a fin line.

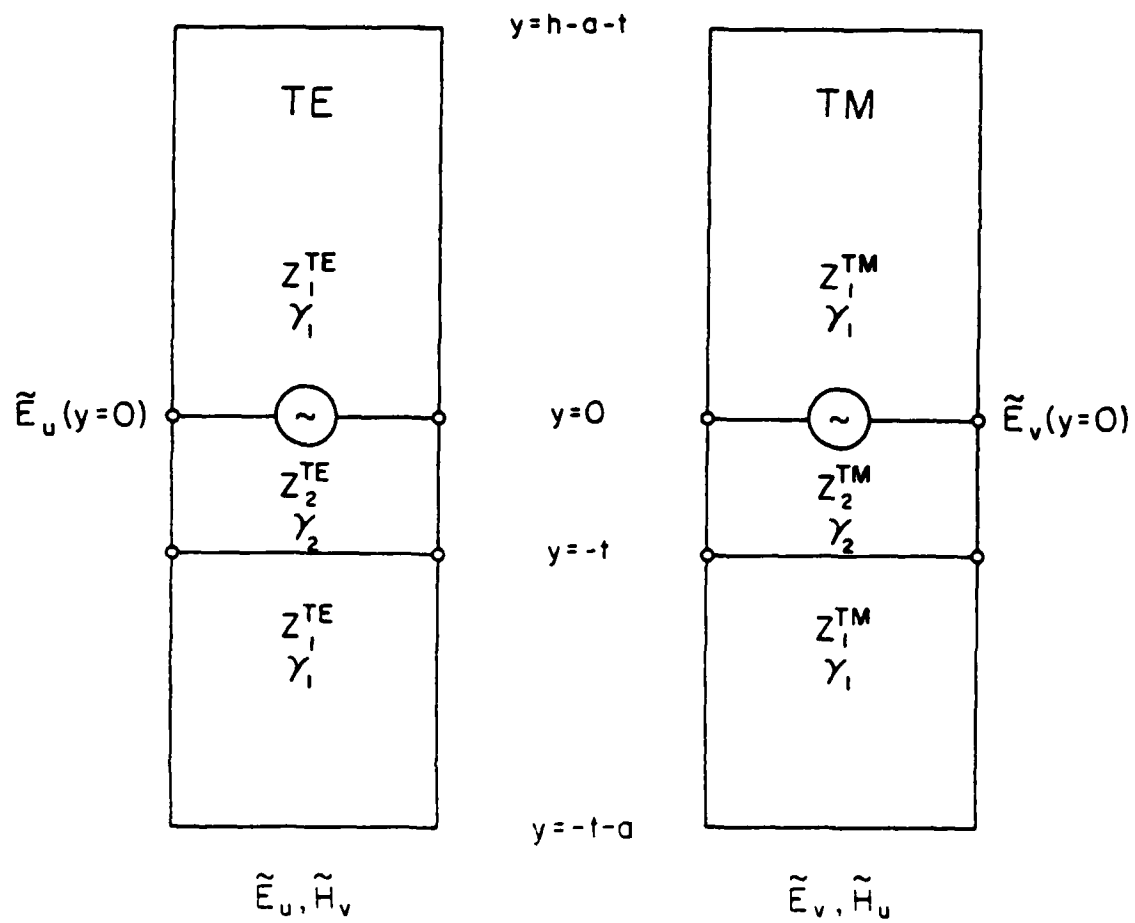


Figure 2.7. Equivalent transmission lines for the TE and TM components of fin-line fields in the transform domain.

$$\tilde{Y}_{zx} = \tilde{Y}_{xz} = N_x N_z \left[-\tilde{Y}^e + \tilde{Y}^h \right] \quad (2.42b)$$

$$\tilde{Y}_{zz} = N_z^2 \tilde{Y}^e + N_x^2 \tilde{Y}^h \quad (2.42c)$$

where

$$\begin{aligned} \tilde{Y}^e &= \frac{1}{Z_1^{TM} \tanh \gamma_1 (h-a-t)} \\ &+ \frac{1}{Z_2^{TM}} \frac{Z_2^{TM} + Z_1^{TM} \tanh \gamma_1 a \tanh \gamma_2 t}{Z_1^{TM} \tanh \gamma_1 a + Z_2^{TM} \tanh \gamma_2 t} \end{aligned} \quad (2.43a)$$

$$\begin{aligned} \tilde{Y}^h &= \frac{1}{Z_1^{TE} \tanh \gamma_1 (h-a-t)} \\ &+ \frac{1}{Z_2^{TE}} \frac{Z_2^{TE} + Z_1^{TE} \tanh \gamma_1 a \tanh \gamma_2 t}{Z_1^{TE} \tanh \gamma_1 a + Z_2^{TE} \tanh \gamma_2 t} \end{aligned} \quad (2.43b)$$

The matrix equation is now solved in a manner very similar to the microstrip matrix equation. We expand \tilde{E}_x and \tilde{E}_z in the same basis functions used previously for \tilde{J}_z and \tilde{J}_x , respectively. These basis functions were given in Equation 2.22.

Finally, we must reconsider the definition of the Fourier transform before we solve the fin line problem. In the transform used previously in Equation 2.3, we used $\alpha_n = (n - 1/2)\pi/b$. This value of α_n , however, is no longer valid for the even (in E_x) modes of the fin line we are calculating, which include the dominant mode. The correct choice is now $\alpha_n = n\pi/b$. This choice enforces the boundary conditions of the zero tangential \vec{E} -field and normal \vec{H} -field at $|x| = b$. If we were interested in the odd modes of the fin line, the first definition of α_n , $\alpha_n = (n - 1/2)\pi/b$ would be correct.

In general, we pick $\alpha_n = n\pi/b$ when $\phi(x)$ is even and $\psi(x)$ is odd, where $\phi(x)$ and $\psi(x)$ were defined previously in Equation 2.2. This occurs for even (in J_z) microstrip modes and in odd (in E_x) fin line modes. Furthermore, we pick $\alpha_n = (n - 1/2)\pi/b$ when $\phi(x)$ is odd in $\psi(x)$ is even. This occurs in odd (in J_z) microstrip modes and in even (in E_x) fin line modes.

2.7 Field Configurations

It is of great interest to plot the fields due to the dominant and higher-order modes over the cross section of the waveguide. This provides verification that the boundary conditions have been satisfied and offers physical insight into the structure of the modes. The field configurations may be obtained from the transformed fields obtained in the characteristic impedance calculation, by performing the inverse Fourier transform of Equations 2.35. Results are presented in the next section.

2.8 Results for Uniform Microstrip and Fin Line

In this section we present numerical results for the techniques discussed previously in this chapter. The first item we consider is the convergence of the dominant mode propagation constant with respect to the number of basis functions and number of spectral terms used. In Table 2.1 we show these calculations and compare our results to those of Mittra and Itoh [5]. From this table we can make a number of observations. First, our values of β are in very good agreement with those of Mittra and Itoh. Second, our values of β have converged sufficiently with two basis functions and 50 spectral terms. Note that "2 basis functions" indicates two functions for J_z and two for J_x . Note furthermore that 50 spectral terms indicates that all series were summed from $n = -49$ to 50.

Next, we present a sample dispersion curve for a shielded microstrip. This is shown in Figure 2.8. Note that the dominant mode is not cut off, while the first higher-order mode is cut off below about 20 GHz.

Next, we present data on the characteristic impedance of a shielded microstrip. This is shown in Figure 2.9. The impedance has been calculated using both the V-I and the V-I definitions, as discussed in Section 2.5, and the results are compared to those of El-Sherbiny [11]. Note that in El-Sherbiny's paper, the impedance was calculated for a shielded microstrip without side walls. In order to account for this, we chose in our calculations to move the side walls far enough from the strip to eliminate their effect. Our results for the

Table 2.1 Convergence of β with respect to the number of basis functions and number of spectral terms. For these calculations, $h = 2$ mm, $b = 1.75$ mm, $t = s = 0.5$ mm, and $\epsilon_r = 9.0$. These results are compared to those of Mittra and Itoh [5].

Number of		$\beta(\text{rad/m})$ at		
Basis Functions	Spectral Terms	10 GHz	20 GHz	30 GHz
1	25	530.64	1110.0	1717.7
1	50	530.50	1109.6	1717.1
2	50	530.27	1108.9	1715.6
2	100	530.17	1108.7	1715.1
3	250	530.11	1108.5	1714.9
Mittra & Itoh [5]		531	1115	1740

V-I definition of a microstrip agree very well with those of El-Sherbiny. Although he does not in his paper specifically identify which definition of characteristic impedance he is using, we may very well guess that it is the V-I definition.

Next, we would like to find modes in a fin line. This is done, as explained earlier, as a check on the microstrip mode calculations. Results for the first three higher-order modes are shown in Figure 2.10, and are compared to those of Helard et al. [17]. From this figure, it is readily apparent that there is excellent agreement between the fin line modes. This leads us to have a high degree of confidence in our microstrip evanescent modes.

Finally, we present field plots for the first five modes of a microstrip. Since a given field component is either purely real or purely imaginary, we have plotted the part of the field that is nonzero. In Figures 2.10-2.13, we have plotted the six components of the dominant mode of a shielded microstrip. Note that these plots satisfy the boundary conditions that E-fields tangential to a conductor and H-fields normal to a conductor are zero. Note also the correct singularity behavior at the edges of the strip. In Figures 2.14-2.17, we have plotted $E_x(x,y)$ and $E_y(x,y)$ for the next four higher-order modes of the same configuration. These are evanescent modes for the dimensions and frequency given. Again, we note that the correct boundary conditions and singularities are observed.

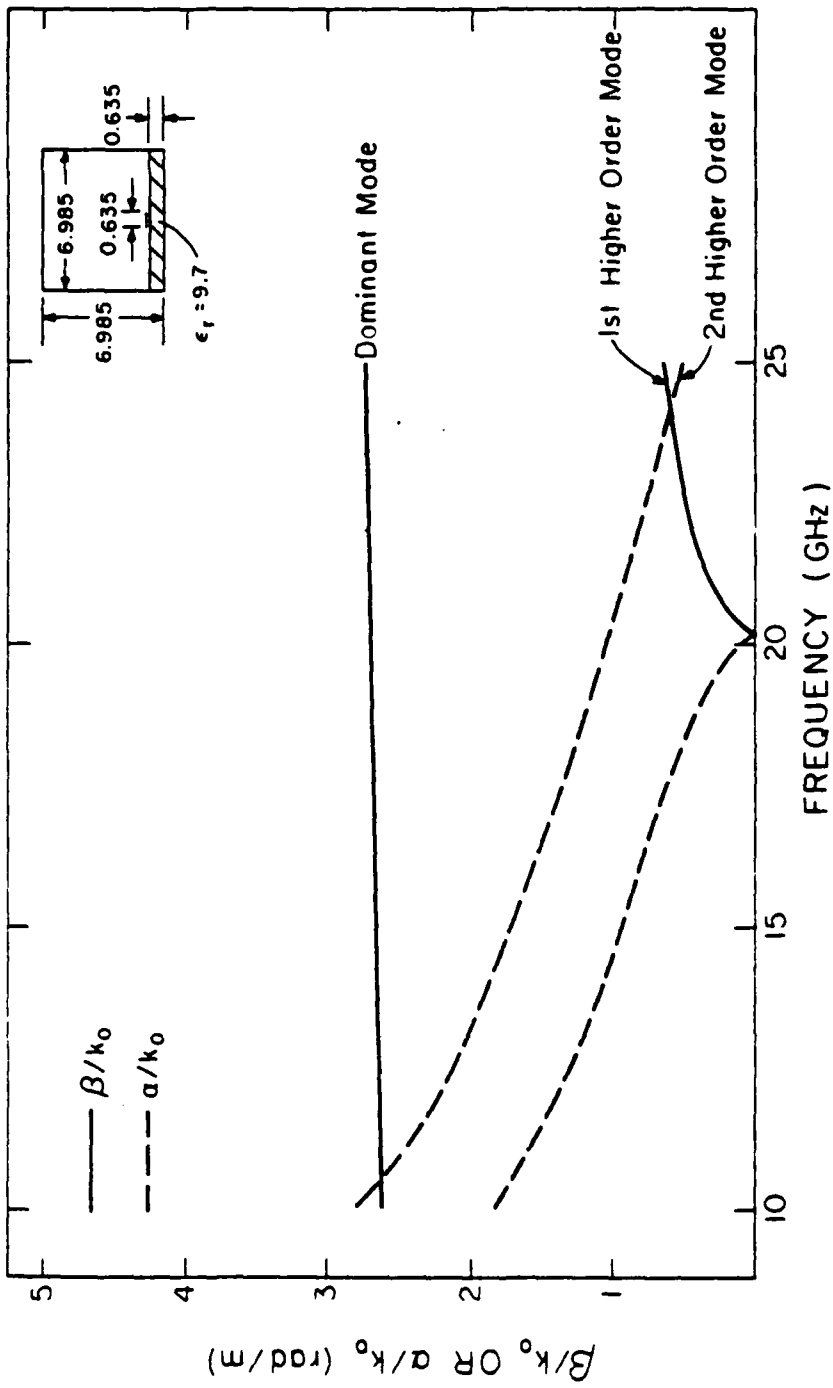


Figure 2.8. The dispersion characteristics of the dominant and first two even higher-order modes of a microstrip. Two basis functions and 100 spectral terms were used.

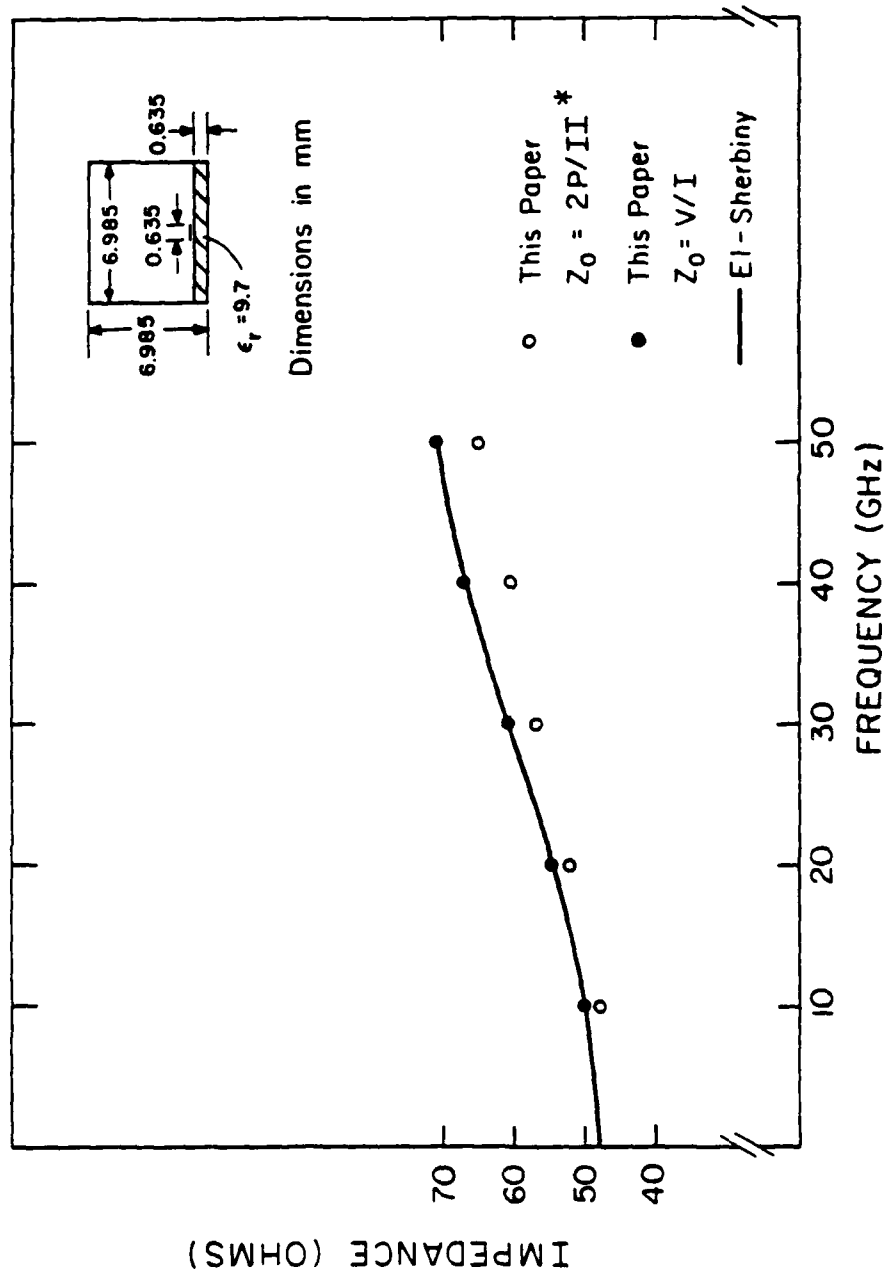


Figure 2.9. The characteristic impedance of a microstrip, calculated with two definitions. (One basis function and .50 spectral terms were used.)

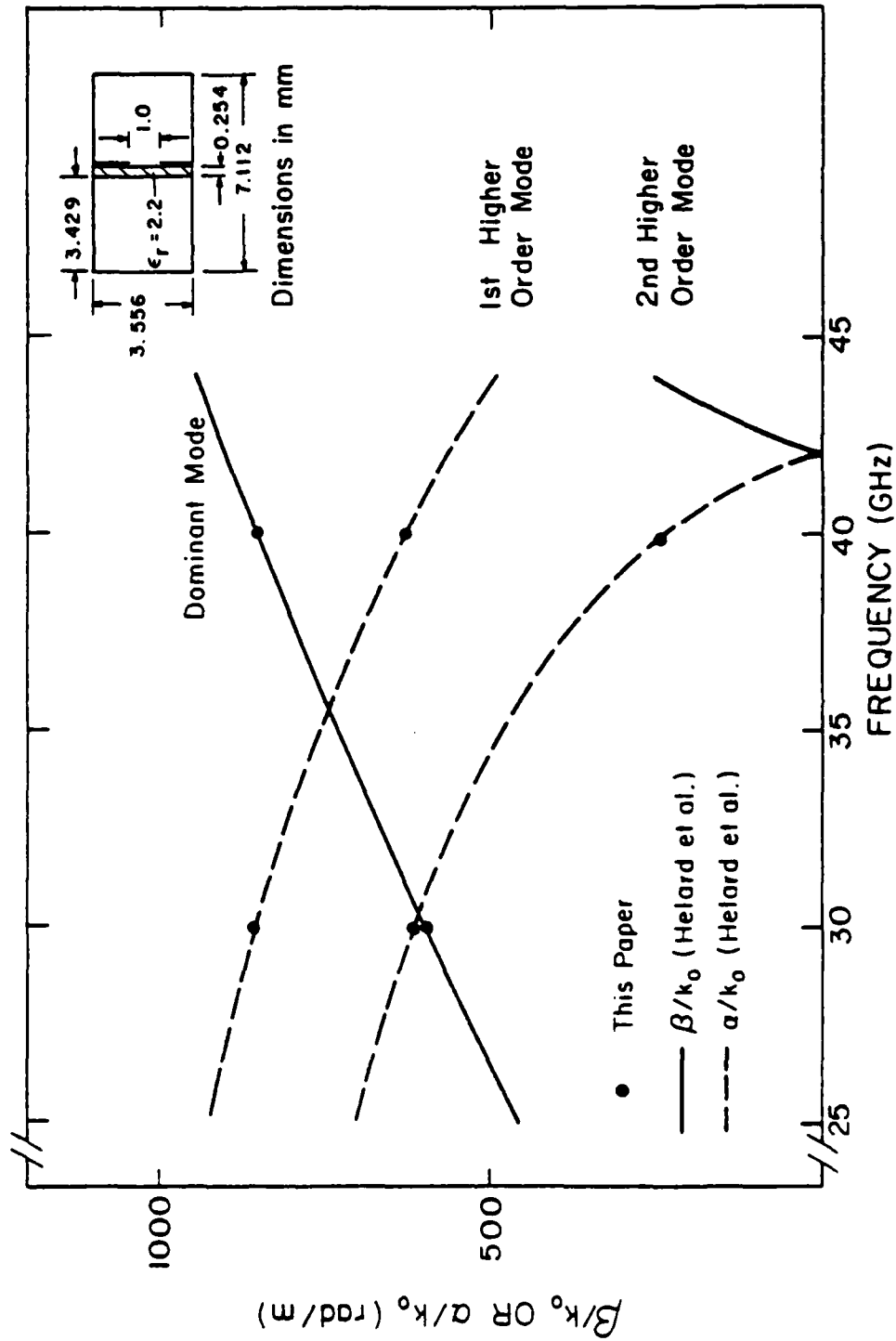


Figure 2.10. Dispersion curve of a fin line. One basis function and 50 spectral terms were used. A comparison is made to the results of Helard et al. [17].

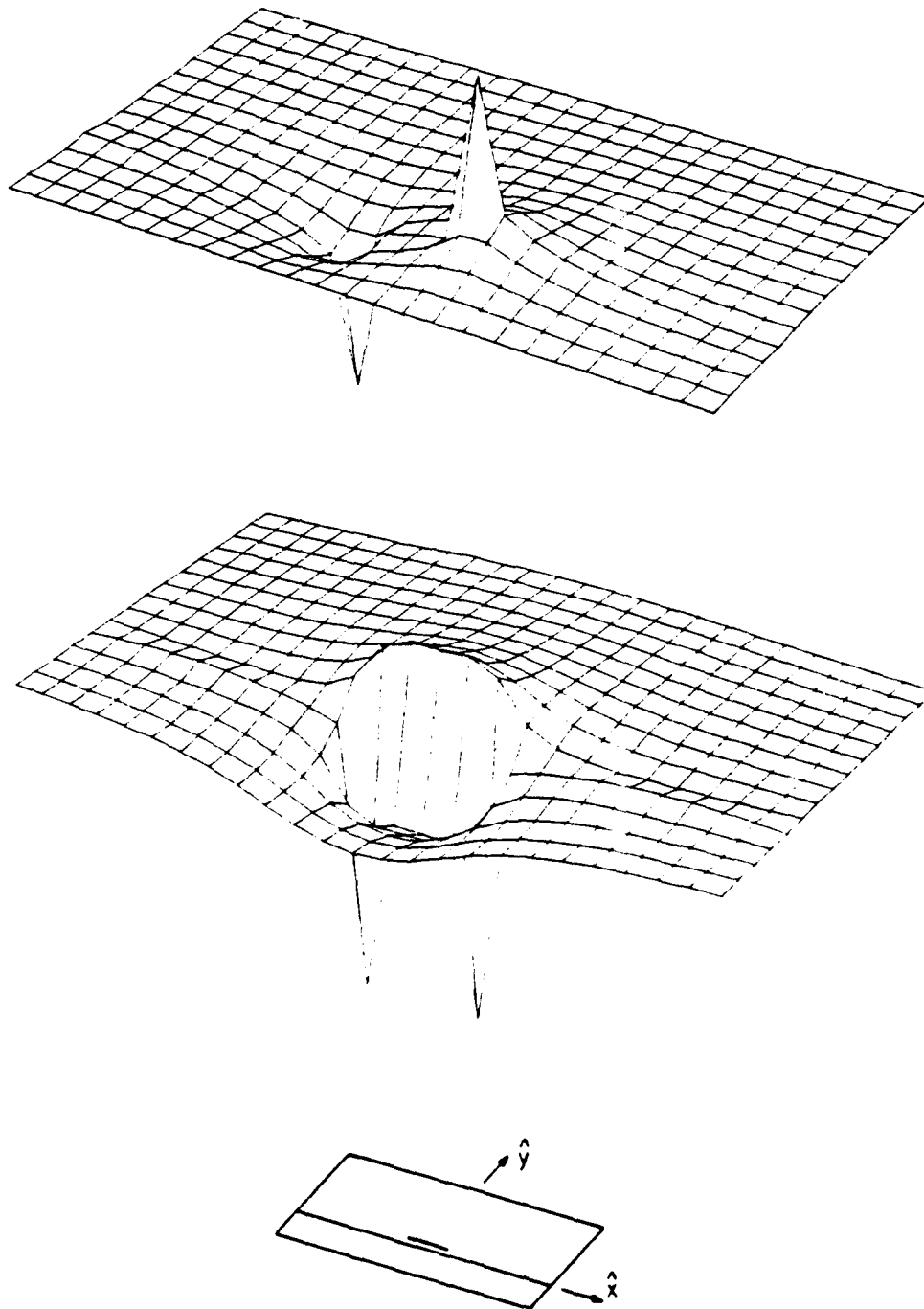


Figure 2.11. Plots of $E_x(x,y)$ and $E_y(x,y)$ for the dominant mode of a microstrip. For this plot, $h = 0.4445$ mm, $b = 0.381$ mm, $t = 0.127$ mm, $s = 0.0635$ mm, $\epsilon_r = 9.6$ mm, freq = 20 GHz, and $\beta = 1037.01$ rad/m.

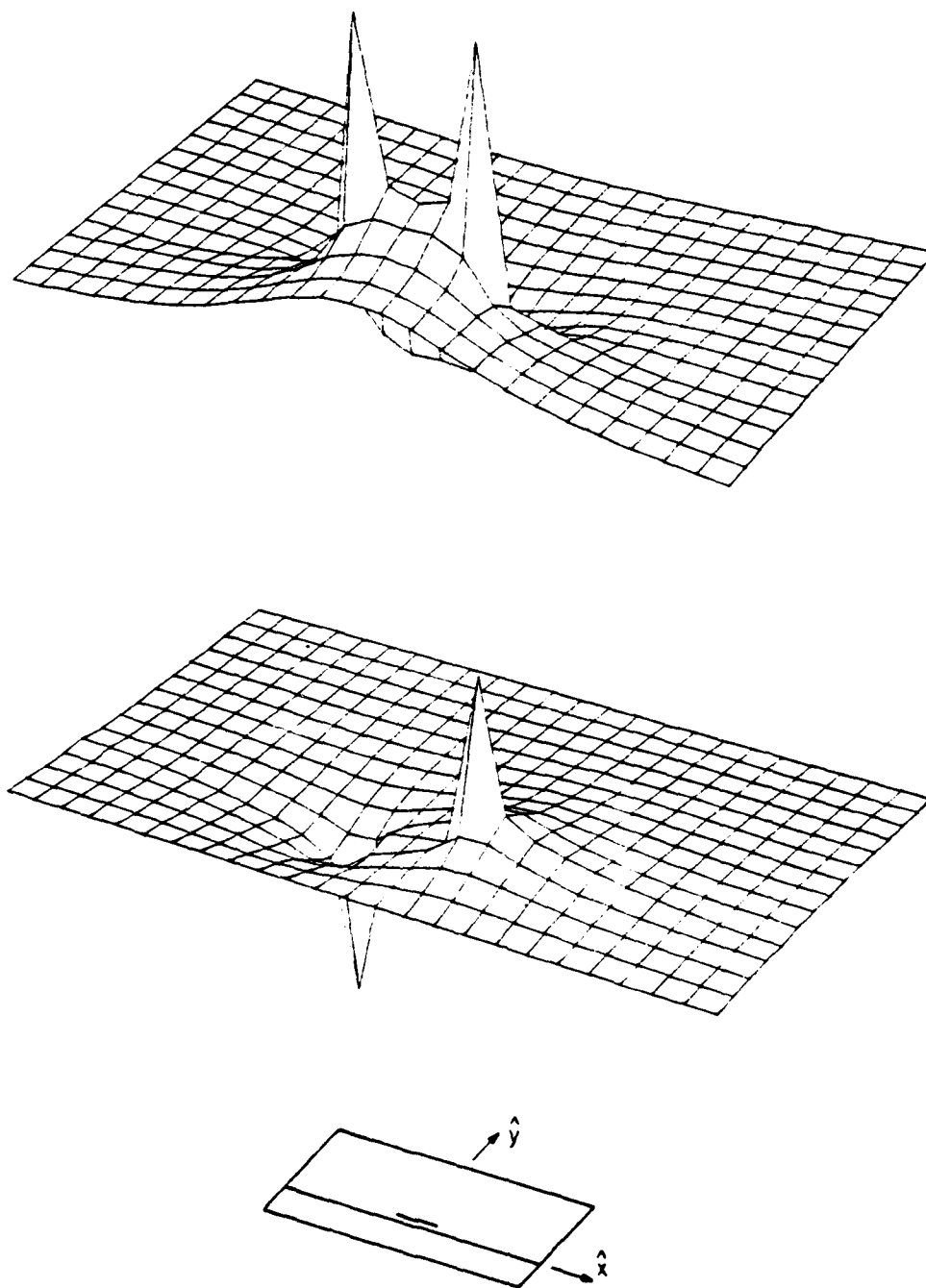


Figure 2.12. H_1 and H_2 of the dominant mode for the same configuration as that in Figure 2.11

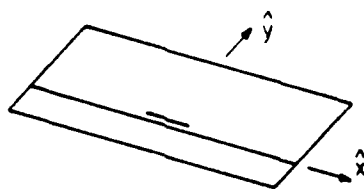
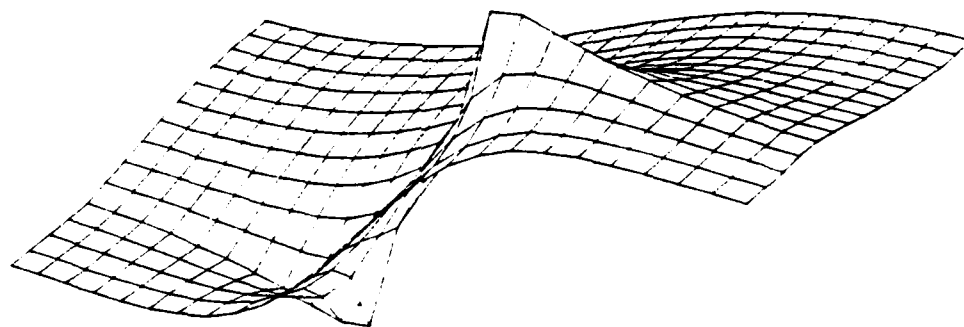
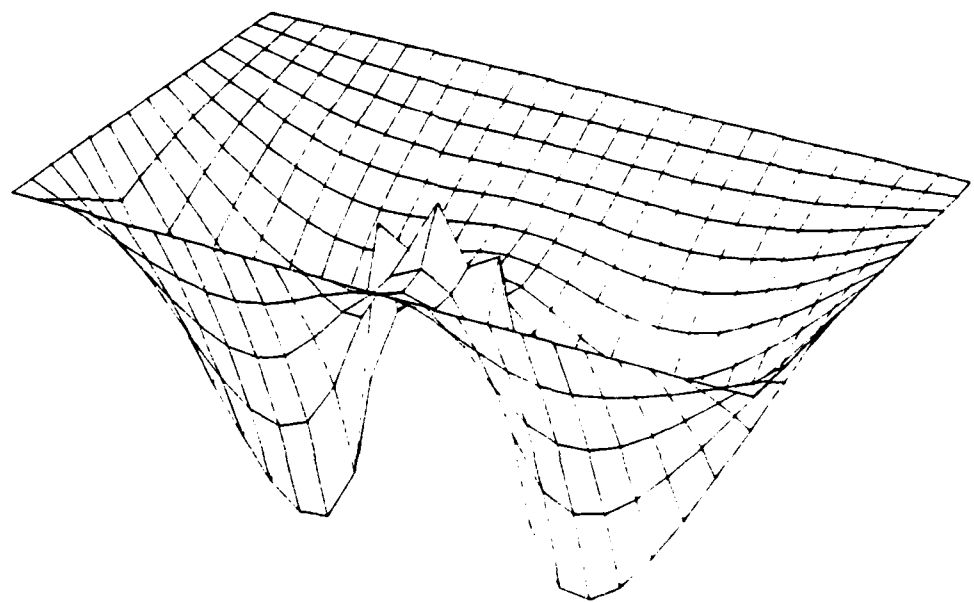


Figure 2.13. E and H of the dominant mode for the same configuration as that in Figure 2.11.

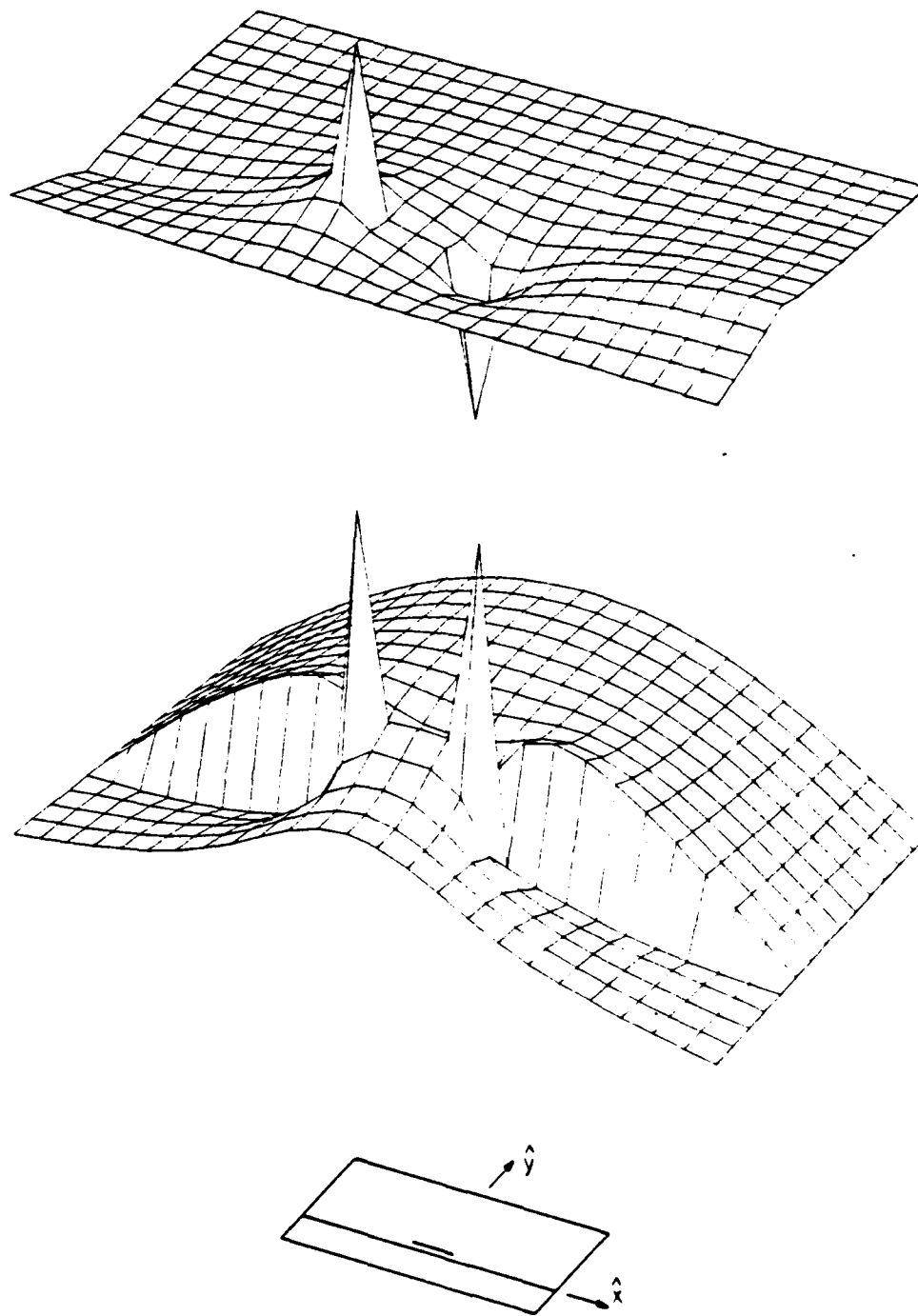


Figure 2.14 E_x and E_y of the second mode for the same configuration as that in Figure 2.9
For this mode, $\beta = -j4068.72$ rad/m.

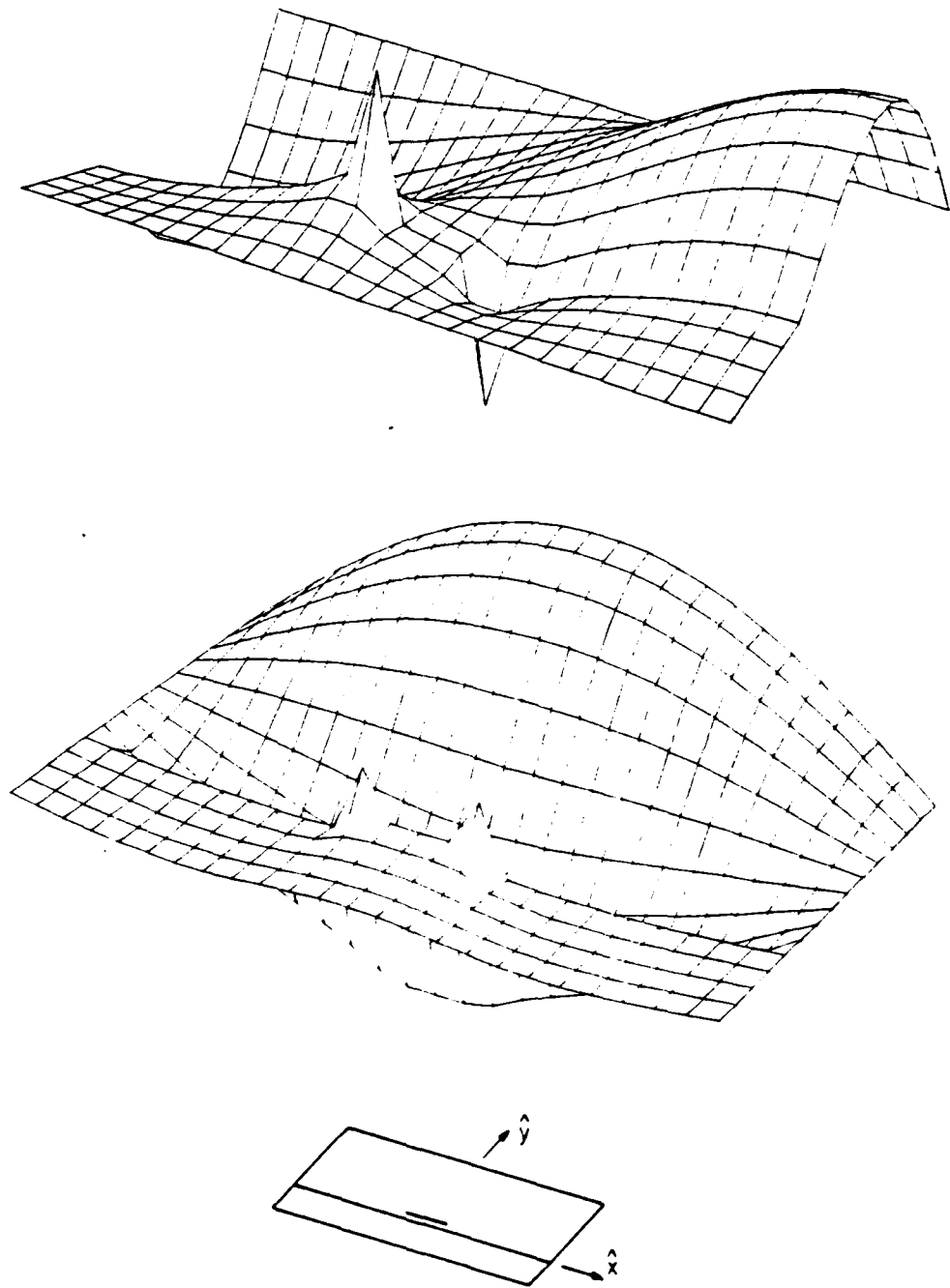


Figure 2.15. E_x and E_y of the third mode for the same configuration as that in Figure 2.9.
For this mode, $\beta = -j10478.5$ rad/m.

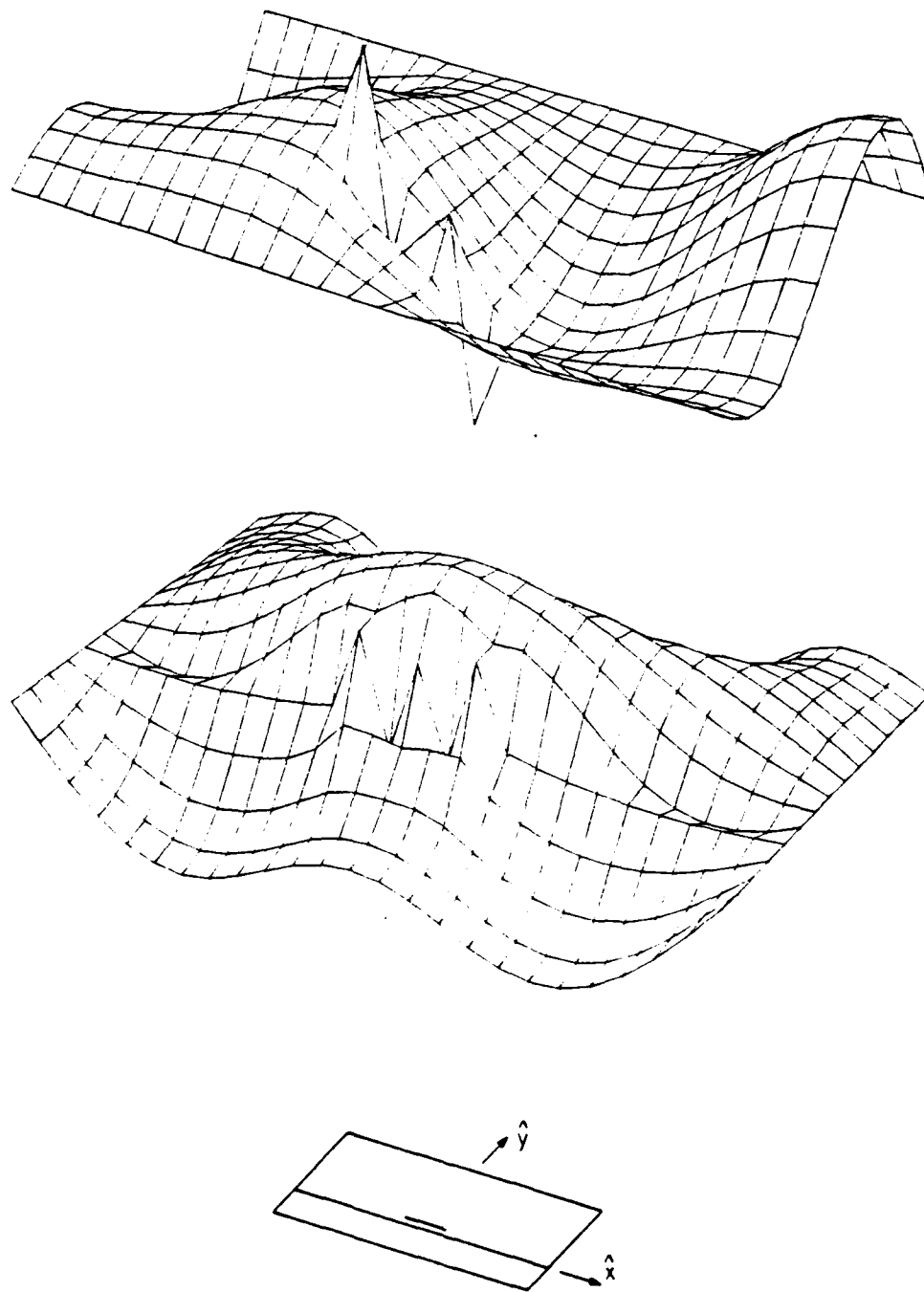


Figure 2.16. E_x and E_y of the fourth mode for the same configuration as that in Figure 2.9.
For this mode, $\beta = -j14694.4$ rad/m

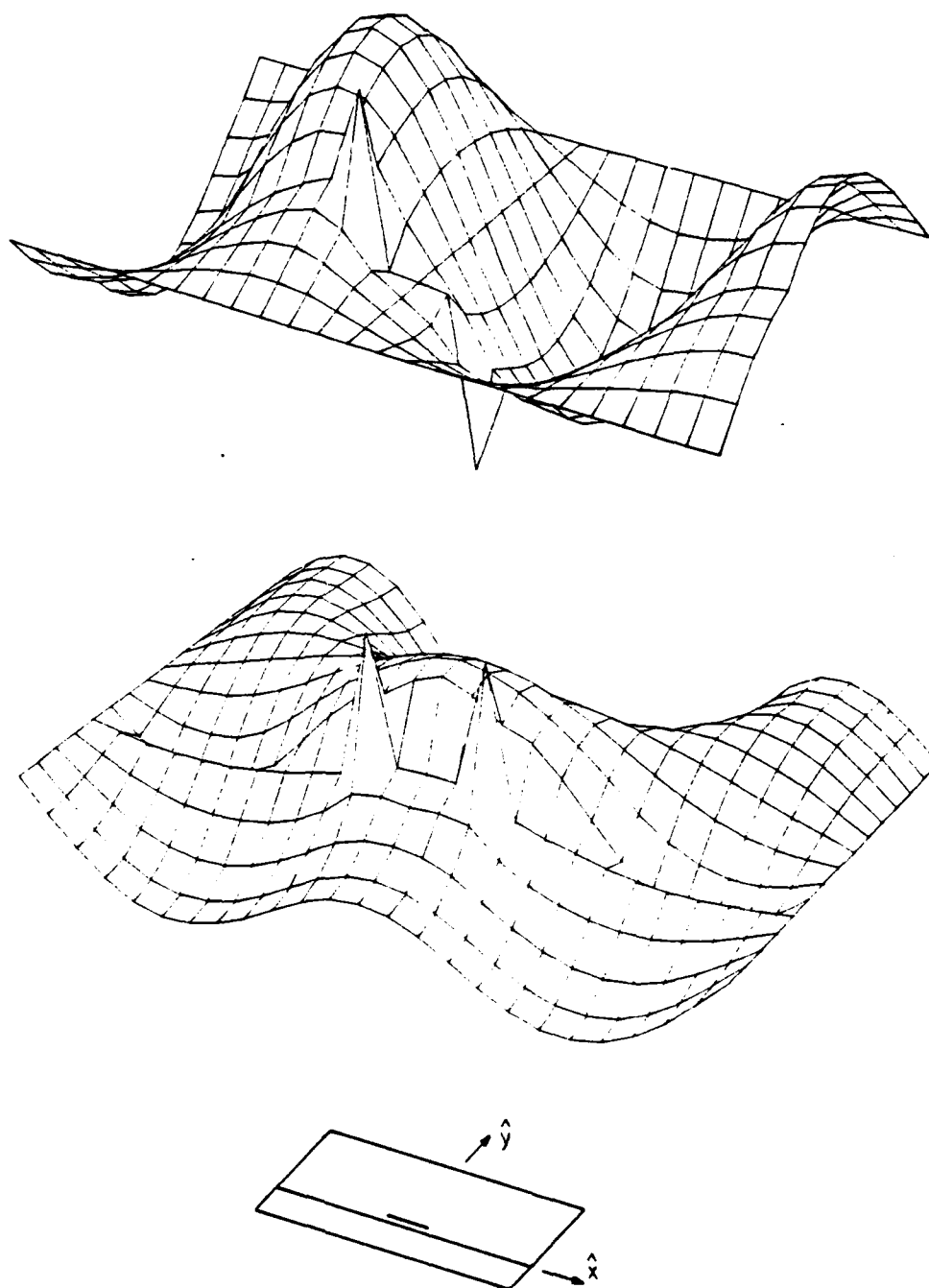


Figure 2.17 E_x and E_y of the fifth mode for the same configuration as that in Figure 2.9
For this mode, $\beta = -j14897.1$ rad/m

2.9 Conclusion

In this section we have demonstrated the capability of calculating microstrip propagating and evanescent modes. This extends the work of previous authors, as very few results for evanescent modes were previously available. In addition, we have generated data on characteristic impedance and fin-line modes, all of which confirm the accuracy of our calculations. Finally, field configurations of microstrip modes have been generated, and these have been shown to satisfy the necessary boundary conditions.

All of the above suggest a basic agreement of the mode calculations with the expected results. The next step is to use these results in a mode matching procedure for calculating discontinuities.

Let us now proceed to the discontinuity calculations.

CHAPTER 3

DISCONTINUITY CALCULATIONS

3.1 Introduction

The calculation of discontinuities associated with printed circuits has been of interest for some time. In particular, abrupt discontinuities in the widths of the strips in the microstrip and in the slots in the fin line seem to offer the best hope for solution, and have been studied by a number of authors.

The earliest attempts at solving one of these types of discontinuities occurred in the realm of microstrip discontinuities. The methods used involved a quasistatic calculation of a step discontinuity of strip width [27-30]. Although these methods in general yielded good results, it must be assumed that at sufficiently high frequencies the quasistatic approximations will break down.

The next generation of solutions involved approximating the microstrip as a rectangular waveguide with perfect electric conductors on the top and bottom walls and perfect magnetic conductors on the side walls [31-34]. Although this method yielded a frequency-dependent solution, it again is expected to break down at higher frequencies due to the approximations of the model. Furthermore, there are many printed circuit discontinuities, such as those in the fin line and strip line, for which no waveguide model is available.

Another attempt at solving this type of problem was made by Lampe [35], who presented a three-region analysis of strip line discontinuities. Recall that the strip line and fin line are analogous to the microstrip because of the generality of the spectral domain immittance approach, as discussed in Section 2.2. In his analysis, Lampe begins by breaking up a discontinuity into three regions, taking the boundaries of the middle region far enough away from the discontinuity on either side so that most of the evanescent modes have decayed enough to become insignificant. Next, he finds the dominant and first few higher-

order modes in the first and third regions. Finally, he formulates an integral equation that relates the magnitude of the mode coefficients in the first and third regions to the unknown current on the strip in the second region. The solution to this integral equation yields the desired reflection and transmission coefficients. This method has limitations also, because it is formulated for an isotropic medium. The strip is assumed to be printed on a thin dielectric substrate; so thin that it is felt to have little effect. Thus, the entire problem is formulated in a homogeneous region whose dielectric constant is the "volume average" dielectric constant. This turns out to be a small perturbation from the free-space dielectric constant of one. This method is appropriate for low frequencies in the strip line, but it seems likely to break down for higher frequencies. In addition, it is not appropriate for a microstrip configuration, in which the dielectric material plays an important role. Finally, this method can not easily be modified to account for the dielectric, since the Green's function in the second region would then become too complicated.

The most recent attempts at solving this type of problem have occurred in the area of fin line discontinuities. The methods used in these cases all involved finding a number of modes for each guide by using a spectral Galerkin method. These modes were then used in either a mode matching procedure [17,36,37] or in an iteration procedure [38] to equate the fields tangent to the plane of the discontinuity.

The results generated in these mode matching papers were not conclusive, but they did suggest that further study would be in order, and that the method might be applicable to a shielded microstrip as well as to the fin line. This will be the topic of study for this chapter.

3.2 Mode Matching

The structure to be analyzed is shown in Figure 3.1a. It involves an abrupt discontinuity in the strip width of the center conductor of shielded microstrip, whose cross section is shown in Figure 2.1.

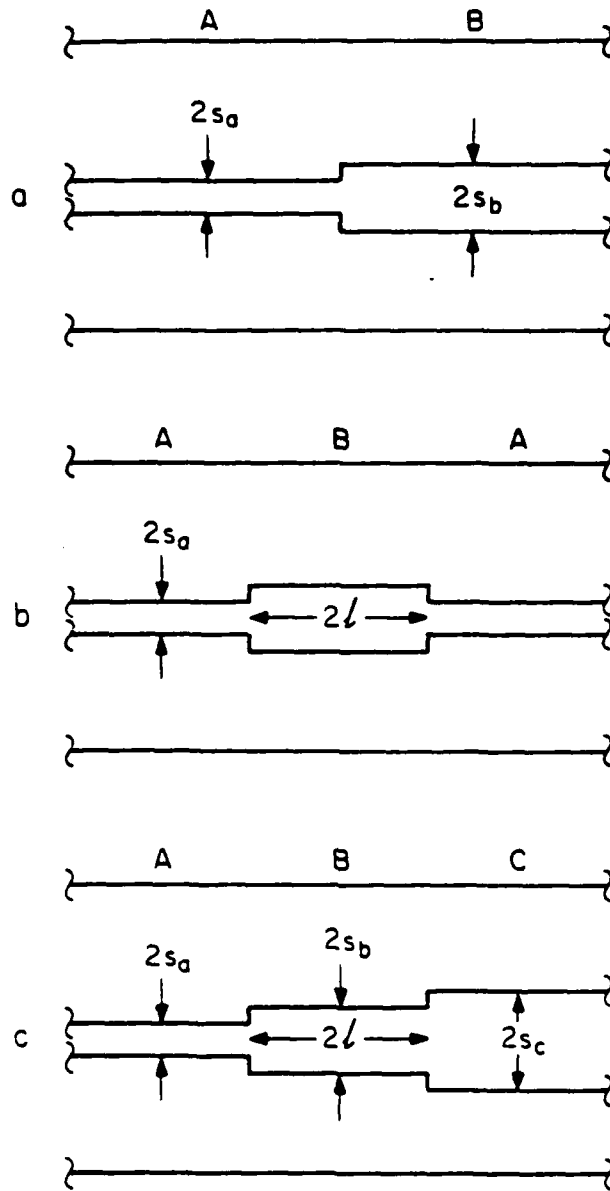


Figure 3.1. Various microstrip discontinuities in the center conductor.

We begin the analysis by generating the propagation constants and field configurations for the dominant and first few higher-order modes of each of the two waveguides. This was discussed in Chapter 2. Next, we express the fields in waveguide A as a sum of the waveguide modes

$$\bar{E}_a(x, y, z) = \sum_{i=1}^{\infty} a_i \bar{e}_{ai}(x, y) e^{-\gamma_{ai} z} \quad (3.1a)$$

$$\bar{H}_a(x, y, z) = \sum_{i=1}^{\infty} a_i \bar{h}_{ai}(x, y) e^{-\gamma_{ai} z} \quad (3.1b)$$

where the a_i are mode coefficients, γ_{ai} are the complex propagation constants of the i th mode, and \bar{e}_{ai} and \bar{h}_{ai} are the vector mode functions of the i th mode, where

$$\bar{e}_{ai}(x, y) = e_{aix}(x, y)\hat{x} + e_{aiy}(x, y)\hat{y} \quad (3.2a)$$

$$\bar{h}_{ai}(x, y) = h_{aix}(x, y)\hat{x} + h_{aiy}(x, y)\hat{y} \quad (3.2b)$$

Similar expressions are formulated for waveguide B by replacing "a" with "b" in the above equations. If we assume the discontinuity occurs at $z = 0$, we may equate the field components tangential to the interface at $z = 0$ as

$$(1+\rho)\bar{e}_{a1}(x, y) + \sum_{i=2}^{\infty} a_i \bar{e}_{ai}(x, y) = \sum_{i=1}^{\infty} b_i \bar{e}_{bi}(x, y) \quad (3.3a)$$

$$(1-\rho)\bar{h}_{a1}(x, y) - \sum_{i=2}^{\infty} a_i \bar{h}_{ai}(x, y) = \sum_{i=1}^{\infty} b_i \bar{h}_{bi}(x, y) \quad (3.3b)$$

This is the equation that is to be solved for the mode coefficients a_i and b_i and for the reflection coefficient ρ .

To solve this equation, we take the inner products of Equation 3.3a with $\bar{h}_{am}(x, y)$, and the inner product of Equation 3.3b with $\bar{e}_{bm}(x, y)$. The inner product is defined as

$$I_{aibj} = \int_S \bar{e}_{ai}(x, y) \times \bar{h}_{bj}(x, y) \cdot \hat{z} \, dx \, dy \quad (3.4)$$

It is calculated most simply in the spectral domain, in a manner analogous to the power

calculation described in Section 2.5. Thus, the integration over x becomes a sum over spectral terms, and the integration over y is analytic in the spectral domain. After taking these inner products, we find

$$-\rho I_{a_{1am}} - \sum_{i=2}^L a_i I_{a_{iam}} + \sum_{i=1}^L b_i I_{b_{iam}} = I_{a_{1am}} \quad m=1, \dots, L \quad (3.5a)$$

$$\rho I_{b_{ma1}} + \sum_{i=2}^L a_i I_{b_{mai}} + \sum_{i=1}^L b_i I_{b_{mbi}} = I_{b_{ma1}} \quad m=1, \dots, L \quad (3.5b)$$

This equation can also be written in the form

$$Ax = b \quad (3.6)$$

where A is a $2L \times 2L$ matrix of inner products, x is the $2L \times 1$ vector containing the unknown mode coefficients, and b is a known $2L \times 1$ matrix of inner products. This can be solved by a standard linear equation solution routine.

The solution to this matrix equation contains within it the reflection coefficient, ρ , and the magnitude of the transmitted wave, b_1 . From ρ , we may calculate an equivalent circuit of the form shown in Figure 3.2. If we let

$$\rho = \rho_r + j \rho_i \quad (3.7)$$

where ρ_r and ρ_i are both real, then

$$Z_N = \frac{Z_2}{Z_1} = \frac{(\rho_r + 1)^2 + \rho_i^2}{(1 - \rho_r^2) - \rho_i^2} \quad (3.8a)$$

$$Y_N = \omega C Z_1 = \frac{-2\rho_i}{(\rho_r + 1)^2 + \rho_i^2} \quad (3.8b)$$

These parameters are useful because they can be checked with other, more approximate methods. Therefore, we expect $Z_N \approx Z_{ob}/Z_{oa}$ where Z_{ob} and Z_{oa} are the characteristic impedances of the second and first waveguides, as calculated in Section 2.5. Furthermore, we may compare our values of Y_N to those generated by quasistatic analysis [29]. We

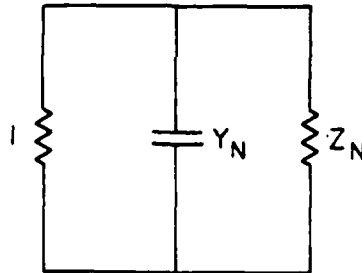
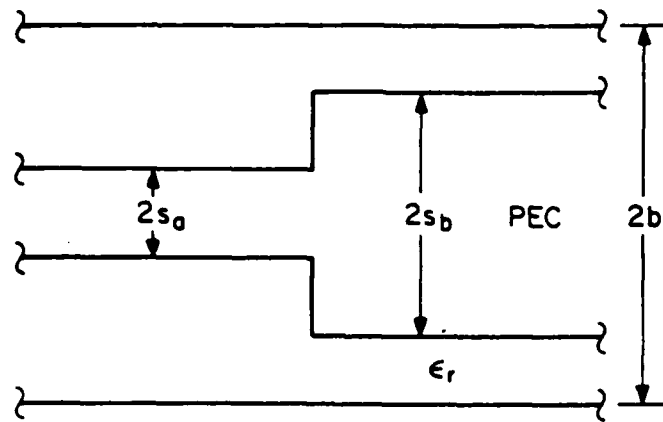


Figure 3.2 Dimensions for a single step discontinuity in strip width and the corresponding equivalent circuit.

should expect only approximate agreement, since we are now using a frequency dependent method to generate the solution.

A second check we can make on our final answer is to verify that all real power is accounted for. This is checked by showing that

$$|S_{11}|^2 + |S_{21}|^2 = 1 \quad (3.9)$$

While this condition is not sufficient to guarantee a good solution, it is necessary, and should be verified.

This concludes the setup of the mode matching procedure. Before we present calculations, there are a number of related issues that need to be dealt with. These are discussed in the following three sections.

3.3 Orthogonality of Inner Products

Upon examination of Equation 3.5 we observe a number of inner products of the form I_{aia_j} where $i \neq j$. We expect the standard orthogonality relationship to hold for the normalized modes of uniform waveguides with perfectly conducting side walls [39]

$$I_{aia_j} = \begin{cases} 1 & i = j \\ 0 & i \neq j \end{cases} \quad (3.10)$$

Thus, we are left with the problem of deciding whether or not to retain in the matrix equation the inner products that are theoretically equal to zero. It must be kept in mind that our modes have been calculated only to a finite accuracy, dictated by the numerical accuracy of our methods. If the accuracy in the mode functions is good, then retaining the cross terms will not matter. If, on the other hand, there is a small error in the mode functions, then it would seem preferable to retain the cross terms rather than discard what may be useful numerical information. This is the approach adopted for these calculations.

3.4 Condition Number of the Matrix

In formulating the mode matching solution, we obtain a matrix equation of the form $Ax = b$. A useful parameter associated with this equation is the condition number of the matrix A . It turns out that if the matrix A has a large condition number, it is very difficult to obtain accurate solutions for the unknown column vector x .

There are a number of methods that may be used to calculate the condition number of a matrix, depending on the norm of the matrix chosen for the problem [40,41]. A reasonable definition of condition number is

$$\text{cond}(A) = \left(\frac{|\lambda_{\max}|}{|\lambda_{\min}|} \right)^{\frac{1}{2}} \quad (3.11)$$

where the λ 's are the maximum and minimum eigenvalues of the matrix $A^H A$, and A^H is the transposed complex conjugate of A . If this condition number is large, we have difficulty in solving the matrix equation, because small errors in the matrix elements generate large errors in the solution for the unknown vector x . This definition of condition number is used in the calculations that follow, in order to check the stability of the matrix equation solution.

3.5 Matrix Theory for Cascaded Discontinuities

In the case where there are multiple discontinuities, we need a method of keeping track of a number of modes between one discontinuity and the next. We consider two cases. First, we study a symmetrical double step, as shown in Figure 3.1b. This is a special case of the second case we will study, that of N discontinuities each spaced an arbitrary distance from the previous discontinuity. An example of this is shown in Figure 3.1c.

In the case of an asymmetrical double step, we may take advantage of symmetry properties to greatly simplify the problem. Thus, instead of launching the dominant mode

from the left with a magnitude of one, we add the results of launching modes of equal magnitude and either equal or opposite phase, as shown in Figure 3.3. These cases are equivalent to placing magnetic and electric conductors at the center of the waveguide B. The solution for each of these cases may easily be adapted from the solution for the single discontinuity, since the waveguide modes are reflected from the electric or magnetic conductor without coupling to other modes. We adapt results from [36] that result in a slight modification of Equation 3.3. Thus, at $z = 0$

$$(1/2 + \rho)\bar{e}_{a1}(x,y) + \sum_{i=2}^{\infty} a_i \bar{e}_{ai}(x,y) = \sum_{i=1}^{\infty} b_i (1 + S_{bii}) \bar{e}_{bi}(x,y) \quad (3.12a)$$

$$(1/2 - \rho)\bar{h}_{a1}(x,y) - \sum_{i=2}^{\infty} a_i \bar{h}_{ai}(x,y) = \sum_{i=1}^{\infty} b_i (1 - S_{bii}) \bar{h}_{bi}(x,y) \quad (3.12b)$$

where

$$S_{bii} = \begin{cases} e^{-2\gamma_{bi}l} & \text{for electric conductor at } z = l \\ -e^{-2\gamma_{bi}l} & \text{for magnetic conductor at } z = l \end{cases} \quad (3.13)$$

and γ_{bi} is the complex propagation constant of the i th mode in waveguide B, and $2l$ is the distance between the discontinuities. The above equation may be solved in a manner analogous to Equation 3.3 by taking appropriate inner products, as described in Section 3.2.

If, on the other hand, we do not have the luxury of having favorable symmetry properties, we have to solve the more general case of N discontinuities, each separated by a length of transmission line. In this case we will have to cascade the generalized S-parameters of each of the discontinuities, and the transmission lines that separate them, to form an S matrix for the entire structure. The method that follows is adapted from a method by Hall [42].

Let us begin with a definition of generalized S- and T-parameters. For the arbitrary circuits shown in Figure 3.4, we define generalized T- and S-parameters as

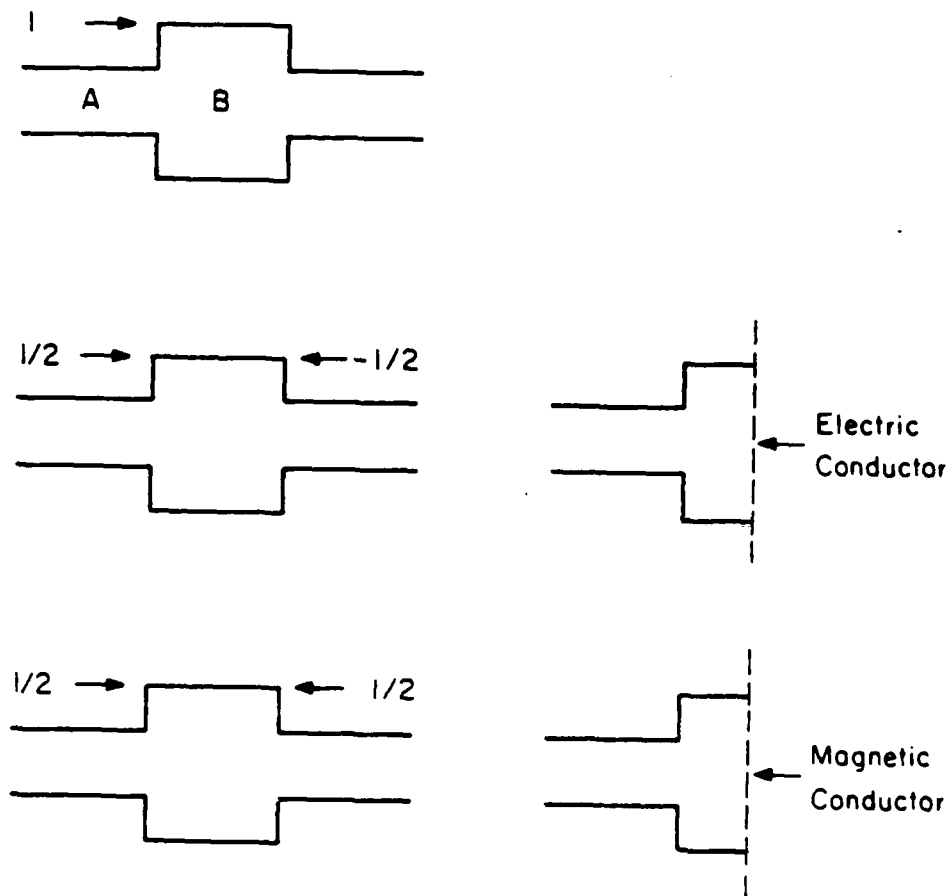


Figure 3.3 Symmetrical discontinuities, and the method of taking advantage of the symmetry, by symmetrical and antisymmetrical excitation of the discontinuity.

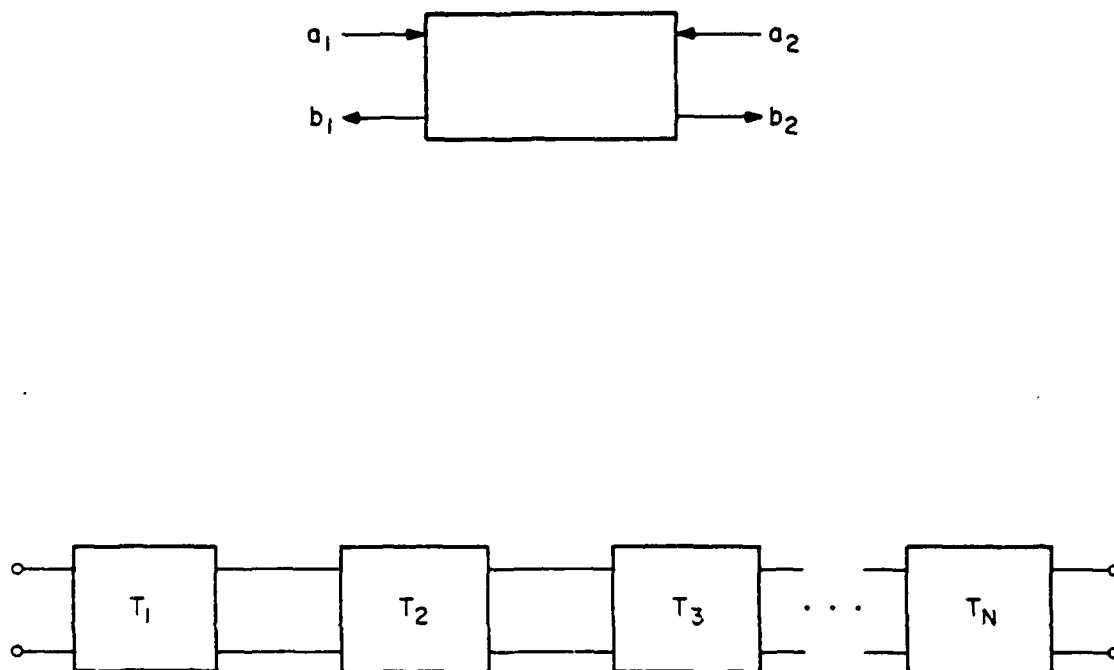


Figure 3.4. Input and output parameters of an arbitrary circuit, and a cascade of such circuits.

$$\begin{bmatrix} b_2 \\ a_2 \end{bmatrix} = \begin{bmatrix} T_{11} & T_{12} \\ T_{21} & T_{22} \end{bmatrix} \begin{bmatrix} a_1 \\ b_1 \end{bmatrix} \quad (3.14a)$$

$$\begin{bmatrix} b_1 \\ b_2 \end{bmatrix} = \begin{bmatrix} S_{11} & S_{12} \\ S_{21} & S_{22} \end{bmatrix} \begin{bmatrix} a_1 \\ a_2 \end{bmatrix} \quad (3.14b)$$

In these equations, a_i and b_i represent $L \times 1$ column vectors representing mode coefficients for the L modes either incident or reflected from the circuit. In addition, terms such as S_{11} represent an $L \times L$ generalized scattering matrix for L modes in each guide.

We generate generalized S-matrices for discontinuities in the manner of Section 3.2, but keeping in mind that we now have to run cases for all L possible modes incident from the left at each discontinuity. Care must be taken with the normalization of these S-parameters, since the modes generated were not normalized. The correct normalization gives, for example

$$S_{21}(i,j) = \frac{b_j}{a_i} \left| \frac{\int \int \epsilon_{b_j} \times \bar{h}_{b_j} \cdot d\bar{S}}{\int \int \epsilon_{a_i} \times \bar{h}_{a_i} \cdot d\bar{S}} \right|^{1/2} \quad (3.15)$$

Once the generalized scattering parameters are normalized, they must be converted to T-parameters. The conversions are

$$T = \begin{bmatrix} S_{21} - S_{22}S_{12}^{-1}S_{11} & S_{22}S_{12}^{-1} \\ -S_{12}^{-1}S_{11} & S_{12}^{-1} \end{bmatrix} \quad (3.16a)$$

$$S = \begin{bmatrix} -T_{22}^{-1}T_{21} & T_{22}^{-1} \\ T_{11} - T_{12}T_{22}^{-1}T_{21} & T_{12}T_{22}^{-1} \end{bmatrix} \quad (3.16b)$$

Next we generate the T-matrices of individual transmission lines. These are

$$T_{11}(i,j) = \begin{cases} e^{-2\gamma_i l} & i=j \\ 0 & \text{else} \end{cases} \quad (3.17a)$$

$$T_{22}(i, j) = \begin{cases} e^{2\gamma_i l} & i = j \\ 0 & \text{else} \end{cases} \quad (3.17b)$$

$$T_{12} = T_{21} = 0 \quad (3.17c)$$

Finally, we cascade a number of discontinuities and transmission lines by multiplying the T-matrices together to obtain a composite T-matrix for the entire structure of N components, as shown in Figure 3.4.

$$T = T_N \cdot T_{N-1} \cdots T_2 \cdot T_1 \quad (3.18)$$

This is now converted to an S matrix using Equation (3.13b), and the problem of cascaded discontinuities is now formulated. Numerical results for single and cascaded discontinuities appear in the next two sections.

3.6 Results for the Single Discontinuity

We now present our results for a single discontinuity in strip width, shown in Figure 3.2. The first step in the solution is to search for propagation constants of the dominant and higher-order modes at a given frequency. This was done, and the results are shown in Table 3.1.

Next, the results for the reflection coefficient, ρ , and for the equivalent circuit

Table 3.1. Propagation constants for a uniform microstrip. For these calculations, $h = 0.4445$ mm, $b = 0.381$ mm, $t = 0.127$ mm, $\epsilon_r = 9.6$, freq = 20 GHz.

	$s_a = .0635$ mm $Z_{oa} = 48.915$	$s_a = .1588$ mm $Z_{ob} = 33.38$
β_1 (rad./m)	1037.01	1065.91
β_2	-j4068.72	-j4056.39
β_3	-j10478.5	-j8050.07
β_4	-j14694.4	-j10648.9
β_5	-j14897.1	-j14505.2
β_6	-j16201.8	-j17358.1

parameters, Z_N and Y_N , are shown in Table 3.2 for calculations with up to six modes in each waveguide. We note here that Z_N converges quickly to the values expected from transmission line theory. The junction capacitance, however, never seems to converge with the small number of modes we have used. We are limited somewhat in the number of modes we can use because the cost of the calculation begins to become quite large with more modes, and because the spectral Galerkin technique tends to break down for large imaginary propagation constants.

Next, we perform a number of checks on these calculations. These include a power check and a calculation of the condition number of the A matrix. These data are shown in Table 3.3. From this table we verify that all the power is accounted for to a reasonable numerical accuracy. This, as stated earlier, is a necessary, but not sufficient condition to guarantee the accuracy of a solution. The condition number of the matrix may be more indicative of what is going on. The condition numbers, which are around 750, suggest that the matrix is ill-conditioned. As a general guideline, we consider a condition number greater than about 100 to indicate a problem in the condition number of the matrix. Thus, unless the matrix elements are computed very accurately, we have to expect a problem in generating highly accurate solutions to the matrix equation.

The issue of condition number turns out to be of a very central importance in these

Table 3.2. Values of the circuit elements in Figure 3.2 for the dimensions in Table 3.1. These calculations were made with 5 basis functions and 200 spectral terms.

# of Modes	ρ_r	ρ_i	Y_N	Z_N
3	-.269978	-.0014	.0060	.575
4	-.270028	-.0011	.0043	.575
5	-.270368	-.0038	.0146	.574
6	-.280095	-.0060	.0233	.562
Expected from Quasi Static (Y_N) and TEM (Z_N) Approaches			.0172	.684

Table 3.3. Power check and condition number for the discontinuity whose dimensions were given in Table 3.1.

Number of Modes	$ S_{11} ^2 + S_{21} ^2$	Condition Number
3	1.0016	754
4	1.0016	759
5	1.0006	752

calculations. Since the imaginary part of the reflection coefficient is several orders of magnitude less than the real part, the reflection coefficient as a whole must be calculated to a high degree of precision in order to get a meaningful ρ_i , and hence Y_N . When the condition number is high, it is very difficult to obtain accurate results without a very high degree of numerical precision in the matrix elements.

Let us now consider the accuracy of the matrix elements. The simplest way of checking this is to consider the degree to which the orthonormality conditions of the waveguide modes, as expressed in Equation 3.10, were satisfied. If the orthogonality conditions are satisfied well, then we may concede the possibility of an accurate solution to the discontinuity problem despite the ill-condition of the matrix. These inner products appear in Table 3.4 for the first five modes of waveguides A and B. From this table, we see that the cross terms are well behaved for the lower-order terms, but the higher-order cross terms tend to become increasingly large. Thus, it is difficult to claim, based on these inner products, that the matrix elements are accurate enough to overcome the large condition number of the A matrix.

Finally, we present data on the number of basis functions and spectral terms that are required to give accurate propagation constants. This may be used to answer a possible objection that an insufficient number of basis functions and spectral terms was used in the discontinuity calculations. The data, shown in Table 3.5, indicate that the propagation constant of the fifth mode in waveguide A is sufficiently converged with only two basis

Table 3.4. Inner product calculations for the first five modes of waveguides A and B, whose dimensions were given in Table 3.1. These were calculated with 5 basis functions and 200 spectral terms.

$ I_{aia_j} $	1.000	0.000	0.000	0.035	0.013
	0.000	1.000	0.000	0.009	0.003
	0.000	0.000	1.000	0.048	0.018
	0.000	0.000	0.000	1.000	0.010
	0.000	0.000	0.001	0.521	1.000
$ I_{bib_j} $	1.000	0.003	0.046	0.001	0.080
	0.000	1.000	0.053	0.000	0.009
	0.000	0.000	1.000	0.001	0.086
	0.000	0.000	0.113	1.000	0.031
	0.000	0.000	0.031	0.000	1.000

functions and 50 spectral terms. Thus, since we used five basis functions, and 200 spectral terms in our discontinuity calculations, it seems likely that we have used a sufficient number of each.

We conclude, therefore, that the mode matching technique is useful only in obtaining good approximations to the circuit parameters. It seems unlikely that the accuracy of this method can be forced to the point where an accurate junction capacitance can be calculated, for a number of reasons. First, the imaginary part of the reflection coefficient is very small compared to the real part, and it is difficult to calculate a small

Table 3.5. Variation of a propagation constant with the number of basis functions and spectral terms. The mode calculated is the fifth mode of waveguide A, whose dimensions were given in Table 3.1.

Number of Basis Functions	Spectral Terms	$\beta_{o5}(\text{rad/m})$
2	50	14897.1
2	100	14894.5
3	50	14897.6
3	100	14894.7
5	250	14893.3

quantity in the shadow of a larger effect. Second, the condition number of the matrix indicates an instability in the matrix that can only be overcome if the matrix elements are calculated to a high degree of accuracy. Finally, the inner product calculations suggest that the matrix elements can only be calculated to a finite degree of accuracy and that the spectral Galerkin technique can not be pushed beyond this point for modes of high order.

With these thoughts in mind, let us now turn to other discontinuities to calculate. Although we have not achieved a high degree of accuracy in the calculations for the single discontinuity, we have demonstrated that the method generates a good approximation for the solution. Thus, there may well be reason to consider other types of discontinuities, and results for these are presented in the section that follows.

3.7 Results for Other Discontinuities

The next configuration we would like to study is the symmetrical double step discontinuity. This is shown in Figure 3.5, and the theory was presented earlier in Section 3.5. Results are presented for a typical case at two different frequencies in Tables 3.6 and 3.7. These calculations were made with up to four waveguide mode functions in each waveguide. Upon examination of these results, we find the reflection coefficient has converged nicely within four modes to a result that is similar to that expected from the transmission line theory. We note, furthermore, that the results for one mode are similar to that for four modes, so in the future we need to use only a single mode for our calculations.

In the next two tables, Tables 3.8 and 3.9, we present data for several of these cases over a range of frequencies and for various values of s_b . We compare them to experimental data, which was generated by U. Feldman [43], and to results generated by the transmission line theory. Based on the data in these tables, we observe that the data calculated by the mode matching technique provide a slightly better fit to the experimental data than the results generated by the transmission line theory.

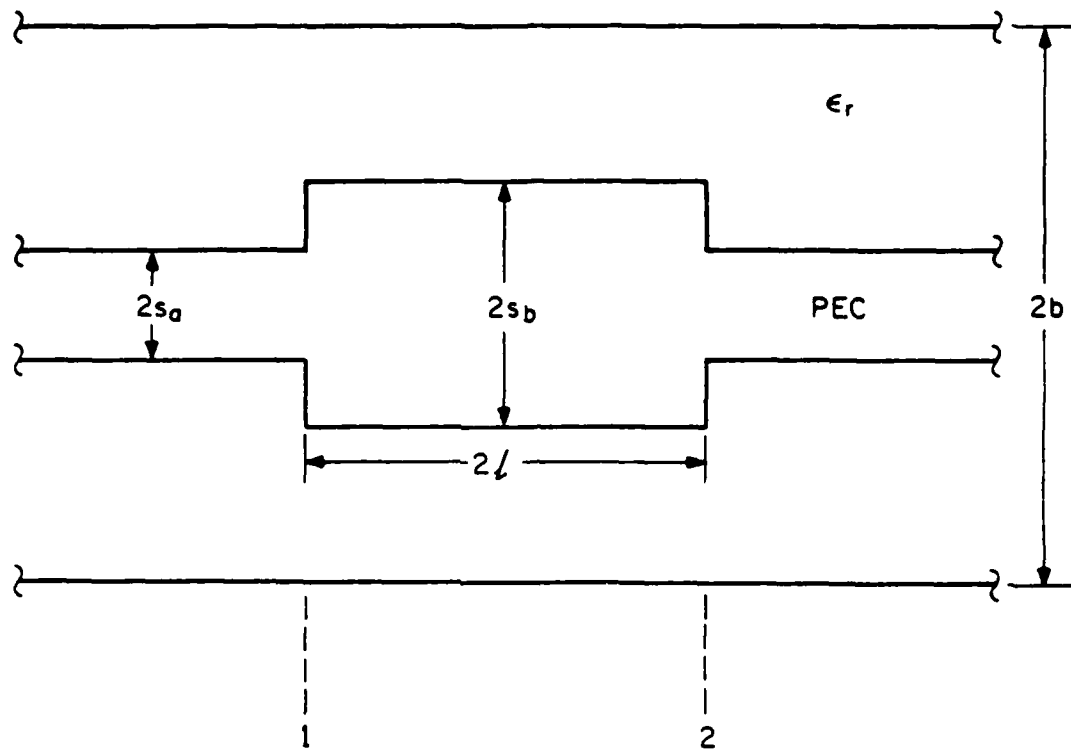


Figure 3.5 Dimensions for a symmetrical double step discontinuity in strip width.

Table 3.6. Propagation constants for the first through fourth modes of a symmetrical double step discontinuity in strip width, and results for S_{11} . For these calculations, $h=5.08$ mm, $b=6.096$ mm, $t=0.7874$ mm, $\epsilon_r=2.2$, $l=1.0$ cm, and $\text{freq}=8.010$ GHz.

	$s_a = 1.17$ mm $Z_{oa} = 51.85 \Omega$	$s_b = 2.41$ mm $Z_{ob} = 3.60 \Omega$
$\beta_1(\text{rad./mm})$	230.056	234.723
β_2	-j187.051	-j186.281
β_3	-j647.067	-j640.983
β_4	-j727.228	-j749.948

Number of Modes	$S_{11} (dB \angle deg)$
1	-6.45 \angle -179.1
2	-6.43 \angle -179.0
3	-6.47 \angle -178.8
4	-6.41 \angle -179.2
From Transmission Line Theory Expect	-8.32 \angle -179.1

Table 3.7. Propagation constants for up to the fourth mode of a symmetrical double step discontinuity in strip width, and results for S_{11} . The configuration is that of Table 3.6, except that the $\text{freq} = 12.02$ GHz.

	$s_a = 1.17$ mm $Z_{oa} = 52.56 \Omega$	$s_b = 2.41$ mm $Z_{ob} = 35.21 \Omega$
$\beta_1(\text{rad./mm})$	341.625	355.340
β_2	55.8937	55.8765
β_3	-j701.537	-j610.145
β_4	-j723.682	-j904.769

Number of Modes	$S_{11} (dB \angle deg)$
1	-8.90 \angle -140.6
2	-8.90 \angle -140.6
3	-8.46 \angle -140.3
4	-8.45 \angle -140.3
From Transmission Line Theory Expect	-10.8 \angle -139.4

Table 3.8. Dominant mode propagation constant and characteristic impedance as a function of frequency and center strip half width (s). For these calculations, $h = 5.08$ mm, $b = 6.096$ mm, $t = 0.7874$ mm, and $\epsilon_r = 2.2$.

FREQ (GHz)	β (rad/m) and Z_0 (Ω) for				
	$s = 2.41$	$s = 1.65$	$s = 1.17$	$s = .026$	$s = .353$
.990	28.6661	28.43	28.1895	27.7751	27.4819
	34.52	42.26	51.74	73.67	97.03
2.025	58.6799	58.1802	57.69	56.8345	56.2296
	34.50	42.23	51.72	73.65	97.01
4.005	116.374	115.330	114.319	112.563	111.330
	34.45	42.19	51.68	73.61	96.97
8.010	234.723	232.338	230.056	226.170	223.470
	34.60	42.35	51.85	73.81	97.19
12.015	355.340	351.391	347.625	341.250	336.825
	35.21	43.01	52.56	74.60	98.06

Table 3.9. S_{11} for the symmetrical double step discontinuity shown in Figure 3.4, as a function of s_b and frequency. For these calculations, $s_a = 1.17$ mm, $l = 1.0$ cm, and all other dimensions are as in Table 3.8. The first number for each case is calculated by mode matching, the second by the transmission line theory, and the third number is from experimental results of Feldman [43].

FREQ (GHz)	S_{11} (dB \angle deg) for			
	$s_b = 2.41$ mm	$s_b = 1.65$ mm	$s_b = .626$ mm	$s_b = .353$ mm
.990	-10.8 \angle -126	-17.6 \angle -123	-13.9 \angle 56	-9.1 \angle 53
	-13.2 \angle -125	-19.2 \angle -123	-14.6 \angle 57	-9.6 \angle 54
	-11.2	-18.3	-13.7	-9.4
2.025	-6.8 \angle -160	-13.1 \angle -157	-9.5 \angle 23	-5.2 \angle 21
	-8.9 \angle -159	-14.7 \angle -157	-10.1 \angle 24	-5.7 \angle 22
	-6.9	-13.3	-9.5	-5.4
4.005	-8.6 \angle 140	-14.9 \angle 138	-10.7 \angle -37	-6.1 \angle -32
	10.8 \angle 139	-16.5 \angle 138	-11.4 \angle -37	-6.6 \angle -33
	-8.9	-15.3	-11.1	-6.6
8.010	-6.4 \angle -179	-12.5 \angle -176	-8.9 \angle 10	-4.9 \angle 11
	-8.3 \angle -179	-14.0 \angle -176	-9.5 \angle 10	-5.3 \angle 12
	-6.4	-12.6	-9.4	-5.2
12.015	-8.9 \angle -141	-15.9 \angle -133	-14.3 \angle 57	-10.7 \angle 59
	-10.8 \angle -139	-17.4 \angle -133	-14.8 \angle 57	-11.1 \angle 60
	-8.8	-16.4	-14.7	-10.3

Next, we consider a nonsymmetrical double discontinuity, shown in Figure 3.6. This configuration may be used to simulate a linear taper. The results for this structure were generated with the matrix theory given in Section 3.5, and are given in Table 3.10. In this table are the propagation constants and characteristic impedances of the three lines, and

the S-parameters of the discontinuity referenced to planes Nos. 1 and 2 as shown in Figure 3.6. In addition, Table 3.10 has a comparison to transmission line theory and a power check of the mode matching results. The results indicate an overall agreement with the transmission line approach, although it is difficult to say which approach is more accurate.

Finally, we consider a single discontinuity in the dielectric constant, strip width, and substrate thickness, a diagram of which is shown in Figure 3.7. This case is one that might be expected to occur when a microstrip printed on gallium arsenide must mate with a microstrip printed on duroid board. Because of the difference in dielectric constants, it will be necessary to have different line widths to maintain a 50 ohm line in each section. Some typical S-parameter data for this configuration are shown in Table 3.11, along with data for a power check and the condition number of the matrix. These data are difficult to interpret since the condition numbers are very large, and since the power check is off by about 0.06. Both transmission lines are 50 ohm lines, so we expect a reflection coefficient of zero from simple transmission line analysis, while we calculate a reflection coefficient of about -10 dB. This -10 dB reflection corresponds to a value of 0.1 in the power check. Since the power check is off by 0.06, it is difficult to get a feel for the accuracy of these results. If we ignore, however, the higher-order modes, and look only at the results when a single mode is used, we still have a reflection coefficient of about -10 dB, but now the power check and condition number of the matrix are both satisfactory. It appears, therefore, that experimental work will be required to verify these calculations.

3.8 Conclusion

In this chapter we have analyzed a number of discontinuities by using a combination of the spectral Galerkin technique to generate modes and mode matching to find the scattering parameters of the discontinuity. In general, our results have been close to what was expected, but it proves difficult to use this technique to give highly accurate results. The factors that limit the accuracy include the small number of waveguide modes

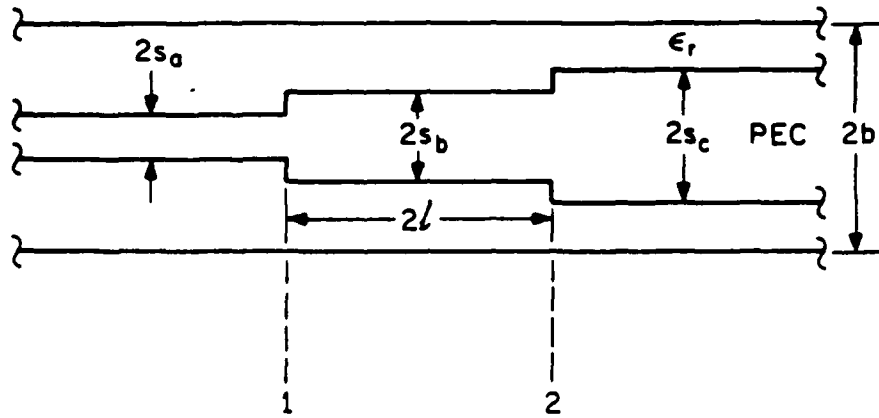


Figure 3.6. Dimensions for a model of a microstrip taper, modeled as a cascade of discrete discontinuities.

Table 3.10. Results for the taper simulation shown in Figure 3.6. For these calculations, $h = 5.08$ mm, $b = 6.096$ mm, $t = 0.7874$ mm, $\epsilon_r = 2.2$, and $l = 1.0$ cm.

		10 GHz	12.5 GHz	15.0 GHz
$s_a = 1.17$ mm	β_a (rad/m)	288.2	261.8	435.9
	Z_{oz} (Ω)	52.14	52.57	53.28
$s_b = 1.65$ mm	β_b	291.2	365.7	440.8
	Z_{ob}	42.63	43.11	43.67
$s_o = 2.41$ mm	β_c	294.36	269.9	445.9
	Z_{oc}	34.86	35.30	35.79
Transmission Line Theory dB \angle deg	S_{11}	-14.95 \angle -154	-19.76 \angle 122	-15.81 \angle -146
	S_{21}	-0.14 \angle 26	-0.05 \angle -59	-0.12 \angle -146
	S_{22}	-14.95 \angle 26	-19.76 \angle -59	-15.81 \angle 34
Mode Matching	S_{11}	-12.78 \angle -152	-17.61 \angle 114	-12.94 \angle -143
	S_{21}	-0.23 \angle 26	-0.76 \angle -58	-0.18 \angle -146
	S_{22}	-12.78 \angle 23	-17.61 \angle -51	-13.94 \angle 31
	$ S_{11} ^2 + S_{21} ^2$	1.00000	0.999998	0.999999

Table 3.11. Results for a step discontinuity in ϵ_r , t , and s . For these calculations $h_a = 0.889$ mm, $h_b = 0.953$ mm, $b = 1.27$ mm, $t_a = 0.127$ mm, $t_b = 0.191$ mm, $s_a = 0.042$ mm, $s_b = 0.298$ mm, $\epsilon_{ra} = 12.3$, $\epsilon_{rb} = 2.2$, freq. = 20 GHz. These calculations were made with 2 basis functions and 50 spectral terms, and $Z_{oa} = Z_{ob} = 50.0 \Omega$.

Number of Modes	S_{11} (dB \angle deg)	S_{21} (dB \angle deg)	$ S_{11} ^2 + S_{21} ^2$	Condition Number
1	-9.92 \angle 180	-46 \angle 0.0	1.00000	26
2	-11.69 \angle -175	-08 \angle -2.2	1.066	6240
3	-11.67 \angle -175	-01 \angle -2.0	1.066	6790
4	-11.67 \angle -172	-02 \angle -3.2	1.063	6800

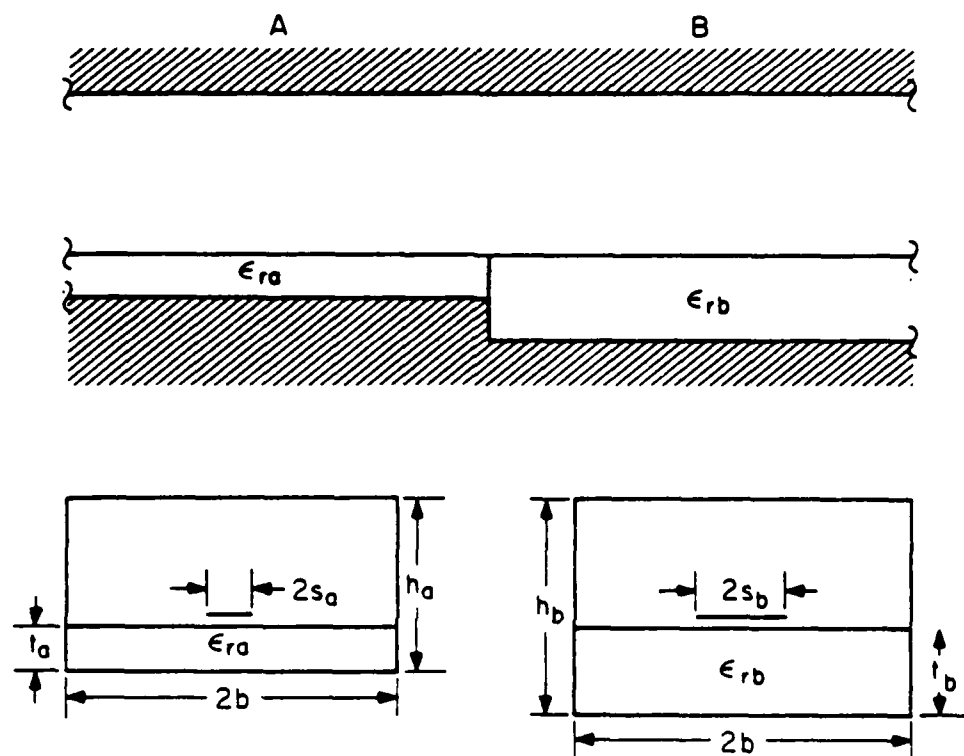


Figure 3.7 Dimensions for a step discontinuity in dielectric constant, strip width, and substrate thickness.

one can calculate with the spectral Galerkin technique, the ill-condition of the set of matrix equations, and the necessity of calculating a small junction capacitance in the shadow of a comparatively large reflection coefficient.

If this method is to be refined to yield more accurate results, we have to find a way to generate a large number of very accurate waveguide modes. In the next chapter, we consider an alternate method of generating these modes, in an effort to increase the accuracy of the mode matching method. Let us now turn our attention to the singular integral equation technique.

CHAPTER 4

THE SINGULAR INTEGRAL EQUATION TECHNIQUE

4.1 Introduction

The singular integral equation technique is an alternate method of finding modes in printed circuit waveguides. This method was first suggested by Mittra and Itoh [5], and has since been expanded upon by Omar and Schunemann [44,45]. Its chief advantage over the spectral Galerkin method is its very high degree of numerical efficiency, requiring, by comparison, very little computer time. Its disadvantage, however, is that it is a much more difficult method to derive and implement, requiring a great deal of effort to derive the matrix equation.

In this chapter, we outline the work of Mittra and Itoh and expand upon it by calculating a larger number of terms in certain series as well as a larger matrix size. In addition, we compare these results to those obtained with the spectral Galerkin technique presented earlier.

4.2 Overview of the Method

In this section we outline the singular integral equation technique as applied to the microstrip, and as explained in [5]. Since the method is somewhat involved, we omit a number of details here that are included in [5]. In spite of this, we include sufficient detail to demonstrate the reasons for the increased efficiency of the method.

Consider the shielded microstrip structure shown in Figure 4.1. We may write the fields in the two regions, denoted by i , as a sum of TE and TM components. This leads to

$$E_{z,i} = j \frac{k_i^2 - \beta^2}{\beta} \psi_i^{(e)} e^{-j\beta z} \quad (4.1a)$$

$$\bar{E}_{i,i}^{(e)} = \nabla_i \psi_i^{(e)} e^{-j\beta z} \quad (4.1b)$$

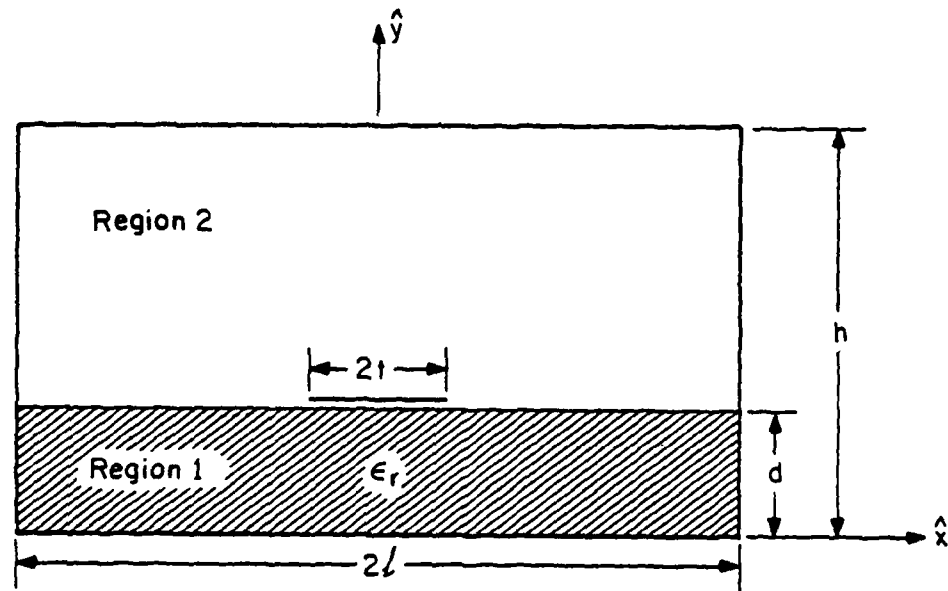


Figure 4.1. Dimensions of a shielded microstrip for this chapter.

$$\bar{H}_{ti}^{(e)} = \frac{\omega \epsilon_i}{\beta} \hat{z} \times \nabla_t \psi_i^{(e)} e^{-j\beta z} \quad (4.1c)$$

for the TM fields and

$$\bar{H}_{zi} = j \frac{k_i^2 - \beta^2}{\beta} \psi_i^{(h)} e^{-j\beta z} \quad (4.2a)$$

$$\bar{E}_{ti}^{(h)} = -\frac{\omega \mu}{\beta} \hat{z} \times \nabla_t \psi_i^{(h)} e^{-j\beta z} \quad (4.2b)$$

$$\bar{H}_{ti}^{(h)} = \nabla_t \psi_i^{(h)} e^{-j\beta z} \quad (4.2c)$$

for the TE fields. In these equations β is the propagation constant in the \hat{z} direction. $\psi_i^{(e)}$ and $\psi_i^{(h)}$ are scalar potentials for the E and H fields, respectively, and the subscript t indicates the transverse direction. The scalar potentials each satisfy a two-dimensional Helmholtz equation as in Equation 2.2 of the spectral Galerkin approach, where $k_i = \omega \sqrt{\mu_0 \epsilon_i}$ is the propagation constant of the medium in regions 1 and 2. By satisfying the boundary conditions on the side and top walls, we expand the scalar potentials as

$$\psi_1^{(e)} = \sum_{n=1}^{\infty} A_n^{(e)} \sinh \alpha_n^{(1)} y \cos \hat{k}_n x \quad (4.3a)$$

$$\psi_2^{(e)} = \sum_{n=1}^{\infty} B_n^{(e)} \sinh \alpha_n^{(2)} (h - y) \cos \hat{k}_n x \quad (4.3b)$$

$$\psi_1^{(h)} = \sum_{n=1}^{\infty} A_n^{(h)} \cosh \alpha_n^{(1)} y \sin \hat{k}_n x \quad (4.3c)$$

$$\psi_2^{(h)} = \sum_{n=1}^{\infty} B_n^{(h)} \cosh \alpha_n^{(2)} (h - y) \sin \hat{k}_n x \quad (4.3d)$$

where

$$\hat{k}_n = \frac{(n - 1/2)\pi}{L} \quad (4.4)$$

$$\alpha_n^{(1)} = \sqrt{\hat{k}_n^2 + \beta^2 - \epsilon_r k_0^2} \quad (4.5a)$$

$$\alpha_n^{(2)} = \sqrt{\hat{k}_n^2 + \beta^2 - k_0^2} \quad (4.5b)$$

and $k_0 = \omega\sqrt{\mu_0\epsilon_0}$.

We may now apply the boundary conditions at $y = d$, which is the interface of the two regions, to obtain

$$\sum_{n=1}^{\infty} \bar{A}_n^{(\epsilon)} \cos \hat{k}_n x = 0, \quad 0 < x < t \quad (4.6a)$$

$$\begin{aligned} \sum_{n=1}^{\infty} \bar{A}_n^{(\epsilon)} \hat{k}_n P_n(\beta) \cos \hat{k}_n x \\ - \sum_{n=1}^{\infty} \bar{A}_n^{(h)} \hat{k}_n T_n(\beta) \cos \hat{k}_n x = 0, \quad t < x < L \end{aligned} \quad (4.6b)$$

$$\begin{aligned} \sum_{n=1}^{\infty} \bar{A}_n^{(\epsilon)} \hat{k}_n \sin \hat{k}_n x \\ - \sum_{n=1}^{\infty} \bar{A}_n^{(h)} \hat{k}_n \sin \hat{k}_n x = 0, \quad 0 < x < t \end{aligned} \quad (4.6c)$$

$$\begin{aligned} \sum_{n=1}^{\infty} \bar{A}_n^{(\epsilon)} Q_n(\beta) \sin \hat{k}_n x \\ - \sum_{n=1}^{\infty} \bar{A}_n^{(h)} W_n(\beta) \sin \hat{k}_n x = 0, \quad t < x < L \end{aligned} \quad (4.6d)$$

where

$$\begin{aligned} P_n(\beta) = \epsilon_r \frac{\alpha_n^{(1)}}{\hat{k}_n} \coth \alpha_n^{(1)} d + \frac{\epsilon_r - \bar{\beta}^2}{1 - \bar{\beta}^2} \frac{\alpha_n^{(2)}}{\hat{k}_n} \coth \alpha_n^{(2)} (h - d) \\ + \bar{\beta}^2 \frac{\hat{k}_n}{\alpha_n^{(2)}} \frac{1 - \epsilon_r}{1 - \bar{\beta}^2} \coth \alpha_n^{(2)} (h - d) \end{aligned} \quad (4.7a)$$

$$T_n(\beta) = \bar{\beta}^2 \left(\frac{\hat{k}_n}{\alpha_n^{(1)}} \coth \alpha_n^{(1)} d + \frac{\hat{k}_n}{\alpha_n^{(2)}} \coth \alpha_n^{(2)} (h - d) \right) \quad (4.7b)$$

$$Q_n(\beta) = \frac{\hat{k}_n}{\alpha_n^{(2)}} \frac{1 - \epsilon_r}{1 - \beta^2} \coth \alpha_n^{(2)}(h - d) \quad (4.7c)$$

$$W_n(\beta) = \frac{\epsilon_r - \bar{\beta}^2}{1 - \beta^2} \frac{\hat{k}_n}{\alpha_n^{(1)}} \coth \alpha_n^{(1)}d + \frac{\hat{k}_n}{\alpha_n^{(2)}} \coth \alpha_n^{(2)}(h - d) \quad (4.7d)$$

and $\bar{\beta} = \beta/k_0$. This set of equations could be solved in their current form, but there would be no savings in computation time, since no effort has yet been made to reduce the number of terms needed for the summation. Let us now consider the method for doing so.

If we differentiate Equation 4.6a with respect to x and substitute the result into Equation 4.6c, we obtain

$$\sum_{n=1}^{\infty} \bar{A}_n^{(e)} \hat{k}_n \sin \hat{k}_n x = 0, \quad 0 < x < t \quad (4.8a)$$

$$\sum_{n=1}^{\infty} \bar{A}_n^{(h)} \hat{k}_n \sin \hat{k}_n x = 0, \quad 0 < x < t \quad (4.8b)$$

Next if we differentiate (4.6d) and rearrange, we find

$$\sum_{n=1}^{\infty} \bar{A}_n^{(e)} \hat{k}_n \cos \hat{k}_n x = f(x), \quad t < x < L \quad (4.8c)$$

$$\sum_{n=1}^{\infty} \bar{A}_n^{(h)} \hat{k}_n \cos \hat{k}_n x = g(x), \quad t < x < L \quad (4.8d)$$

where

$$f(x) = \sum_{m=1}^{\infty} (a_m \bar{A}_m^{(e)} + b_m \bar{A}_m^{(h)}) \cos \hat{k}_m x, \quad (4.9a)$$

$$g(x) = \sum_{m=1}^{\infty} (c_m \bar{A}_m^{(e)} + d_m \bar{A}_m^{(h)}) \cos \hat{k}_m x \quad (4.9b)$$

and

$$a_m = \hat{k}_m \left[1 - \frac{P_m(\beta)W(\beta) - T(\beta)Q_m(\beta)}{P(\beta)W(\beta) - T(\beta)Q(\beta)} \right] \quad (4.10a)$$

$$b_m = \hat{k}_m \frac{T_m(\beta)W(\beta) - T(\beta)W_m(\beta)}{P(\beta)W(\beta) - T(\beta)Q(\beta)} \quad (4.10b)$$

$$c_m = \hat{k}_m \frac{P(\beta)Q_m(\beta) - P_m(\beta)Q(\beta)}{P(\beta)W(\beta) - T(\beta)Q(\beta)} \quad (4.10c)$$

$$d_m = \hat{k}_m \left[1 - \frac{P(\beta)W_m(\beta) - T_m(\beta)Q(\beta)}{P(\beta)W(\beta) - T(\beta)Q(\beta)} \right] \quad (4.10d)$$

The functions $P(\beta)$, $T(\beta)$, $Q(\beta)$, and $W(\beta)$ are the asymptotic limits of $P_m(\beta)$, $T_m(\beta)$, $Q_m(\beta)$, and $W_m(\beta)$, respectively, as $m \rightarrow \infty$. These are

$$P(\beta) = 2\epsilon_r \quad (4.11a)$$

$$T(\beta) = 2\bar{\beta}^2 \quad (4.11b)$$

$$Q(\beta) = \frac{1 - \epsilon_r}{1 - \bar{\beta}^2} \quad (4.11c)$$

$$W(\beta) = \frac{\epsilon_r - \bar{\beta}^2}{1 - \bar{\beta}^2} + 1 \quad (4.11d)$$

It turns out that a_m , b_m , c_m , and d_m can be written in terms of expressions such as $P - P_m$ and $T - T_m$, and that these expressions decay rapidly for large m . Thus, for example

$$P - P_m \sim 2\epsilon_r \left[e^{-(2m-1)\pi d/L} + e^{-(m-1/2)\pi(h-d)/L} \right] \quad (4.12)$$

for large m . Since these terms decay very rapidly, the a_m , b_m , c_m , and d_m coefficients in Equation 4.9 also decay rapidly. Therefore, only a small number of terms are necessary for the summations in Equation 4.8. This is the reason that the method is numerically very efficient.

There is a standard method of solving an equation of the form of Equation 4.8, which appears in a number of texts [46-49], as well as in [5]. We therefore forego the detailed explanation of the solution, and instead quote the result from [5]. The solution to Equation 4.8 is the following matrix equation.

$$\begin{aligned}
& \sum_{m=1}^{\infty} (\hat{k}_p \delta_{pm} - a_m D_{pm} - M_m K_p) \bar{A}_m^{(\epsilon)} \\
& - \sum_{n=1}^{\infty} (b_n D_{pn} + N_n K_p) \bar{A}_n^{(\lambda)} = 0, \quad p = 1, 2, \dots \\
& \sum_{m=1}^{\infty} (-c_m D_{qm} - X_m K_q) \bar{A}_m^{(\epsilon)} \\
& + \sum_{n=1}^{\infty} (\hat{k}_q \delta_{qn} - d_n D_{qn} - Y_n K_q) \bar{A}_n^{(\lambda)} = 0 \quad q = 1, 2, \dots
\end{aligned} \tag{4.13}$$

where δ_{nm} is the Kronecker delta. As before, in the spectral Galerkin technique, the solution for β is found when the determinant of the coefficient matrix vanishes.

Let us identify the missing terms in Equation (4.13). It turns out that

$$M_m = - \frac{a_m \sum_{q=0}^{m-1} P_{mq} I_q}{I_h} \tag{4.14a}$$

$$N_m = - \frac{b_m \sum_{q=0}^{m-1} P_{mq} I_q}{I_h} \tag{4.14b}$$

where P_{mq} is identified by

$$\frac{\cos \hat{k}_m x}{\cos \hat{k}_1 x} = \sum_{q=0}^{m-1} P_{mq} \cos q\theta \tag{4.15}$$

and

$$I_h = \int_0^{\pi} \frac{d\theta}{\sqrt{1 - \alpha_1 - \alpha_2 \cos \theta}} \tag{4.16}$$

$$I_q = \begin{cases} -\int_0^{\pi} \frac{\cos \theta d\theta}{\sqrt{1 - \alpha_1 - \alpha_2 \cos \theta}} & q = 0 \\ \int_0^{\pi} \frac{\sin q\theta \sin \theta d\theta}{\sqrt{1 - \alpha_1 - \alpha_2 \cos \theta}} & q = 1, 2, \dots, m-1 \end{cases} \tag{4.17}$$

We note, furthermore, from Equation (4.13) that

$$X_m = \frac{S_m - M_m Q I_g - (Q a_m - W c_m) E_m}{S - W I_g} \quad (4.18a)$$

$$Y_m = \frac{S'_m - N_m Q I_g - (Q b_m - W d_m) E_m}{S - W I_g} \quad (4.18b)$$

where

$$S = \sum_{n=1}^{\infty} \frac{\sin \hat{k}_n t}{\hat{k}_n} (W - W_n) K_n \quad (4.19a)$$

$$S_m = \sum_{n=1}^{\infty} \frac{\sin \hat{k}_n t}{\hat{k}_n} \left[D_{nm} \{ (Q - Q_n) a_m - (W - W_n) c_m \} + K_n (Q - Q_n) M_m \right] \quad (4.19b)$$

$$S'_m = \sum_{n=1}^{\infty} \frac{\sin \hat{k}_n t}{\hat{k}_n} \left[D_{nm} \{ (Q - Q_n) b_m - (W - W_n) d_m \} + K_n (Q - Q_n) N_m \right] \quad (4.19c)$$

and

$$I_g = \frac{\alpha_2 L}{\sqrt{2\pi^2}} \int_0^{\pi} \ln \left| \frac{\sqrt{1 - \alpha_1 - \alpha_2 \cos \theta'} + \sqrt{1 - \alpha_1 - \alpha_2}}{\sqrt{1 - \alpha_1 - \alpha_2 \cos \theta'} - \sqrt{1 - \alpha_1 - \alpha_2}} \right| \frac{d\theta'}{\sqrt{1 - \alpha_1 - \alpha_2 \cos \theta'}} \quad (4.20)$$

$$E_m = \frac{\alpha_2 L}{\sqrt{2\pi^2}} \left[\sum_{q=1}^{m-1} P_{mq} J_q + P_{m0} J_0 \right] \quad (4.21)$$

where

$$J_0 = - \int_0^{\pi} \ln \left| \frac{\sqrt{1 - \alpha_1 - \alpha_2 \cos \theta'} + \sqrt{1 - \alpha_1 - \alpha_2}}{\sqrt{1 - \alpha_1 - \alpha_2 \cos \theta'} - \sqrt{1 - \alpha_1 - \alpha_2}} \right| \frac{\cos \theta' d\theta'}{\sqrt{1 - \alpha_1 - \alpha_2 \cos \theta'}} \quad (4.22a)$$

$$J_q = \int_0^{\pi} \ln \left| \frac{\sqrt{1 - \alpha_1 - \alpha_2 \cos \theta'} + \sqrt{1 - \alpha_1 - \alpha_2}}{\sqrt{1 - \alpha_1 - \alpha_2 \cos \theta'} - \sqrt{1 - \alpha_1 - \alpha_2}} \right| \frac{\sin q\theta' \sin \theta' d\theta'}{\sqrt{1 - \alpha_1 - \alpha_2 \cos \theta'}} \quad (4.22b)$$

Finally, the last two terms in Equation 4.13 that need to be defined are K_n and D_{nm} . These

are

$$K_n = \frac{2}{L} \int_0^L \frac{\cos \hat{k}_1 x \sin \hat{k}_n x}{\sin \theta} dx \quad (4.23)$$

$$D_{nm} = \frac{2}{L} \int_0^L \cos \hat{k}_1 x \left[\sum_{q=1}^{m-1} P_{mq} \sin q\theta - P_{m0} \frac{\cos \theta}{\sin \theta} \right] \sin \hat{k}_n x dx \quad (4.24)$$

where the variable θ is defined by the coordinate transformation

$$\cos \frac{\pi x}{L} = \alpha_1 + \alpha_2 \cos \theta \quad (4.25)$$

and

$$\alpha_1 = \frac{1}{2} \left[\cos \frac{\pi t}{L} - 1 \right] \quad (4.26a)$$

$$\alpha_2 = \frac{1}{2} \left[\cos \frac{\pi t}{L} + 1 \right] \quad (4.26b)$$

This completes the description of the final solution, which was stated in Equation 4.13.

The integrals shown in Equations 4.16 and 4.17 are well behaved, and can be easily calculated with a numerical quadrature subroutine. The integrals in Equations 4.20 and 4.22, however, have an integrable logarithmic singularity at $\theta' = 0$. We therefore must use a small angle approximation for $\cos \theta'$ inside the logarithm in the region $0 < \theta' < \theta_p$, where $\theta_p \ll 1$, and use an integration routine in the region $\theta_p < \theta' < \pi$.

We now have only to calculate P_{mq} , K_n , and D_{nm} , as shown in Equations 4.15, 4.23, and 4.24. In [5] these terms were calculated only to the second or third order. We now would like to extend the work of [5] by calculating these terms out to the fifth order. These are calculated in the next section.

4.3 Calculation of P_{mq} , K_n , and D_{nm}

In reference [5], Mitra and Itoh calculated P_{mq} , K_n , and D_{nm} to the second or third

order. We would like to extend this work by calculating these terms to the fifth order. For convenience, we repeat the equations from the last section in which these quantities were defined. Hence,

$$\frac{\cos \hat{k}_m x}{\cos \hat{k}_1 x} = \sum_{q=0}^{m-1} P_{mq} \cos q \theta \quad (4.15)$$

$$K_{nm} = \frac{2}{L} \int_0^L \frac{\cos \hat{k}_1 x \sin \hat{k}_n x}{\sin \theta} dx \quad (4.23)$$

$$D_{nm} = \frac{2}{L} \int_0^L \cos \hat{k}_1 x \left\{ \sum_{q=1}^{m-1} P_{mq} \sin q \theta - P_{m0} \frac{\cos \theta}{\sin \theta} \right\} \sin \hat{k}_n x dx \quad (4.24)$$

The calculations of P_{mq} and K_n are straightforward, although somewhat tedious. The results are

$$P_{10} = 1$$

$$P_{20} = 2\alpha_1 - 1$$

$$P_{21} = 2\alpha_2$$

$$P_{30} = 4\alpha_1^2 - 2\alpha_1 - 1 + 2\alpha_2^2$$

$$P_{31} = 8\alpha_1\alpha_2 - 2\alpha_2$$

$$P_{32} = 2\alpha_2^2$$

$$P_{40} = 8\alpha_1^3 - 4\alpha_1^2 - 4\alpha_1 + 1 + 12\alpha_1\alpha_2^2 - 2\alpha_2^2$$

$$P_{41} = 24\alpha_1^2\alpha_2 - 8\alpha_1\alpha_2 - 4\alpha_2 + 6\alpha_2^3$$

$$P_{42} = 12\alpha_1\alpha_2^2 - 2\alpha_2^2$$

$$P_{43} = 2\alpha_2^3$$

$$P_{50} = 16\alpha_1^4 - 8\alpha_1^3 - 12\alpha_1^2 + 4\alpha_1 + 1 + 48\alpha_1^2\alpha_2^2 - 12\alpha_1\alpha_2^2 - 6\alpha_2^2 + 6\alpha_2^4$$

$$P_{51} = 64\alpha_1^3\alpha_2 - 24\alpha_1^2\alpha_2 - 24\alpha_1\alpha_2 + 4\alpha_2 + 48\alpha_1\alpha_2^3 - 6\alpha_2^3$$

$$P_{52} = 48\alpha_1^2\alpha_2^2 - 12\alpha_1\alpha_2^2 - 6\alpha_2^2 + 8\alpha_2^4$$

$$P_{53} = 16\alpha_1\alpha_2^3 - 2\alpha_2^3$$

$$P_{34} = 2\alpha_2^4 \quad (4.27)$$

for P_{mq} , and

$$\begin{aligned} K_1 &= \alpha_2 \\ K_2 &= \alpha_2(1 + 2\alpha_1) \\ K_3 &= \alpha_2(4\alpha_1^2 + 2\alpha_1 - 1 + 2\alpha_2^2) \\ K_4 &= \alpha_2(-1 - 4\alpha_1 - 4\alpha_1^2 + 2\alpha_2^2 + 8\alpha_1^3 + 12\alpha_1\alpha_2^2) \\ K_5 &= \alpha_2(1 - 4\alpha_1 - 12\alpha_1^2 - 6\alpha_2^2 + 8\alpha_1^3 + 12\alpha_1\alpha_2^2 + 16\alpha_1^4 + 48\alpha_1^2\alpha_2^2 + 6\alpha_2^4) \end{aligned} \quad (4.28)$$

for K_n , where α_1 and α_2 were defined in Equation 4.26.

The calculation of D_{nm} requires a rearrangement of terms, because the algebra becomes somewhat involved above $n=2$. Proceeding from Equation 4.24, it can be shown that

$$D_{nm} = \frac{2\alpha_2}{\pi} \sum_{p=0}^{n-1} \sum_{q=0}^{m-1} C_{np} P_{mq} I_{qp} \quad \begin{array}{l} n = 1, 2, \dots \\ m = 1, 2, \dots, n \end{array} \quad (4.29)$$

where C_{np} is defined by

$$\frac{\sin \hat{k}_n x \cos \hat{k}_1 x}{\sin \frac{\pi x}{L}} = \sum_{p=0}^{n-1} C_{np} \cos^p \theta \quad n = 1, 2, \dots \quad (4.30)$$

and I_{qp} is given by

$$I_{qp} = \begin{cases} \int_0^{\pi} -\sin q\theta \cos^{p+1} \theta d\theta & q=0 \\ \int_0^{\pi} \sin q\theta \sin \theta \cos^p \theta d\theta & q=1, 2, \dots \quad p=0, 1, 2, \dots \end{cases} \quad (4.31)$$

The elements C_{np} and I_{qp} are considerably easier to calculate than D_{nm} . We obtain for C_{np}

$$C_{10} = 1/2$$

$$C_{20} = \alpha_1 + 1/2$$

$$C_{21} = \alpha_2$$

$$\begin{aligned}
C_{30} &= \alpha_1 - 1/2 + 2\alpha_2^2 \\
C_{31} &= \alpha_2 + 4\alpha_1\alpha_2 \\
C_{32} &= 2\alpha_2^2 \\
C_{40} &= -1/2 - 2\alpha_1 + 2\alpha_1^2 + 4\alpha_1^3 \\
C_{41} &= -2\alpha_2 + 4\alpha_1\alpha_2 + 12\alpha_1^2\alpha_2 \\
C_{42} &= 2\alpha_2^2 + 12\alpha_1\alpha_2^2 \\
C_{43} &= 4\alpha_2^3 \\
C_{50} &= 1/2 - 2\alpha_1 - 6\alpha_1^2 + 4\alpha_1^3 + 8\alpha_1^4 \\
C_{51} &= -2\alpha_2 - 12\alpha_1\alpha_2 + 12\alpha_1^2\alpha_2 + 32\alpha_1^3\alpha_2 \\
C_{52} &= -6\alpha_2^2 + 12\alpha_1\alpha_2^2 + 48\alpha_1^2\alpha_2^2 \\
C_{53} &= 4\alpha_2^3 + 32\alpha_1\alpha_2^3 \\
C_{54} &= 8\alpha_2^4
\end{aligned} \tag{4.32}$$

and the values of I_{qp} are listed in Table 4.1. By using this method of generating D_{nm} , we reduce slightly the efficiency of the program, by introducing a double summation over p and q . We save, however, a great deal of algebra that would otherwise have to be carried out by hand, so it seems like a small price to pay.

Now that the singular integral equation technique has been formulated and extended to the fifth order; we consider some results in the next section.

Table 4.1. Values of I_{qp} as defined in Equation 4.29.

I_{qp}	p				
	0	1	2	3	4
q 0	0	$-\pi/2$	0	$-3\pi/8$	0
1	$\pi/2$	0	$\pi/8$	0	$\pi/16$
2	0	$\pi/4$	0	$\pi/8$	0
3	0	0	$\pi/8$	0	$3\pi/32$
4	0	0	0	$\pi/16$	0

4.4 Results

The propagation constant of the dominant mode of a shielded microstrip, as shown in Figure 4.1, was calculated with the singular integral equation technique. A comparison is made to results generated from the spectral Galerkin technique, and to the results from Mitra and Itoh [5]. These data are shown in Table 4.2 for three different frequencies. We can make several observations about these data.

It is clear that there is very good agreement between the calculations using the singular integral equation technique and the spectral Galerkin technique. We note, furthermore, that the results are in agreement to within about four significant figures. This extends somewhat the accuracy achieved by Mitra and Itoh, whose results are shown in Table 4.2. This increase in accuracy is due to the larger matrix size that was used in our calculations.

The excellent correlation between the results generated by the singular integral equation and spectral Galerkin techniques is noteworthy because the two methods are of

Table 4.2. Calculation of the dominant mode propagation constant of shielded microstrip as shown in Figure 4.1. These calculations were made with the singular integral equation (SIE) technique and the spectral Galerkin (SG) technique. The notation 2×2 indicates the matrix size in the SIE technique, while the notation $2/50$ indicates that two basis functions and 50 spectral terms were used in the SG technique. For these calculations, $h = 2.0$ mm, $L = 1.75$ mm, $t = d = 0.5$ mm, and $\epsilon_r = 9.0$.

		β (rad/m) at		
		10 GHz	20 GHz	30GHz
SIE, this paper	2×2	525.574	1094.59	1685.50
	4×4	530.007	1108.09	1713.74
	6×6	530.042	1108.25	1714.26
	10×10	530.065	1108.38	1714.61
SIE, Mitra and Itoh [5]	2×2	530.	1100.	1710.
	4×4	531.	1115.	1740.
SG, this paper	$2/50$	530.272	1108.94	1715.56
	$5/100$	530.166	1108.66	1715.10

very different natures. It was not clear, based on previous work, that the spectral Galerkin technique could be used to generate the dominant mode propagation constant to such a high degree of accuracy.

An attempt was made to calculate higher-order evanescent modes with the singular integral equation technique. This, in theory, is easy to do by changing the propagation constant from purely real to purely imaginary. In practice, it turns out that the determinant function that must go through zero is ill-behaved, and does not have any clear zeros. Thus, the method doesn't seem to work for evanescent modes. One explanation for this result could be that we have only calculated enough matrix elements to fill a 10×10 matrix. We could, of course, have calculated more elements, but the amount of algebra required to do so tends to become very large, very fast. This places a practical limit on the matrix size.

4.5 Conclusion

Although the original goal of the singular integral equation technique, that of finding higher-order evanescent modes, was not met, we did achieve excellent success in verifying the propagation constant of the propagating modes. In doing so, we have demonstrated agreement between two very different methods, the singular integral equation method and the spectral Galerkin technique, to four significant figures in the final answer. This degree of accuracy is very high, given the complexity of the calculation and the very different natures of the two methods used for the comparison.

CHAPTER 5

COUPLED-MODE ANALYSIS OF MULTICONDUCTOR MICROSTRIP LINES

5.1 Introduction

Recent advances in microelectronic packaging have generated a number of difficulties associated with interconnections between VLSI logic devices. These interconnections are typically made with large numbers of microstrip lines that run parallel to each other. It is possible, under certain conditions, that a signal propagating on one line can couple to other lines. This cross-talk can trigger false signals on nearby lines. Therefore, it is important to fully analyze multiple microstrip lines, in order to determine the performance of the overall system. These cross-talk problems become more serious as switching speeds and packing densities are increased.

Coupled microstrip lines have been analyzed with several different methods [6,7,50,51]. More recently, multiconductor transmission lines with more than two lines have received some attention [52,53]. These analyses, however, are all based on a quasi-static approximation which is valid only for digital devices with switching speeds in the order of one nanosecond. When the rise time of the switching pulse is reduced to hundreds of picoseconds, the spectral content of the pulse contains higher-frequency components. Since quasi-static approximations break down at high frequencies, a full-wave analysis of multiconductor microstrip transmission lines becomes necessary.

The configuration under study is shown in Figure 5.1. It is composed of five microstrip lines, each of the same width and strip separation. In this chapter we would like to demonstrate, using a frequency-dependent analysis, the mechanism whereby current that is excited on one line is transferred to other lines. We begin with an analysis of the modes of propagation on the line.

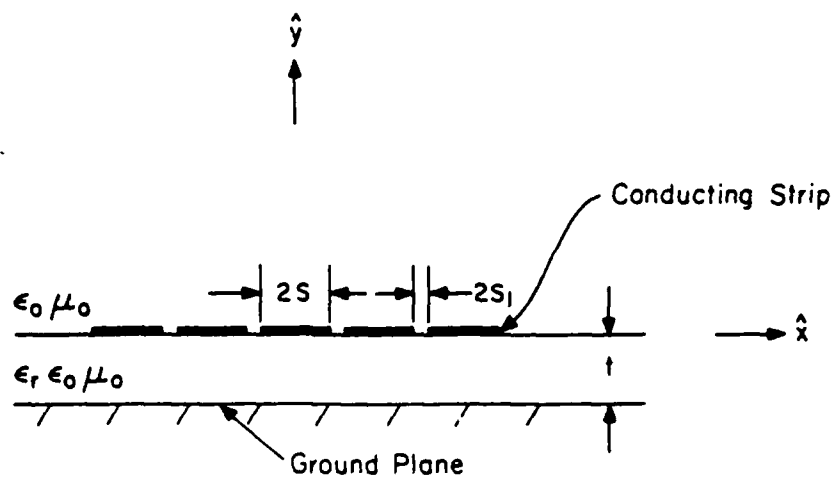


Figure 5.1. Configuration of microstrip with five lines. For these calculations, $t = 2s = 1$ mm, $2s_1 = 0.2$ mm, and $\epsilon_r = 10$.

5.2 Calculation of Modes

In a multiple microstrip configuration with N strips, there are N modes of propagation down these lines. In order to analyze the crosstalk and propagation delay of these lines, the propagation constant for each of the N propagating modes is needed. The method we use for this calculation is the spectral Galerkin technique, described in Chapter 2. By making a number of alterations, the same theory can handle multiple lines as well as a single one.

We begin the analysis with the matrix equation generated by the spectral Galerkin technique for a single shielded line. This equation was given previously in Equation 2.16, for the configuration shown in Figure 2.1. In order to remove the top wall, we make a modification in the spectral Green's function. This is done by replacing the short circuits in the equivalent transmission lines, at $y = h - d$, shown in Figure 2.3, with matched loads. The side walls, on the other hand, are removed by moving them far enough away from the strips that they have no effect. Care must be taken, however, not to move them too far away, since the number of spectral terms required for this calculation can become large with wide side walls.

All that remains now is to generate a reasonable set of basis functions for the current on the lines. We choose to build our basis functions up from a set of functions that would be suitable for finding the odd and even modes in a microstrip containing only a single strip. These building block functions are

$$\begin{aligned} \xi_{ei}(x) &= \frac{\cos((i-1)\pi(x/s+1))}{\sqrt{1-(x/s)^2}} & \eta_{ei}(x) &= \frac{\sin((i-1/2)\pi(x/s+1))}{\sqrt{1-(x/s)^2}} \\ \xi_{oi}(x) &= \frac{\cos((i-1/2)\pi(x/s+1))}{\sqrt{1-(x/s)^2}} & \eta_{oi}(x) &= \frac{\sin(i\pi(x/s+1))}{\sqrt{1-(x/s)^2}} \end{aligned} \quad (5.1)$$

We note that ξ_{ei} and η_{oi} are the same basis functions used for the even modes in a single line in Chapter 2. These were given in Equation 2.22 and shown in Figures 2.6 and 2.7.

We now take advantage of the symmetry inherent in the structure to find basis

functions that are either even in J_z and odd in J_x , or odd in J_z and even in J_x . Although the method that follows is general for N lines, we show as an example the basis functions used for five lines as

$$\begin{aligned} J_z(x) &= \sum_{j=1}^{N_z} \sum_{i=1}^5 c_{ij} P_{ij}(x) \\ J_x(x) &= \sum_{j=1}^{N_x} \sum_{i=1}^5 d_{ij} Q_{ij}(x) \end{aligned} \quad (5.2)$$

where, for even J_z and odd J_x

$$\begin{aligned} P_{1i}(x) &= \xi_{ei}(x) & Q_{1i}(x) &= \eta_{oi}(x) \\ P_{2i}(x) &= \xi_{ei}(x+q) + \xi_{ei}(x-q) & Q_{2i}(x) &= \eta_{oi}(x+q) + \eta_{oi}(x-q) \\ P_{3i}(x) &= \xi_{oi}(x+q) - \xi_{oi}(x-q) & Q_{3i}(x) &= \eta_{ei}(x+q) - \eta_{ei}(x-q) \\ P_{4i}(x) &= \xi_{ei}(x+2q) + \xi_{ei}(x-2q) & Q_{4i}(x) &= \eta_{oi}(x+2q) + \eta_{oi}(x-2q) \\ P_{5i}(x) &= \xi_{oi}(x+2q) - \xi_{oi}(x-2q) & Q_{5i}(x) &= \eta_{ei}(x+2q) - \eta_{ei}(x-2q) \end{aligned} \quad (5.3a)$$

and for odd J_z and even J_x ,

$$\begin{aligned} P_{1i}(x) &= \xi_{oi}(x) & Q_{1i}(x) &= \eta_{ei}(x) \\ P_{2i}(x) &= \xi_{ei}(x+q) - \xi_{ei}(x-q) & Q_{2i}(x) &= \eta_{oi}(x+q) - \eta_{oi}(x-q) \\ P_{3i}(x) &= \xi_{oi}(x+q) + \xi_{oi}(x-q) & Q_{3i}(x) &= \eta_{ei}(x+q) + \eta_{ei}(x-q) \\ P_{4i}(x) &= \xi_{ei}(x+2q) - \xi_{ei}(x-2q) & Q_{4i}(x) &= \eta_{oi}(x+2q) - \eta_{oi}(x-2q) \\ P_{5i}(x) &= \xi_{oi}(x+2q) + \xi_{oi}(x-2q) & Q_{5i}(x) &= \eta_{ei}(x+2q) + \eta_{ei}(x-2q) \end{aligned} \quad (5.3b)$$

where

$$q = 2(s + s_1) \quad (5.4)$$

With these basis functions, we now search for the three even-mode and two odd-mode propagation constants that satisfy Equation 2.16. Results showing dispersion curves and comparisons to the quasi-static theory are presented in Section 5.4.

Let us now turn to the coupled mode theory used to explain the transfer of current between lines.

5.3 Coupled-mode Theory

When a single line of an N-line system is excited, one may consider this to be an excitation of a linear combination of the five modes, whose weighting coefficients must be determined. We may consider the integral of J_z over an individual strip to be the quantity that is coupled between the lines. Therefore, we carry out a procedure similar to that described by Bhartia and Bahl [54] for image guide couplers. For each mode, we find the longitudinal current on strip i due to mode j as

$$I_{ji} = \int_{\text{strip } i} J_{zj}(x) dx \quad i, j = 1, \dots, 5 \quad (5.5)$$

We consider an excitation of the first line alone to be one where the first line has a magnitude of one and the others have a magnitude of zero at $z = 0$. Therefore, we set up a fifth-order linear equation to find the combination of modes that satisfies the condition

$$\sum_{j=1}^5 a_j I_{ji} = \begin{cases} 1 & i = 1 \\ 0 & i = 2, \dots, 5 \end{cases} \quad (5.6)$$

where the a_j 's are the unknown mode coefficients.

Once the mode coefficients are determined, we may assume they propagate down the five-line system, with their respective propagation constants and mode coefficients that were calculated in the previous section. Thus,

$$I_i'(z) = \sum_{j=1}^5 a_j I_{ji} e^{-j\beta_j z} \quad (5.7)$$

where β_j is the propagation constant of the j^{th} mode, and $I_i'(z)$ is the current on the i^{th} strip due to all j modes, at a distance z from the original excitation. This can be calculated

for each strip as a function of z , and results are shown in the next section.

5.4 Results

Let us now examine the results obtained with the method described above. The first step of the procedure involved calculating the propagation constants of the various propagating modes associated with the configuration in Figure 5.1. We have calculated the modes at 1 GHz for a three-line configuration using the spectral Galerkin technique, and then we compare them to those of Chan's quasi-static approach [53]. This comparison is shown in Table 5.1. At this comparatively low frequency, the two methods are in excellent agreement. At higher frequencies, however, the quasi-static method is expected to break down.

This point is demonstrated in Figure 5.2, where the five propagation constants of a five-strip system are plotted as a function of frequency. At low frequencies, the curves are level, as would be expected by quasi-static theory. At higher frequencies, however, the relative propagation constants squared are no longer constant, indicating that a frequency-dependent theory is now necessary.

Next, we checked the convergence of the calculated propagation constants with respect to the number of modes. These results, shown in Table 5.2, demonstrate a very rapid convergence with respect to the number of modes and suggest that probably one basis function of each type ($N_z = N_x = 1$) will be sufficient for most calculations.

Table 5.1. Comparison of propagation constants calculated by two different methods. Shown here are the two even and one odd modes of a three-microstrip system at 1 GHz, where $t = 2s = 1$ mm, and $2s_1 = 0.2$ mm.

	Spectral Galerkin	Quasi-static
β_{e1} (rad/m)	50.53	50.61
β_{e2}	58.12	58.60
β_o	52.80	52.88

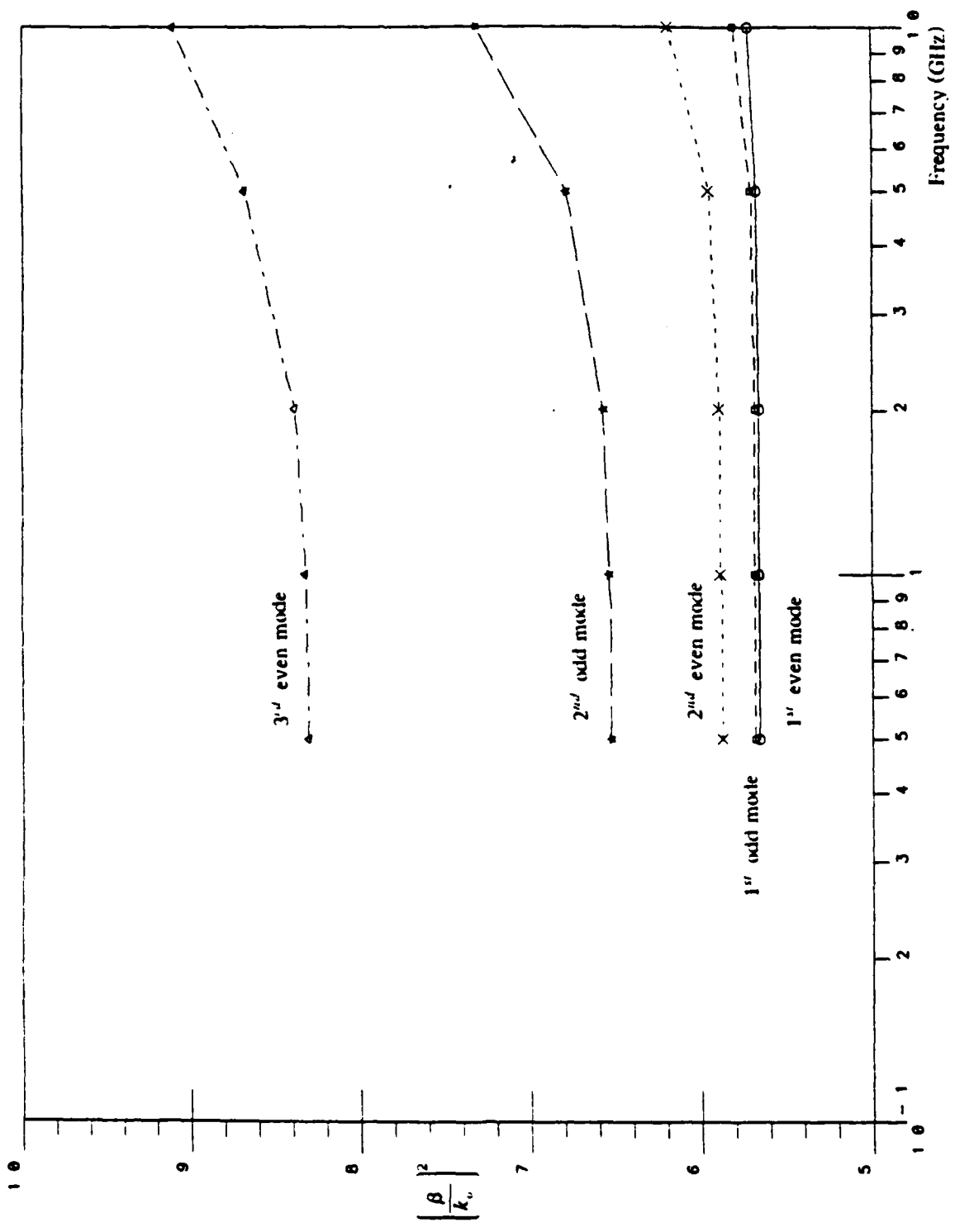


Figure 5.2. Dispersion curves for the first five modes of propagation of a microstrip with five lines. The dimensions are the same as those in Figure 5.1.

Table 5.2. Variation of the five propagation constants in a five line system with the number of basis functions. For this configuration, $t = 2s = 1$ mm, $2s_1 = 0.2$ mm, and $f=1$ GHz.

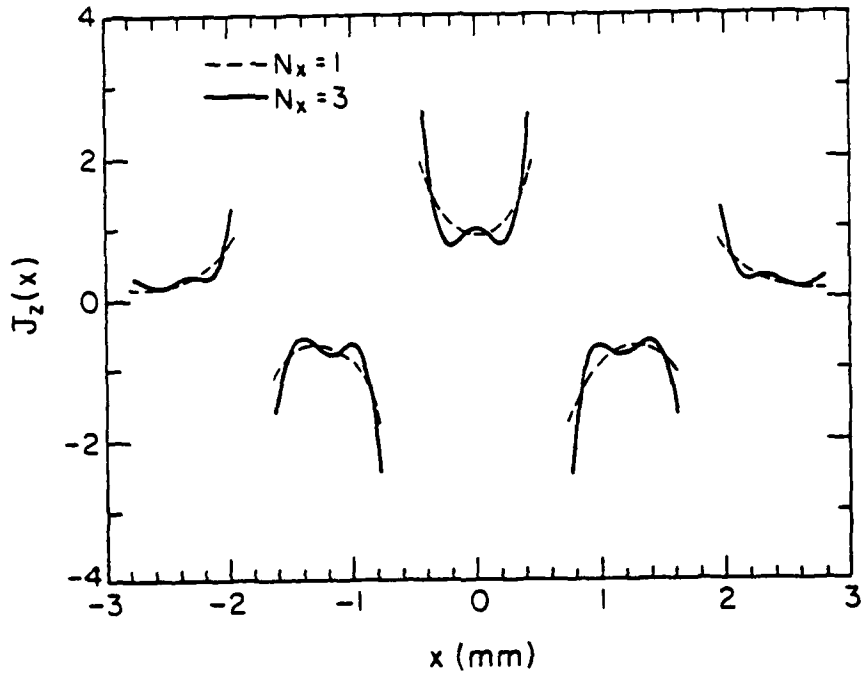
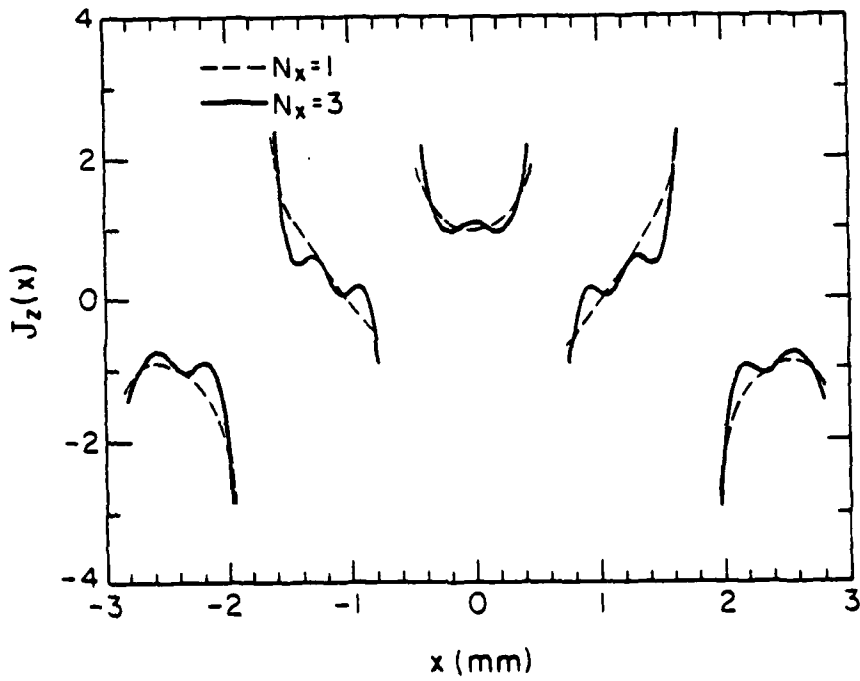
$N_z = N_x$	$\beta_{e,1}$	$\beta_{e,2}$	$\beta_{e,3}$	$\beta_{o,1}$	$\beta_{o,2}$
1	49.86	50.83	60.50	49.97	53.58
2	49.45	50.77	60.40	49.75	53.57
3	49.42	50.77	60.40	49.73	53.57

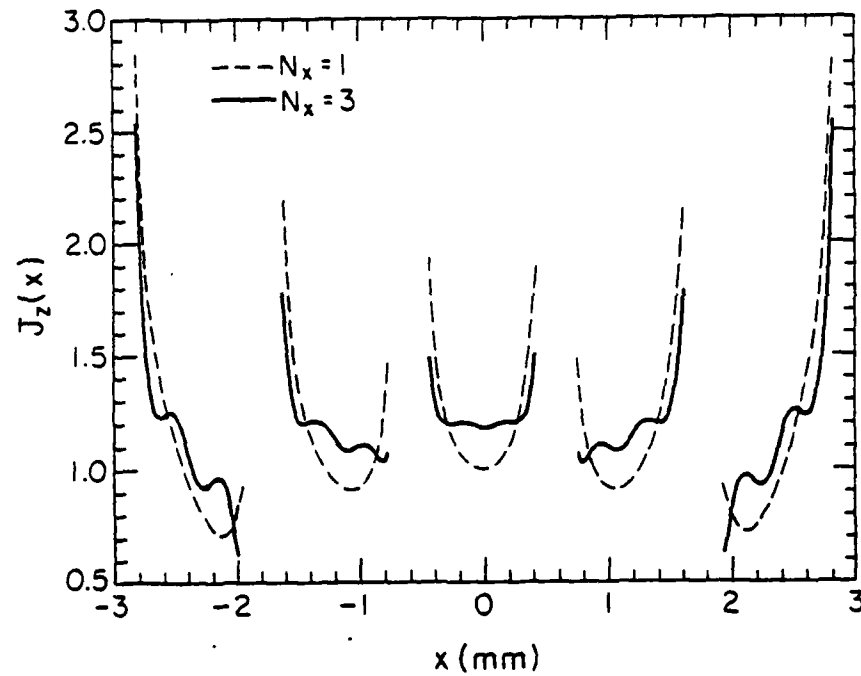
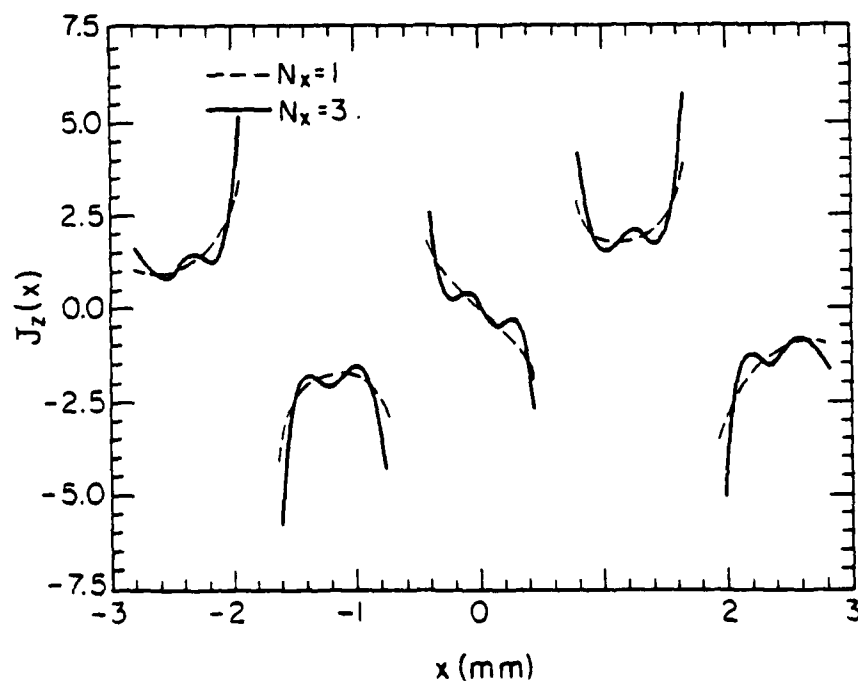
In order to get a physical feel for the shape of the five modes, we have plotted J_z as a function of x over a cross section of the strip for each of the five modes. These are shown in Figures 5.3-5.7 for $N_z = N_x = 1$ and for $N_z = N_x = 3$. We note that for most of the modes, we may obtain a very reasonable representation of the currents with just one basis function of each type.

Finally, we demonstrate the coupling of current from one strip to the next. In Figure 5.8, we present results for the configuration of Figure 5.1 at 1 GHz, and of Figure 5.9 at 10 GHz. We start with a unit excitation on the first strip and note that the current on the first strip very rapidly decreases, while the current on the other strips rapidly increases. Thus, when microstrips are closely spaced, the coupling between strips is predicted to be quite severe.

5.5 Conclusion

In this chapter, a frequency-dependent method of calculating the coupling between a large number of parallel microstrips has been demonstrated. Using this method, it has been shown that coupling between closely spaced lines can be quite severe. This has significance in the area of VLSI interconnectivity, where parallel microstrip lines are packed as densely as possible.

Figure 5.3. $J_z(x)$ for the first even mode.Figure 5.4. $J_z(x)$ for the second even mode.

Figure 5.5. $J_z(x)$ for the third even mode.Figure 5.6. $J_z(x)$ for the first odd mode.

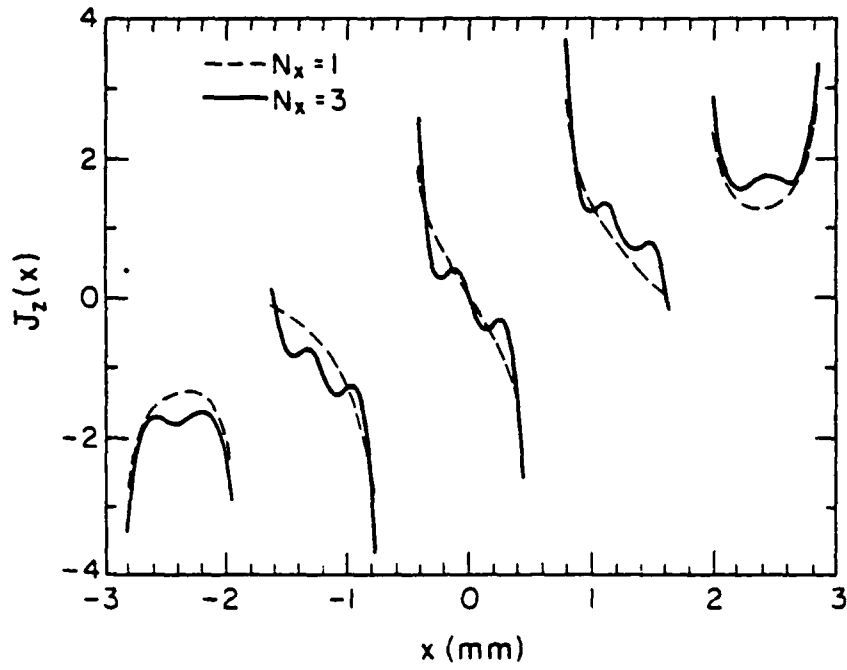


Figure 5.7. $J_z(x)$ for the second odd mode.

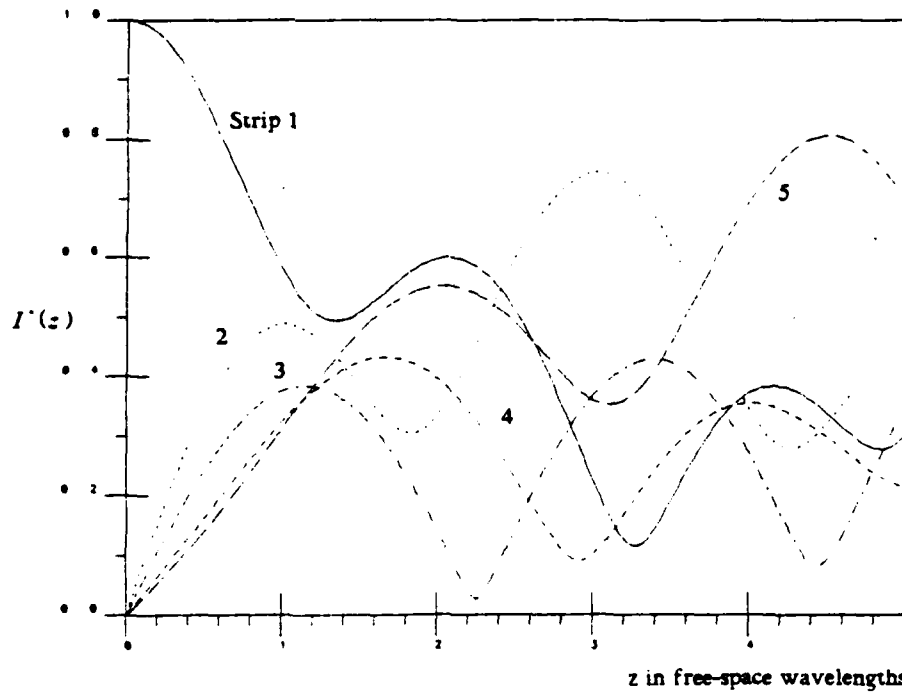


Figure 5.8. Variation of I with z at 1 GHz for each of the five strips.

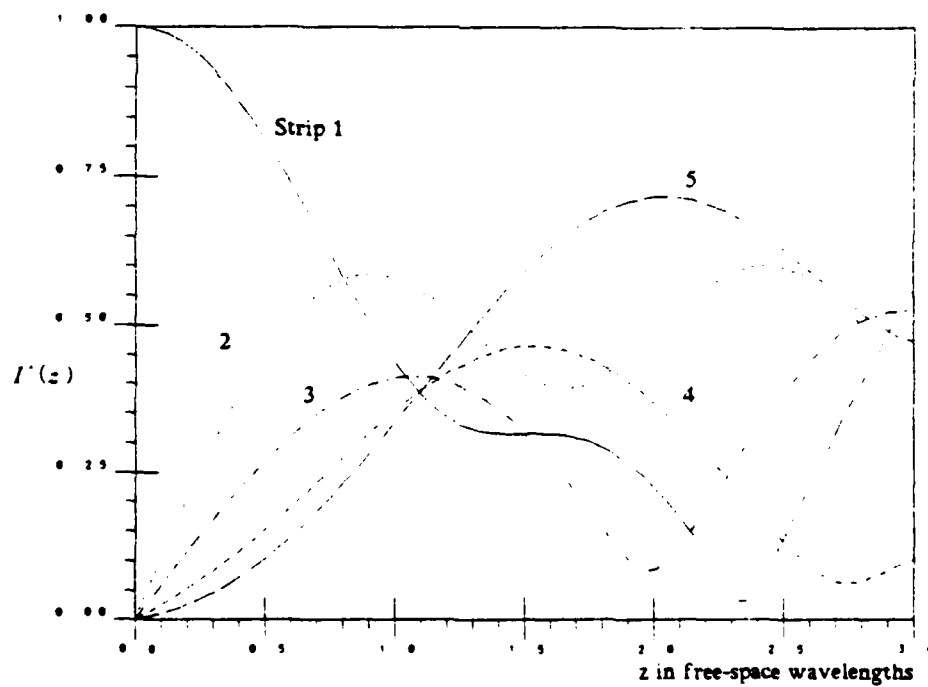


Figure 5.9. Variation of I with z at 10 GHz for each of the five strips.

CHAPTER 6

SUMMARIES OF OTHER ACTIVITIES AND IMPORTANT RESULTS

Other activities in this effort that have been reported previously in various technical reports have included the study of coplanar transmission lines [55, 56] and fin lines [57, 58] and the investigation of dielectric antennas for millimeter-wave imaging applications [59]. In addition, a study of planar waveguides and components for millimeter-wave integrated circuits has been carried out [60]. In Ref. 60, the problem of discontinuities in planar guides has been treated using the generalized variational method and the conjugate gradient technique.

Summarizing the important results, we have shown that the spectral Galerkin method is useful for calculating the evanescent as well as propagating modes in a shielded microstrip. We have demonstrated that the accuracy of these modes is quite reasonable; the field distributions corresponding to these modes have been plotted to provide a physical insight of their structures.

Next, these modes have been used in a mode-matching analysis to calculate the scattering from discontinuities in various microstrip configurations. Again, reasonable results have been obtained for single and cascaded discontinuities; however, the problem of accurately calculating the junction capacitance has presented some difficulties that have yet to be overcome.

We conjecture that this is due primarily to our inability to calculate a sufficient number of modes with enough accuracy, as evidenced by our check on the orthogonality of these modes. In addition, the matrix generated by these modes was also found to be ill-conditioned.

Next, we investigated an alternate method, viz., the Singular Integral Equation technique, for calculating the modes in a shielded microstrip line. The calculated values of the propagation constant of the dominant mode were in agreement to four significant

figures, with results generated with the spectral Galerkin technique. This degree of accuracy is exceptional, because the two methods that are being compared are quite different. An attempt was made to calculate evanescent modes using the singular integral equation technique, but these modes were not found. One possible explanation was that the size of the matrix we could use was too small. Using a larger matrix was not practical because the complexity of the matrix elements increases rapidly with matrix size.

The generalized variational method and the conjugate gradient method, both of which are iterative techniques, have been employed to derive the solution to the discontinuity problems in planar guides, but they have also yielded only limited success in terms of the realized accuracy of the results. Thus, our conclusion is that further effort in this direction is critically needed.

Finally, the dielectric antenna we have developed has been demonstrated to be useful as an array element of an imaging system at 80 GHz and 220 GHz. Again, a monolithic imaging system would be better suited for this purpose and it would be worthwhile, in the future, to investigate such a monolithic system.

LIST OF PUBLICATIONS AND TECHNICAL REPORTS

Publications

1. Y. Hayashi and R. Mittra. "An analytical investigation of finlines with magnetized ferrite substrate." *IEEE Trans. Microwave Theory Tech.*, vol. MTT-31, no. 67, pp. 495-498, June 1983.
2. N. Deo and R. Mittra. "A technique for analyzing planar dielectric waveguides for millimeter wave integrated circuits." *AEU*, Band 37, Heft 7/8, July/Aug. 1983, pp. 236-244.
3. K. Webb and R. Mittra. "Dielectric waveguide grating filter." *AEU*, Band 38, Heft 1, pp. 51-54, Jan./Feb., 1984.
4. T. Kitazawa and R. Mittra. "An investigation of striplines and fin lines with periodic stubs." *IEEE Trans. Microwave Theory Tech.*, vol. MTT-32, no. 7, pp. 684-688, July 1984.
5. T. Kitazawa and R. Mittra. "Analysis of finline with finite metallization thickness." *IEEE Trans. Microwave Theory Tech.*, vol. MTT-32, no. 11, pp. 1484-1487, November 1984.
6. E. Farr, K. Webb and R. Mittra. "Studies in fin-line antenna design for imaging array applications." *AEU*, Band 39, Heft 2, pp. 87-89, March/April 1985.
7. T. Kitazawa and R. Mittra. "Analysis of Asymmetric Coupled Striplines." *IEEE Trans. Microwave Theory Tech.*, vol. MTT-33, no. 7, pp. 643-646, July 1985.
8. T. Kitazawa and R. Mittra. "Quasi-static characteristics of asymmetrical and coupled coplanar-type transmission lines." *IEEE Trans. Microwave Theory Tech.*, vol. MTT-33, no. 9, pp. 771-778, September 1985.
9. K. J. Webb and R. Mittra. "A variational solution of the fin-line discontinuity problem." *Proceedings of the 15th European Microwave Conference*, September 1985.

AD-A161 444

MILLIMETER-WAVE INTEGRATED CIRCUITS(U) ILLINOIS UNIV AT
URBANA ELECTROMAGNETIC COMMUNICATION LAB R MITTRA
OCT 85 UIEC-85-8 ARO-18054. 16-EL DAAG29-82-K-0004

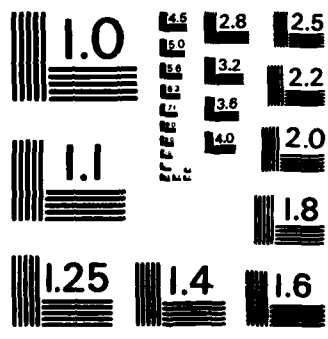
2/2

UNCLASSIFIED

F/G 9/5

NL





MICROCOPY RESOLUTION TEST CHART
NATIONAL BUREAU OF STANDARDS - 1963 - A

10. K. Webb, E. Farr and R. Mittra, "A note on the numerical solution for finline and microstrip modes," to be published in *IEEE Trans. Microwave Theory Tech.*
11. E. Farr, C. Chan and R. Mittra, "A frequency-dependent coupled-mode analysis of multiconductor microstrip lines with application to VLSI interconnection problems," to be published in *IEEE Trans. Microwave Theory Tech.*
12. K. Webb and R. Mittra, "Solution of the fin-line discontinuity problem using the generalized variational technique," to be published in *IEEE Trans. Microwave Theory Tech.*

Technical Reports

1. Y. Hayashi and R. Mittra, "An analytical investigation of fin lines with magnetized ferrite substrate," EM Lab Report 82-4, University of Illinois, June 1982.
2. J. S. Wilson and R. Mittra, "Analysis of fin-line at millimeter wavelengths," EM Lab Report 82-6, University of Illinois, July 1982.
3. Y. Hayashi, E. Farr and R. Mittra, "Analysis of dominant and higher-order modes in unilateral fin lines," EM Lab Report 82-9, University of Illinois, August 1982.
4. K. Webb and R. Mittra, "Dielectric waveguide grating filter," EM Lab Report 82-11, University of Illinois, November 1982.
5. T. N. Trinh and R. Mittra, "Analysis of the suspended H-waveguide and other related dielectric waveguide structures," EM Lab Report 83-1, University of Illinois, January 1983.
6. T. Kitazawa and R. Mittra, "Analysis of fin-lines with the finite metallization thickness," EM Lab Report 83-11, University of Illinois, October 1983.
7. T. Kitazawa and R. Mittra, "An investigation of strip lines and fin lines with periodic stubs," EM Lab Report 83-13, University of Illinois, October 1983.
8. E. Farr, K. Webb and R. Mittra, "Studies in fin-line antenna design for phased array applications," EM Lab Report 83-14, University of Illinois, November 1983.

9. T. Kitazawa and R. Mittra. "Asymmetrical coplanar transmission lines." EM Lab Report 84-9. University of Illinois. June 1984.
10. K. Webb and R. Mittra. "Investigation of planar waveguides and components for millimeter-wave integrated circuits." EM Lab Report 84-3. University of Illinois. October 1984.
11. S. H. Doran and R. Mittra. "An experimental study of dielectric rod antennas for millimeter-wave imaging applications." EMC Lab Report 85-3. University of Illinois. March 1985.
12. T. Kitazawa and R. Mittra. "Quasistatic characteristics of asymmetrical and coupled coplanar-type transmission lines." EMC Lab Report 85-4. University of Illinois. April 1985.

SCIENTIFIC PERSONNEL AND DEGREES AWARDED**Scientific Personnel**

Professor Raj Mittra, Principal Investigator

Visiting Scholars

Dr. Y. Hayashi
Dr. T. Kitazawa
Dr. Z. Pantic

Research Students

Mr. Sunil Bhooshan
Mr. Chi Chan
Mr. Albert Chang
Mr. Sean Doran
Mr. Everett Farr
Mr. Ben Halpern
Mr. Charles Smith
Mr. Trang Trinh
Mr. Kevin Webb
Mr. Scott Wilson

Theses

1. "Analysis of fin-line at millimeter wavelengths." M.S. thesis, John S. Wilson, May 1982.
2. "Analysis of the suspended H-waveguide and other related dielectric waveguide structures." Ph.D. thesis, Trang N. Trinh, December 1982.
3. "Investigation of planar waveguides and components for millimeter-wave integrated circuits." Ph.D. thesis, Kevin J. Webb, August 1984.
4. "A novel technique for the analysis of dielectric waveguides." Ph.D. thesis, Sunil V. Bhooshan, January 1985.
5. "Analysis of microstrip discontinuities using the finite element method." M.S. thesis, Albert H. Chang, January 1985.
6. "An experimental study of dielectric rod antennas for millimeter-wave imaging applications." M.S. thesis, Sean H. Doran, January 1985.
7. "An investigation of modal characteristics and discontinuities in printed circuit transmission lines." Ph.D. thesis, Everett G. Farr, August 1985.

REFERENCES

- [1] T. Itoh and R. Mittra, "Spectral domain approach for calculating the dispersion characteristics of microstrip lines," *IEEE Trans. Microwave Theory Tech.*, vol. MTT-19, pp. 30-39, Jan. 1971.
- [2] T. Itoh and R. Mittra, "A technique for computing dispersion characteristics of shielded microstrip lines," *IEEE Trans. Microwave Theory Tech.*, vol. MTT-22, pp. 896-898, Oct. 1974.
- [3] R. Mittra and S.W. Lee, *Analytical Techniques in the Theory of Guided Waves*. New York: Macmillan, 1971.
- [4] A. Wexler, "Solution of waveguide discontinuities by modal analysis," *IEEE Trans. Microwave Theory Tech.*, vol. MTT-15, pp. 508-517, Sept. 1967.
- [5] R. Mittra and T. Itoh, "A new technique for the analysis of the dispersion characteristics of microstrip lines," *IEEE Trans. Microwave Theory Tech.*, vol. MTT-19, pp. 47-56, Jan. 1971.
- [6] H.A. Wheeler, "Transmission line properties of parallel strips separated by a dielectric sheet," *IEEE Trans. Microwave Theory Tech.*, vol. MTT-13, pp. 172-175, Mar. 1965.
- [7] T.G. Bryant and J.A. Weiss, "Parameters of microstrip transmission lines and of coupled pairs of microstrip lines," *IEEE Trans. Microwave Theory Tech.*, vol. MTT-16, pp. 1021-1027, Dec. 1968.
- [8] R.D. Ward, "Application of Galerkin's Method for Analyzing Microstrip Transmission Line," M.S. Thesis, University of Illinois at Urbana-Champaign, 1971.
- [9] Y. Rahmat-Samii, "Application of Fourier and Galerkin Techniques for Analyzing Discontinuities and Coupling Phenomena in Microstrip Lines," M.S. Thesis, University of Illinois at Urbana-Champaign, 1972.
- [10] E. Yamashita and K. Atsuki, "Analysis of microstrip-like transmission lines by nonuniform discretization of integral equations," *IEEE Trans. Microwave Theory Tech.*, vol. MTT-24, pp. 194-200, Apr. 1976.
- [11] A.-M. A. El Sherbiny, "Exact analysis of shielded microstrip lines and bilateral fin-lines," *IEEE Trans. Microwave Theory Tech.*, vol. MTT-29, pp. 669-675, July 1981.
- [12] D. Mirshekar-Syahkal and J. Brian Davies, "Accurate solution of microstrip and coplanar structures for dispersion and for dielectric and conductor losses," *IEEE Trans. Microwave Theory Tech.*, vol. MTT-27, pp. 694-699, July 1979.

- [13] T. Itoh, "Spectral domain immittance approach for dispersion characteristics of generalized printed transmission lines." *IEEE Trans. Microwave Theory Tech.*, vol. MTT-28, pp. 733-736, July 1980.
- [14] J.B. Knorr and P.M. Shayda, "Millimeter-wave fin-line characteristics." *IEEE Trans. Microwave Theory Tech.*, vol. MTT-28, pp. 737-743, July 1980.
- [15] L.P. Schmidt and T. Itoh, "Spectral domain analysis of dominant and higher-order modes in fin-lines." *IEEE Trans. Microwave Theory Tech.*, vol. MTT-28, pp. 981-985, Sept. 1980.
- [16] L.P. Schmidt, T. Itoh, and H. Hofmann, "Characteristics of unilateral fin-line structures with arbitrarily located slots." *IEEE Trans. Microwave Theory Tech.*, vol. MTT-29, pp. 352-355, Apr. 1981.
- [17] M. Helard et al., "Exact calculations of scattering parameters of a step slot width discontinuity in a unilateral fin-line." *Electron. Lett.*, vol. 19, pp. 537-539, July 7, 1983.
- [18] R.F. Harrington, *Time Harmonic Electromagnetic Fields*. New York: McGraw Hill, 1961, pp. 129-132.
- [19] H. Bateman, *Tables of Integral Transforms* vol. 1. New York: McGraw Hill, 1954, p. 139.
- [20] F. Arndt and G.V. Paul, "The reflection definition of the characteristic impedance of microstrips." *IEEE Trans. Microwave Theory Tech.*, vol. MTT-27, pp. 724-731, Aug. 1979.
- [21] R.H. Jansen, "Unified user-oriented computation of shielded, covered, and open planar microwave and millimeter-wave transmission-line characteristics." *IEEE Proc. Pt. H, Microwaves Opt. Acoust.*, vol. MOA-1, pp. 14-22, Jan. 1979.
- [22] B. Bianco et al., "Some considerations about the frequency dependence of uniform microstrips." *IEEE Trans. Microwave Theory Tech.*, vol. MTT-26, pp. 182-185, Mar. 1978.
- [23] W.J. Getsinger, "Microstrip characteristic impedance." *IEEE Trans. Microwave Theory Tech.*, vol. MTT-27, p. 293, Apr. 1979.
- [24] R.F. Harrington, *Time Harmonic Electromagnetic Fields*. New York: McGraw Hill, 1960, pp. 458-459.
- [25] P.E. Mayes, *Electromagnetics for Engineers*. Ann Arbor: Edwards Bros., 1965, pp. 63-65.

- [26] D.W. Dearholt and W.R. McSpadden, *Electromagnetic Wave Propagation*. New York: McGraw Hill, 1973, p. 151.
- [27] A. Farrar and A.T. Adams, "Matrix methods for microstrip three-dimensional problems." *IEEE Trans. Microwave Theory Tech.*, vol. MTT-20, pp. 497-504, Aug. 1982.
- [28] P. Benedek and P. Silvester, "Equivalent capacitances for microstrip gaps and steps." *IEEE Trans. Microwave Theory Tech.*, vol. MTT-20, pp. 729-733, Nov. 1972.
- [29] R. Horton, "Equivalent representation of an abrupt impedance step in microstrip line." *IEEE Trans. Microwave Theory Tech.*, vol. MTT-21, pp. 562-564, Aug. 1973.
- [30] A. Gopinath, A.F. Thompson, and I.M. Stephenson, "Equivalent circuit parameters of microstrip step change in width and cross junctions." *IEEE Trans. Microwave Theory Tech.*, vol. MTT-24, pp. 144, March 1976.
- [31] I. Wolf, G. Kompa, and R. Mehran, "Calculation method for microstrip discontinuities and T-junctions." *Electron. Lett.*, vol. 8, pp. 177-179, April 1972.
- [32] G. Kompa, "S-matrix computation of microstrip discontinuities with a planar waveguide model." *Arch. Elek. Ubertragung.*, vol. 30, pp. 58-64, 1975.
- [33] W. Menzel and I. Wolff, "A method for calculating the frequency-dependent properties of microstrip discontinuities." *IEEE Trans. Microwave Theory Tech.*, vol. MTT-25, pp. 107-112, Feb. 1977.
- [34] Y.C. Shih, T.S. Chu, and T. Itoh, "Comparative study of mode matching formulations for microstrip discontinuities." *IEEE MTT-S International Microwave Symposium Digest*, pp. 435-438, June 1985.
- [35] R. Lampe, "Discontinuities in Suspended Substrate Strip Transmission Lines." Ph.D. Thesis, University of Illinois at Urbana-Champaign, 1983.
- [36] H. El Hennawy and K. Schunemann, "Impedance transformation in fin-lines." *IEEE Proc. Pt. H, Microwaves, Opt. Acoust.*, vol. 129, pp. 342-350, Dec. 1982.
- [37] H. El Hennawy and K. Schunemann, "Hybrid fin-line matching structures." *IEEE Trans. Microwave Theory Tech.*, vol. MTT-30, pp. 2132-2139, Dec. 1982.
- [38] K. Webb, "Investigation of Planar Waveguides and Components for Millimeter Wave Applications." Ph.D. Thesis, University of Illinois at Urbana-Champaign, 1984.
- [39] R.E. Collin, *Field Theory of Guided Waves*. New York: McGraw Hill, 1960, pp. 174-179.

- [40] C.A. Klein and R. Mittra, "Stability of matrix equations arising in electromagnetics." *IEEE Trans. Antennas Propagat.*, vol. AP-21, pp. 902-905, Nov. 1973.
- [41] R. Mittra, ed., *Numerical and Asymptotic Techniques in Electromagnetics*. Berlin: Springer-Verlag, 1975, pp. 129-134.
- [42] R. Hall, Ph.D. Thesis, University of Illinois at Urbana-Champaign, (to be published).
- [43] U. Feldman, "Characterization of Microstrip Discontinuities in the Time and Frequency Domains." M.S. Thesis, University of Illinois, 1985, p. 40.
- [44] A.S. Omar and K. Schunemann, "Space-domain decoupling of LSE and LSM fields in generalized planar guiding structures." *IEEE Trans. Microwave Theory Tech.*, vol. MTT-32, pp. 1626-1632, Dec. 1984.
- [45] A.S. Omar and K. Schunemann, "Formulation of the singular integral equation technique for general planar transmission lines." *IEEE MTT-S International Microwave Symposium Digest*, pp. 135-138, June 1985.
- [46] L. Lewin, *Advanced Theory of Waveguides*. London: Iliffe, 1951.
- [47] L. Lewin, "The use of singular integral equations in the solution of waveguide problems." in *Advances in Microwaves*, vol. 1, L. Young, Ed. New York: Academic Press, 1966, pp. 212-284.
- [48] L. Lewin, *Theory of Waveguides*. New York: Wiley, 1975.
- [49] F.G. Tricomi, *Integral Equations*. New York: Interscience, 1957, pp. 161-217.
- [50] E. Yamashita and R. Mittra, "Variational method for the analysis of microstrip lines." *IEEE Trans. Microwave Theory Tech.*, Vol. MTT-16, pp. 251-256, Apr. 1968.
- [51] Y. Rahmat-Samii, T. Itoh, and R. Mittra, "A spectral domain technique for solving coupled microstrip line problems." *Archiv. fur Elek. Ubertragung.*, Vol. 27, pp. 69-71, Feb. 1973.
- [52] Cao Wei et al., "Multiconductor transmission lines in multilayered dielectric media." *IEEE Trans. Microwave Theory Tech.*, Vol. MTT-32, pp. 439-449, Apr. 1984.
- [53] C. Chan and R. Mittra, "Spectral iterative techniques for analyzing multiconductor microstrip lines." *IEEE MTT Symposium Digest*, pp. 463-465, May 1984.
- [54] P. Bhartia and I. J. Bahl, *Millimeter Wave Engineering and Applications*. New York: Wiley, 1984, pp. 379-380.

- [55] T. Kitazawa and R. Mittra. "Asymmetrical coplanar transmission lines." EM Lab Report No. 84-9, University of Illinois, June 1984
- [56] T. Kitazawa and R. Mittra. "Quasistatic characteristics of asymmetrical and coupled coplanar-type transmission lines." EM Lab Report No. 85-4, University of Illinois, April 1985.
- [57] T. Kitazawa and R. Mittra. "Analysis of fin-lines with the finite metallization thickness." EM Lab Report No. 83-11, University of Illinois, October 1983.
- [58] T. Kitazawa and R. Mittra. "An investigation of strip lines and fin lines with periodic stubs." EM Lab Report No. 83-13, University of Illinois, October 1983.
- [59] S. H. Doran and R. Mittra. "An experimental study of dielectric rod antennas for millimeter-wave imaging applications." EMC Lab Report No. 85-3, University of Illinois, March 1985.
- [60] K. J. Webb and R. Mittra. "Investigation of planar waveguides and components for millimeter-wave integrated circuits." EMC Lab Report No. 84-3, University of Illinois, October 1984.

END

FILMED

1-86

DTIC